

FEDERAL UNIVERSITY OF ESPÍRITO SANTO - UFES
TECHNOLOGICAL CENTER
ELECTRICAL ENGINEERING POSTGRADUATE PROGRAM

CAIO MARCIANO SANTOS

**LONG-HAUL OFDM TRANSMISSION USING A
RECIRCULATING FIBER LOOP**

VITÓRIA
2019

CAIO MARCIANO SANTOS

LONG-HAUL OFDM TRANSMISSION USING A
RECIRCULATING FIBER LOOP

Dissertation submitted to the Electrical Engineering
Postgraduate Program of the Technological Center of the
Federal University of Espírito Santo, as partial requirement
for obtaining a Master's Degree in Electrical Engineering.

Supervisor:

Prof. Dr. Marcelo Eduardo Vieira Segatto

Co-Supervisor:

Prof. Dr. Maria José Pontes

Co-Supervisor:

Prof. Dr. Jair Adriano Lima Silva

VITÓRIA
2019

Ficha catalográfica disponibilizada pelo Sistema Integrado de Bibliotecas - SIBI/UFES e elaborada pelo autor

S2371 Santos, Caio Marciano, 1993-
Long-Haul OFDM Transmission Using a Recirculating Fiber Loop / Caio Marciano Santos. - 2019.
114 f. : il.

Orientador: Marcelo Eduardo Vieira Segatto.
Coorientadores: Maria José Pontes, Jair Adriano Lima Silva.
Dissertação (Mestrado em Engenharia Elétrica) -
Universidade Federal do Espírito Santo, Centro Tecnológico.

1. Telecomunicações. 2. Comunicações ópticas. I. Segatto, Marcelo Eduardo Vieira. II. Pontes, Maria José. III. Silva, Jair Adriano Lima. IV. Universidade Federal do Espírito Santo. Centro Tecnológico. V. Título.

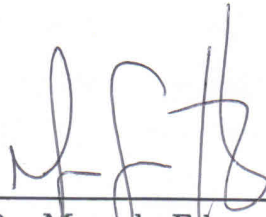
CDU: 621.3

CAIO MARCIANO SANTOS

**LONG-HAUL OFDM TRANSMISSION USING A
RECIRCULATING FIBER LOOP**

Dissertation submitted to the Electrical Engineering Postgraduate Program of the Technological Center of the Federal University of Espírito Santo, as partial requirement for obtaining a Master's Degree in Electrical Engineering.

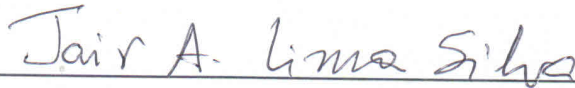
Approved on 17/06/2019.



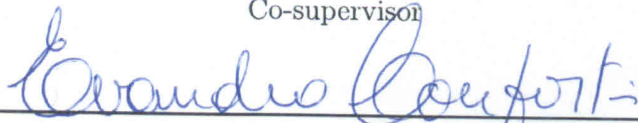
Prof. Dr. Marcelo Eduardo Vieira Segatto
Supervisor



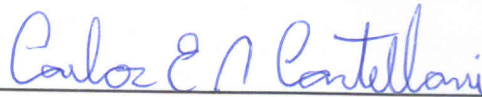
Prof. Dr. Maria José Pontes
Co-supervisor



Prof. Dr. Jair Adriano Lima Silva
Co-supervisor



Prof. Dr. Evandro Conforti
Examiner



Prof. Dr. Carlos Eduardo Schmidt Castellani
Examiner

VITÓRIA
2019

Acknowledgments

Since my first days in engineering I have been building up knowledge to present a considerable research to positively affect society. Through this work, the goal was achieved by presenting tools and analysis that contribute to future researchers in the telecommunications field. Everything contained in this text is fruit of the hard work of numerous people that should be acknowledged individually.

First off, I would like to thank my supervisor, Marcelo Eduardo Vieira Segatto, for the numerous conferences and adjustments required to piece this work together. As for my co-supervisors, Maria José Pontes and Jair Adriano Lima Silva, I am grateful for all the time taken to discuss every detail of the work thoroughly. Without all the invaluable meetings and discussions provided by these three individuals, none of this would be possible.

I also desire to express my gratitude to the Brazilian National Council for Scientific and Technological Development (CNPq, Portuguese: Conselho Nacional de Desenvolvimento Científico e Tecnológico) for the funding during the time required to produce this research. I would also like to extend my thanks to the Telecommunications Laboratory (LabTel) and the Federal University of Espírito Santo (UFES) for providing the space and technological equipment necessary for the development of this work.

Other contributors such as Reginaldo Barbosa Nunes should also be appreciated since the invaluable knowledge of the system coding and technical laboratory aspects helped in guaranteeing the functionality of the setup. The contribution acknowledgment should also be extended to the examiners: Evandro Conforti and Carlos Eduardo Schmidt Castellani for discussing the work thoroughly and bringing improvements to the overall quality of the research.

My family as a whole should be thanked for the support and motivation throughout the whole process. In specific, I would like to thank my grandparents: Jacir Rodrigues Marciano, Arlinda Almeida de Souza and Valdiria Alves Santos for all the positive remarks and loving concern for my future. Regarding support, I would also like to thank my brother Victor Marciano Santos. The largest portion of my gratitude is reserved for my parents, Jacimara de Souza Marciano Santos and Sanderson Alves Santos, whose knowledge and concern for my wellness reflect in all the success I have achieved to this day.

Last, but definitely not least, I would like to express my deepest gratitude to my girlfriend Mariana Lyra Silveira, whose loving care, support and togetherness have guided me through all of this process and more.

Abstract

Optical recirculating loops have been employed systematically over the years in the study of long-haul transmission systems. The loop technique attempts to simulate the performance of these systems by recirculating optical data through fiber spans and amplifier chains. The technique became widely accepted due to the reduced number of components used to achieve simulations of long-distance communications.

Orthogonal frequency division multiplexing (OFDM) is an important method due to its resilience towards polarization mode (PMD) and fiber chromatic dispersions (CD). However, a high peak-to-average power ratio (PAPR) is usually common in these signals, presenting peaks that are saturated by amplitude-limited equipment, consequently distorting the signals and reducing system performance. To overcome this limitation a phase modulation of the conventional OFDM is employed, generating a Constant Envelope OFDM (CE-OFDM), reducing the PAPR significantly. Both methods may be realized either with direct detection (DDO) or with coherent optical detection (CO). For long-haul systems, CO has shown superior performance. On the other hand, DDO has a simpler layout, making it more cost-effective.

By designing and testing a recirculating fiber loop, the parameters of long distance communications can be tested efficiently, acquiring an important tool for performance comparisons over different optical communications systems. Through this technique a DDO-OFDM and a DDO-CE-OFDM systems are tested for long distance optical communications with regards to numerous different parameters. The modulator bias, phase modulation index, fiber input power, transmission distances and modulation formats are thoroughly discussed for both systems and performance comparisons are made. Distances as long as 1.300 km are reached at rates of 1.41 Gb/s and 700 km for 2.82 Gb/s.

Keywords: Recirculating Loop, OFDM, CE-OFDM, Optical Communications, Optical Components, Optical Characterization.

Contents

1 – Introduction	27
1.1 Motivation	29
1.2 Objectives	29
1.3 Methodology	29
1.4 Structure	30
2 – Theoretical Background	31
2.1 Key Optical Components	31
2.1.1 Transmitter	32
2.1.1.1 Light Sources	32
2.1.1.2 Optical Modulators	33
2.1.2 Optical Channel	35
2.1.2.1 Optical Fibers	35
2.1.2.2 Optical Amplifiers	38
2.1.3 Receiver	41
2.1.4 Other Optical Components	42
2.1.4.1 Polarization Controller	42
2.1.4.2 Optical Switch	42
2.1.4.3 Optical Couplers	43
2.1.4.4 Optical Attenuator	44
2.1.4.5 Optical Filter	44
2.1.4.6 Isolators	44
2.2 Recirculating Fiber Loop	45
2.3 OFDM	47
2.3.1 MCM Basics	47
2.3.2 OFDM Principles	49
2.3.3 Hermitian Symmetry	50
2.3.4 Cyclic Prefix	50
2.3.5 Peak-to-Average Power Ratio of OFDM Signals	52
2.4 CE-OFDM Principles	52
2.5 Evaluation Parameters	55
2.5.1 BER	55
2.5.2 EVM	56
3 – Design and Characterization	57
3.1 Main Optical Components	57

3.1.1	Transmitter	57
3.1.1.1	Light Source	58
3.1.1.2	Optical Modulator	59
3.1.1.3	Optical Amplifier (Booster)	60
3.1.2	Optical Channel	61
3.1.2.1	Optical Fiber	61
3.1.2.2	Optical Amplifier (In-Line)	62
3.1.3	Receiver	63
3.1.3.1	Photodetector	63
3.1.3.2	Optical Amplifier (Pre-Amplifier)	65
3.1.3.3	Optical Filter	66
3.2	Recirculating Fiber Loop	67
3.2.1	Optical Switch	68
3.2.2	Couplers	69
3.2.3	Optical Amplifier (Compensator)	71
3.2.4	Loop Control Hardware	72
3.3	OFDM	74
3.3.1	Signal Generation and Reception	74
3.3.2	OFDM System Design	75
3.4	CE-OFDM	78
4	Experimental Results	79
4.1	Modulator's Point of Operation	80
4.2	CE-OFDM Phase Modulation Index	82
4.3	Optimum Fiber Launch Power	84
4.4	Transmission Distance Analysis	85
4.5	16-QAM System Analysis	88
5	Conclusion and Future Research	91
	Bibliography	94
A	Safety Considerations	97
A.1	Optical Safety Considerations	97
A.2	Inspection and Cleaning Procedures	98
A.3	Electrostatic-sensitive Devices	100
B	Measurement Procedures	101
B.1	Light Source Measurement	101

B.2	Optical Modulator Measurements	102
B.3	Optical Amplifier Measurements	103
B.4	Optical Fiber Measurements	107
B.5	Optical Switch Measurements	109
B.6	Optical Coupler Measurements	111
B.7	Optical Filter Measurements	112

List of Figures

Figure 1 – Simplified Optical Communication System.	31
Figure 2 – Mach-Zehnder Modulator.	33
Figure 3 – Mach-Zehnder Modulator Transfer Function.	34
Figure 4 – Silica Fiber Losses. Source: [Photonics 2019] (Modified).	35
Figure 5 – Side view of an optical fiber, with light confinement demonstration through total internal reflection and step-index refractive profile.	37
Figure 6 – Erbium transitions and energetic states for 980 and 1480 nm pumping.	39
Figure 7 – EDFA typical Gain Saturation. Source: [Becker, Olsson e Simpson 1999] (Modified).	40
Figure 8 – Optical spectrum before and after an EDFA. Source: [Derickson 1998] (Modified).	41
Figure 9 – Typical p-i-n photodiode: a) structure and b) equivalent model.	42
Figure 10 – Typical fiber coupler: a) fiber fusing based and b) coupling ratio example.	43
Figure 11 – Basic loop setup.	45
Figure 12 – Loop switch timing diagram, demonstrating how the switches should synchronize during operation.	46
Figure 13 – Typical MCM Transmitter Diagram.	47
Figure 14 – Typical MCM Receiver Diagram.	48
Figure 15 – Symbol transmission time diagram, with and without the CP. Modified: [Klenner 2004]	51
Figure 16 – Basic OFDM Setup.	51
Figure 17 – Signal modulation example a) Sinusoidal signal, b) Amplitude modulated (AM) signal and c) Phase modulated (PM) signal.	53
Figure 18 – Basic CE-OFDM Setup.	54
Figure 19 – Basic Transmitter Setup.	57
Figure 20 – LS5-C-25A-20-NM DFB Laser Measured Optical Spectrum ($P_{out} = +5$ dBm).	58
Figure 21 – Optical Modulator Characterization Setup.	59
Figure 22 – Mach-10 081 Characterization: Analytical and Measured Transfer Function.	59
Figure 23 – EDFA Characterization Setup: (a) input signal measurement and (b) output signal measurement.	60
Figure 24 – AP3370A Booster EDFA Module Characterization: (a) Output Power and (b) Amplifier Gain.	61
Figure 25 – AP3370C Pre-Amplifier EDFA Module Characterization: (a) Output Power and (b) Amplifier Gain.	62

Figure 26 – Basic Receiver Setup.	63
Figure 27 – Mach-10 081 and PDA8GS Frequency Response Characterization Setup.	64
Figure 28 – Mach-10 081 and PDA8GS Frequency Response Characterization.	64
Figure 29 – NOAPF25 Pre-Amplifier EDFA Characterization: a) Output Power and b) Amplifier Gain.	65
Figure 30 – AP3380A Optical Tunable Filter module Characterization Setup: a) Broadband source measurement and b) Filtered source measurement.	66
Figure 31 – AP3380A Optical Tunable Filter module Characterization.	67
Figure 32 – Experimental Loop Setup.	67
Figure 33 – Optical switch characterization: a) Measurement setup and b) Response Time diagram.	68
Figure 34 – Singlemode 1x2 Coupler Characterization Setup: a) Broadband source measurement and b) Coupler output measurement.	69
Figure 35 – Singlemode 1x2 Coupler Insertion Loss Characterization: a) 50/50 cou- pler and b) 80/20 coupler.	70
Figure 36 – NOABF10 Booster EDFA Characterization: a) Output Power and b) Amplifier Gain.	71
Figure 37 – Optical Switch and Amplifiers Hardware Design Setup.	72
Figure 38 – Adopted switching and triggering diagrams for the loop technique.	73
Figure 39 – Tektronix AWG7122C Frequency Characterization for signals generated at 24 GS/s.	74
Figure 40 – Designed OFDM system: a) Time domain signal and b) Power Spectral Density (PSD).	77
Figure 41 – PAPR Comparison between signals: a) OFDM and b) CE-OFDM.	78
Figure 42 – CE-OFDM Spectrum for different phase modulation indexes: a) $h = 0.10$, b) $h = 0.25$ and c) $h = 0.40$	78
Figure 43 – Complete Experimental Setup.	79
Figure 44 – MZM Point of Operation Analysis: a) OFDM signals and b) CE-OFDM signals.	81
Figure 45 – Measured OFDM Optical Spectrum for a) $0.33V_\pi$ and b) $0.64V_\pi$	82
Figure 46 – Measured CE-OFDM Optical Spectrum for a) $0.26V_\pi$ and b) $0.71V_\pi$	82
Figure 47 – CE-OFDM Phase Modulation Index Analysis.	83
Figure 48 – Measured CE-OFDM Optical Spectrum for different phase modulation indexes: a) $h = 0.10$, b) $h = 0.25$ and c) $h = 0.40$	84
Figure 49 – Fiber Launch Power Analysis: a) OFDM and b) CE-OFDM.	85
Figure 50 – BER as a function of transmission distance for different fiber launch powers (P_{in}) in the optimal region for: a) OFDM and b) CE-OFDM systems.	86

Figure 51 – 4-QAM constellation diagram for a transmission distance of 1.300 km at a fiber launch power of $P_{in} = 2$ dBm for a) OFDM and b) CE-OFDM.	87
Figure 52 – BER as a function of transmission distance for different fiber launch powers (P_{in}) in the high fiber nonlinearity region for: a) OFDM and b) CE-OFDM systems.	87
Figure 53 – 4-QAM constellation diagram for a transmission distance of 1,000 km at a fiber launch power of $P_{in} = 8$ dBm for a) OFDM and b) CE-OFDM.	88
Figure 54 – BER as a function of transmission distance for 16-QAM the a) OFDM and b) CE-OFDM system.	89
Figure 55 – 16-QAM constellation diagram for a transmission distance of 700 km at a fiber launch power of $P_{in} = 2$ dBm for a) OFDM and b) CE-OFDM.	90
Figure 56 – Typical laser hazard labels.	97
Figure 57 – Inspection of contaminated connector faces: a) protective end cap removal, b) fingerprint exposure, c) cross-contamination from unclean connector and d) lint from clothing. Source: [Chemtronics 2019].	99
Figure 58 – Connector cleaning: a) fiber cleaning cloth spool usage example and b) clean connector inspection. Source: [Chemtronics 2019].	99
Figure 59 – DPO with ESD sensitive inputs. The wrist wrap grounds the user, protecting the equipment from ESD.	100
Figure 60 – ASE Fitting methods: a) Gaussian fitting and b) Mean Fitting.	104
Figure 61 – MS9740a Optical Amplifier Characterization Test Parameters Example.	104
Figure 62 – MS9740a Optical Amplifier Characterization Test Example.	106
Figure 63 – Anritsu MT9083A2 Graphical Events and Event Table for SSMF characterization.	108
Figure 64 – Anritsu MT9083A2 SSMF characterization trace.	108
Figure 65 – Switch Rise Time (T_r) Measurement.	110
Figure 66 – Switch Fall Time (T_f) Measurement.	110
Figure 67 – Switch Rise Speed (S_r) Measurement.	110
Figure 68 – Switch Fall Speed (S_f) Measurement.	110

List of Tables

Table 1 – LS5-C-25A-20-NM DFB Laser Module Technical Data.	58
Table 2 – AP3370A Booster EDFA Module Technical Data.	60
Table 3 – Corning [®] SMF-28e+ [®] Technical Data.	61
Table 4 – AP3370C Pre-Amplifier EDFA Module Technical Data.	62
Table 5 – PDA8GS Technical Data.	64
Table 6 – NOAPF25 Pre-Amplifier EDFA Technical Data.	65
Table 7 – AP3380A Optical Tunable Filter module Technical Data.	66
Table 8 – Agiltron NanoSpeed [™] Technical Data.	69
Table 9 – SSD-1X2-35-50/50-R-2-1 Technical Data @ 1550 nm.	70
Table 10 – SSD-1X2-35-80/20-R-2-1 Technical Data @ 1550 nm.	70
Table 11 – NOABF10 Booster EDFA Technical Data.	71
Table 12 – OFDM System Parameters.	77
Table 13 – Summarized IEC 60825-1:2014 standard light source classification.	98

List of abbreviations and acronyms

A/D	Analog-to-Digital
APD	Avalanche Photodiode
ASE	Amplified Spontaneous Emission
AWG	Arbitrary Waveform Generator
BER	Bit Error Rate
CD	Chromatic Dispersion
CE	Constant Envelope
CO	Coherent Optical
CP	Cyclic Prefix
D/A	Digital-to-Analog
DBR	Distributed Bragg Reflector
DDO	Direct Detection Optical
DFB	Distributed Feedback Laser
DFT	Discrete Fourier Transform
DPO	Digital Phosphor Oscilloscope
DSF	Dispersion-Shifted Fiber
EAM	Electro-Absorption Modulator
EDFA	Erbium-Doped Fiber Amplifier
ESD	Electrostatic Discharge
EVM	Error Vector Magnitude
FEC	Forward Error Correction
FFT	Fast Fourier Transform
FP	Fabry-Perot
FSR	Free Spectral Range

FT Fourier Transform

FWM Four-Wave Mixing

GVD Differential Group Delay

GVD Group Velocity Dispersion

ICI Interchannel Interference

IDFT Inverse Discrete Fourier Transform

IFFT Inverse Fast Fourier Transform

ISI Inter-Symbol Interference

ITU International Telecommunication Union

LED Light Emitting Diode

MCM Multicarrier Modulation

MDO Mixed Domain Oscilloscope

MZM Mach-Zehnder Modulator

NA Numerical Aperture

NF Noise Figure

NRZ Non-Return-To-Zero

OCSA Optical Complex Spectrum Analyzer

OF Optical Filter

OFDM Orthogonal Frequency Division Multiplexing

OSA Optical Spectrum Analyzer

OSNR Optical Signal-to-Noise Ratio

PAPR Peak-to-Average Power Ratio

PC Polarization Controller

PC Polarization Controllers

PM Power Meter

PMD Polarization Mode Dispersion

PSD Power Spectral Density

QAM Quadrature Amplitude Modulation

RF Radio Frequency

SMSR Side Mode Suppression Ratio

SNR Signal-to-Noise Ratio

SPM Self-Phase Modulation

SRS Stimulated Raman Scattering

SSMF Standard Single Mode Fibers

VCSEL Vertical Cavity Surface Emitting Laser

VLC Visible Light Communication

VNA Vector Network Analyzer

VOA Variable Optical Attenuator

WDM Wavelength Division Multiplexing

List of symbols

λ	Wavelength
T_x	Transmitter
R_x	Receiver
ν	Frequency
$\Delta\nu$	Bandwidth
n	Refractive Index
L	Length
V	Voltage
V_b	Bias Voltage
Δn	Refractive Index Difference
Γ	Confinement Factor
r_{33}	Electro-Optic Coefficient
d_e	Distance Between Electrodes
$\Delta\phi$	Phase Variation
E_i	Input Electrical Field
E_o	Output Electrical Field
P_i	Input Power
P_o	Output Power
n_0	Refractive Index Outside the Fiber
θ_i	Angle of Incidence
n_1	Core Refractive Index
n_2	Cladding Refractive Index
Δ	Relative Refractive Index
V	Normalized Frequency

a	Core Radius
M	Modes in a Step-Index Fiber
G	Amplifier Gain
G_0	Full Gain Coefficient
g_0	Gain Coefficient
P_{sat}	Saturation Power
P_{sat}^{out}	Output Saturation Power
P_{in}	Input Power
P_{out}	Output Power
P_{ASE}	ASE Power
SNR_{in}	Input SNR
SNR_{out}	Output SNR
R_s	Series Resistance
R_{sh}	Shunt Resistance
C_p	Junction Capacitance
i_{ph}	Photocurrent
P_{inc}	Incident Optical Power
R	Responsivity
η	Quantum Efficiency
C	Coupling Coefficient
s_{ij}	Scattering Matrix Elements
β	Propagation Constant
H	Transfer Function
r	Reflectivity of Mirrors
τ	Round-Trip Time within a Cavity
ν_g	Group Velocity

F	Finesse
$\Delta\nu_{FP}$	FP Transmission Peak Width
τ_{loop}	Loop Round Trip Time
L_{loop}	Loop Length
τ_{data}	Duration of the Signal
R_b	Serial Bitstream Rate
R_n	Parallel Bitstream Rate
N	Number of Parallel Bitstreams
s_i	Transmitted Complex Symbols
g_{Tx}	Transmission Filter
f_i	Subcarrier Frequency
g_{Rx}	Reception Filter
\hat{s}_i	Received Complex Symbols
T_s	Symbol Duration
G_{Tx}	Frequency Domain Transmission Filter
G_{Rx}	Frequency Domain Reception Filter
\mathfrak{F}	Discrete Fourier Transform
\mathfrak{F}^{-1}	Inverse Discrete Fourier Transform
T_g	Guard Interval
ϕ	Phase
A	Amplitude
h	Phase Modulation Index
C_N	Variance Normalization Constant
B_i	Resonance Point Intensity
τ_g	Group Delay
ν_g	Group Velocity

$\Delta\tau_g$	Pulse Broadening
D	Dispersion Parameter
β_2	Group Velocity Dispersion
$\Delta\tau$	Differential Group Delay
F_s	Sample Rate
N_c	Useful Subcarriers
N_{FFT}	FFT Size
Δf	Subcarrier Channel Spacing
T_u	Useful Symbol Duration
N_u	Useful Symbol Sample Size
f_c	Optical Carrier Frequency
D_L	Total Chromatic Dispersion
N_g	Cyclic Prefix Sample Size
N_{pr}	Preamble Sample Size
n_{fr}	Frame Size
R_{total}	Total bitrate
$R_{nominal}$	Nominal bitrate
R_{raw}	Raw bitrate
ε_{pr}	Preamble Overhead
ε_{cp}	Cyclic Prefix Overhead
τ_{pr}	Preamble Duration
N_{err}	Number of incorrect bit measurements
N_{bits}	Number of compared bits
μ	Governing Parameter of the Poisson Distribution
CL	Confidence Level

1 Introduction

The growing request for information, due to Internet advances, demanded an evolution of communication systems to the optical domain. In the mid 1990s, the world experienced a considerable expansion of fiber optic networks, demonstrating the potential of optical communication systems. Until 1997, approximately 366,000 km of fiber optic cables were installed undersea, interconnecting the whole world [Becker, Olsson e Simpson 1999].

One of the main concerns when dealing with global interconnection is the attenuation of transmitted data. The optical fiber domination is due to its significantly low loss when compared to conventional transmission methods. Alas, amplification was still needed and optical communication repeaters were expensive due to the high rate electronics that were employed. It was only in 1987 that Erbium-doped fiber amplifiers (EDFAs) appeared, demonstrating efficient amplification of light in the 1.5 μm spectral region [Becker, Olsson e Simpson 1999] [Freitas 2006].

Optical systems made undersea cable applications possible, but the structure of this task was extremely complicated and costly. Before resources could be committed, an experimental proof needed to be provided. A transoceanic length experiment would require more equipment than could be supplied, so a technique needed to be developed in order to test such structures. The solution was an experiment where data was circulated through a shorter amplifier chain. Feasibility of transoceanic transmissions was demonstrated in 1991, where 2.5 Gb/s non-return-to-zero (NRZ) signals were measured over 9,000 km with a bit error rate (BER) lower than 10^{-9} , using a 120 km EDFA chain [Bergano et al. 1991]. Numerous other experiments were realized and the recirculating loop technique became widely accepted for long distance transmission experiments [Bergano e Davidson 1995].

As demand continually increased, different applications and increased rates were necessary, splitting the spectrum and increasing the bandwidth of the systems. In order to keep up with demand, multicarrier modulation (MCM) formats became common in communication systems, dividing the information into numerous lower rate channels. A type of MCM known as orthogonal frequency division multiplexing (OFDM) soon became popular in the early 1990s, due to advantages such as robustness against channel dispersion and the ease of phase and channel estimation in time-varying environments [Chang 1966] [Hanzo, Webb e Keller 2000] [Chang 2000].

Increasing bandwidth for multicarrier systems presented complications that needed to be overcome. In optical fibers, different wavelengths propagate differently due to variations of the refractive index at each frequency and waveguided effects. This phenomenon

is known as chromatic dispersion (CD), being a considerable contributor to interchannel interference (ICI) and signal distortions. OFDM was widely accepted in the optical domain, in part, due to its resilience toward fiber dispersion. This resilience permitted system designers to realize part of the dispersion compensation through OFDM, reducing the quantity of especial dispersion-shifted fibers (DSF), that were used for CD compensation [Nunes et al. 2014].

With the growing importance of OFDM systems, the following years introduced various contributions using either direct detection optical (DDO) or coherent optical (CO) detection [Shieh e Djordjevic 2010]. For long-haul systems, CO-OFDM has shown superior performance, with experiments demonstrating high rates at distances over 1,000 km. On the other hand, DDO-OFDM has a much simpler layout, making it more cost-effective at short distances. Another drawback of DDO-OFDM systems is that a guard band must be inserted between the optical carrier and the OFDM band. This guard band is necessary in order to avoid intermodulation impairments at the photodiode, improving performance while reducing significantly the spectral efficiency of the system [Jansen et al. 2007].

One of the main drawbacks of OFDM systems is the high peak-to-average power ratio (PAPR) of the signal. The multiple frequencies from the subcarriers generate a time domain signal with very different maximum and average power values. This means that the signal is extremely susceptible to distortions generated by devices that saturate high power values. Such devices are common in the electro-optical domain, such as radio frequency (RF) amplifiers and optical modulators. Even after such distortions, signals containing high power values are prone to provoke nonlinear effects in optical fibers, further degrading the transmitted data [Silva 2011].

Various techniques were presented to reduce PAPR, such as signal clipping, amplitude filtering, predistortion, etc. In the midst of all techniques, clipping is usually the most used due to simplicity and efficiency. However, in 2003, a promising technique was introduced aiming to nullify PAPR by modulating the phase of the conventional OFDM. This method was named Constant Envelope OFDM, or CE-OFDM, since it generates a signal with constant amplitude. The drawbacks are increased complexity and spectral inefficiency when compared to conventional OFDM systems [Thompson et al. 2004] [Thompson et al. 2008] [Nunes et al. 2014]. Since then, researches have been proposed demonstrating how CE-OFDM reduces PAPR while mitigating optical fiber nonlinearity [Silva, Cartaxo e Segatto 2012].

1.1 Motivation

This dissertation aims to study the performance of OFDM and CE-OFDM systems over long distance optical channels. The recirculating fiber loop technique is used in order to reach higher distances and analyze an optical communication system. The analysis should provide a concrete comparison of both techniques with regard to optical fiber nonlinearity and overall system performance. It should also prove useful to study the parameters of CE-OFDM over long distance transmissions.

1.2 Objectives

The main goal of this work is to evaluate optical system performance over long distances using a recirculating fiber loop. OFDM and CE-OFDM are compared by analyzing their traits over the optical channel and discussing advantages and disadvantages of each technique. Other characteristics of the system are discussed, such as increasing bandwidth and data rates. It is possible to divide the objective into three specific objectives:

- Recirculating loop construction/characterization;
- OFDM and CE-OFDM design/characterization;
- OFDM and CE-OFDM long-haul analysis;

1.3 Methodology

The recirculating loop technique is discussed in numerous researches but replicating the system requires an understanding of a vast number of optical components and characteristics. All components should be studied and characterized, separately and thoroughly, in order to comprehend the system completely. In the end, the technique will be responsible for leading the signals through numerous optical components and thousands of kilometers of fiber. This bibliographic study demonstrates the exploratory nature of the research.

OFDM and CE-OFDM signals are generated through software, so all coding should be revised and improved to acquire the desired systems. Numerous parts of the software were inherited by past contributions from [Silva 2011], [Almeida 2014] [Nunes 2016] and [Pereira 2017]. A conventional OFDM design should be employed for long distance communications, taking into account bandwidth, data rates and chromatic dispersion compensation. From the conventional system, the phase modulation should be realized and characterized properly for the CE-OFDM. These steps demonstrate the explanatory nature of the experiments, aiming to have every piece of equipment characterized and understood before actual testing.

Each technique is then analyzed separately, utilizing the recirculating fiber loop. Both results are compared in order to evaluate the similarities and differences between OFDM and CE-OFDM. With this combined understanding of both techniques, it is possible to take conclusions on whether CE-OFDM functions as expected in long-haul systems. System performance and parameter evaluation highlight the quantitative nature of the research.

1.4 Structure

After a brief introduction to the topics under discussion, it is noteworthy to define the structure of the dissertation. Chapter 2 will layout the theoretical background required for comprehending the setups and analysis discussed throughout the text. The characterization of all components and the OFDM system design is introduced in Chapter 3. By combining the acquired knowledge from Chapters 2 and 3, the experimental results are appropriately discussed in Chapter 4 and, finally, a conclusion of the experiments is laid out in Chapter 5.

2 Theoretical Background

This chapter summarizes the basics of optical communication systems. The key optical components are discussed in detail, from transmission to reception. The recirculating loop technique is introduced and described thoroughly, defining possible setups and procedures. Finally, OFDM and CE-OFDM principles are discussed, demonstrating how these systems function.

2.1 Key Optical Components

An optical communications system can be divided, in general, into three sections: transmitter, optical channel and receiver, as shown in Figure 1. Each section needs to be taken into account carefully for the system to function as desired. T_x and R_x refer to the transmitter and receiver respectively, λ is the wavelength of the signal and WDM the wavelength division multiplexing.

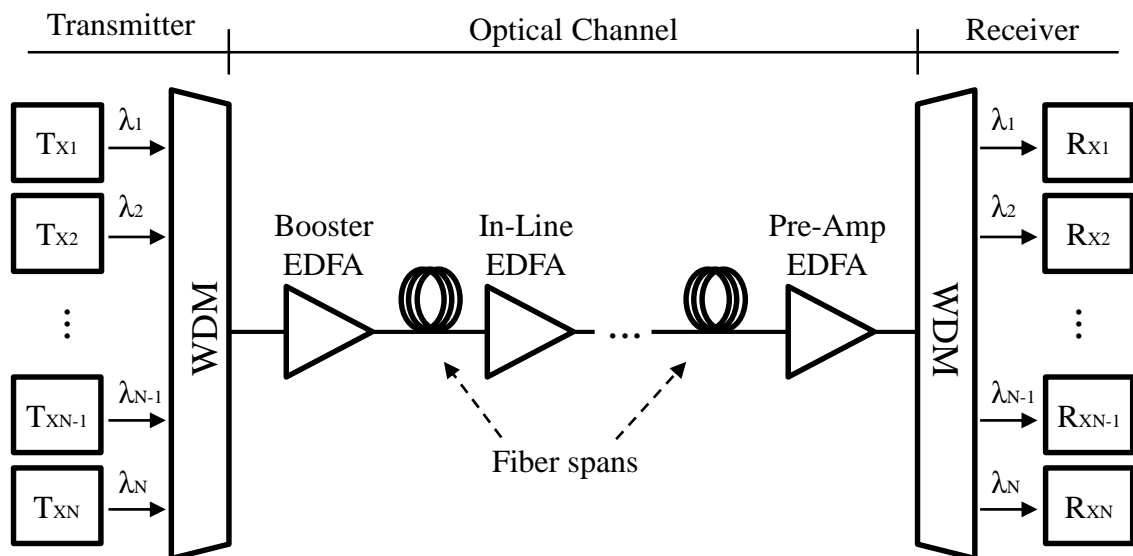


Figure 1 – Simplified Optical Communication System.

2.1.1 Transmitter

The main purpose of the transmitter is to generate and prepare the optical signal for propagation through the optical channel. Semiconductor light sources are usually used in modern optical communication systems. The characteristics of the light source determines a series of factors, such as transmission distance and achievable data rate [Derickson 1998]. Optical modulators are introduced to act as electro-optic converters of the radio frequency (RF) signal.

2.1.1.1 Light Sources

Fabry-Perot (FP) lasers are well known due to their simplicity of fabrication and low cost. The basic structure consists of a semiconductor optical amplifier and mirrors to form a resonator. An injection current flows through the amplifier, stimulating the creation of photons that are reflected by the mirrors and successively amplified by the same amplifier [Derickson 1998]. Lasing begins to occur when the collective gain is larger than the loss after a round trip through the cavity. This configuration will generate different longitudinal modes of frequency $\nu_q = qc/(2nL)$, where q denotes different integers, c is the speed of light, n is the refractive index of the active medium and L is the length of the active medium [Djordjevic, Ryan e Vasic 2010]. The spacing between neighboring modes is known as free-spectral range (FSR) and is achievable through the following equation:

$$\Delta\nu = \nu_q - \nu_{q-1} = q\frac{c}{2nL} - (q-1)\frac{c}{2nL} = \frac{c}{2nL}. \quad (1)$$

Distributed feedback lasers (DFBs) were designed to overcome the flaws of the FP lasers. This type of laser improves the coherence of output light and modulation speed by selecting one of the longitudinal modes while suppressing the others. The structure is similar to that of the FP lasers with the addition of a Bragg grating inside the laser cavity. This grating will select a longitudinal mode according to the Bragg condition [Djordjevic, Ryan e Vasic 2010]. Another possibility is placing the grating element outside of the active region or instead of the mirrors, creating a distributed Bragg reflector (DBR). The outcome of this structure will have effects similar to that of the DFBs. Both of these lasers are usually used in single-mode applications.

A laser that uses a similar concept as DBRs is the vertical cavity surface emitting laser (VCSEL), with the exception of emitting the light vertical to the active layer plane. VCSEL usually offers higher output power and higher modulation rates than light-emitting diodes (LEDs) used in data communications links [Derickson 1998]. They are inserted in the multi-mode laser domain, usually offering high rates in short distances.

2.1.1.2 Optical Modulators

Modulation is required to perform electro-optic conversion of the RF signal. DFBs and DBRs are the best contenders for modulation due to their narrow spectral width. Unfortunately, if high-speed direct current modulation is applied to these lasers, the center wavelength is pulled up and down. This phenomenon is referred to as frequency chirp, causing substantial broadening of the laser linewidth [Derickson 1998]. To avoid this problem, external modulation may be used while the laser is biased at a continuous point of operation.

In this context, Mach-Zehnder modulators (MZM) are widely accepted. They operate using interferometry techniques based on the electro-optic effect, present in certain materials such as $LiNbO_3$ and $GaAs$. The optical signal is split into two separate paths and then recombined at the output as seen in Figure 2. Its main principle is the variation of the refractive index of the material with respect to the voltage applied across the electrodes ($V = V_1 - V_2$), generating a phase variation as equated by [Dubovitsky et al. 2002] [Agrawal 2004] [Djordjevic, Ryan e Vasic 2010]:

$$\Delta n = -\frac{1}{2}\Gamma n^3 r_{33}(V/d_e) \Rightarrow \Delta\phi = \frac{2\pi}{\lambda}\Delta nL, \quad (2)$$

where Δn denotes the variation of the refractive index, Γ is the confinement factor, r_{33} is the electro-optic coefficient, d_e is the distance between the electrodes, $\Delta\phi$ the phase variation, λ is the wavelength of the signal and L is the electrode length.

An important modulator parameter is V_π , also known as the differential voltage that results in a differential phase shift of π rad between the branches of the MZM. To simplify the knowledge of the optical properties of MZMs, manufacturers usually use V_π to express some of the terms in equation 2 in one meaningful variable that can be expressed

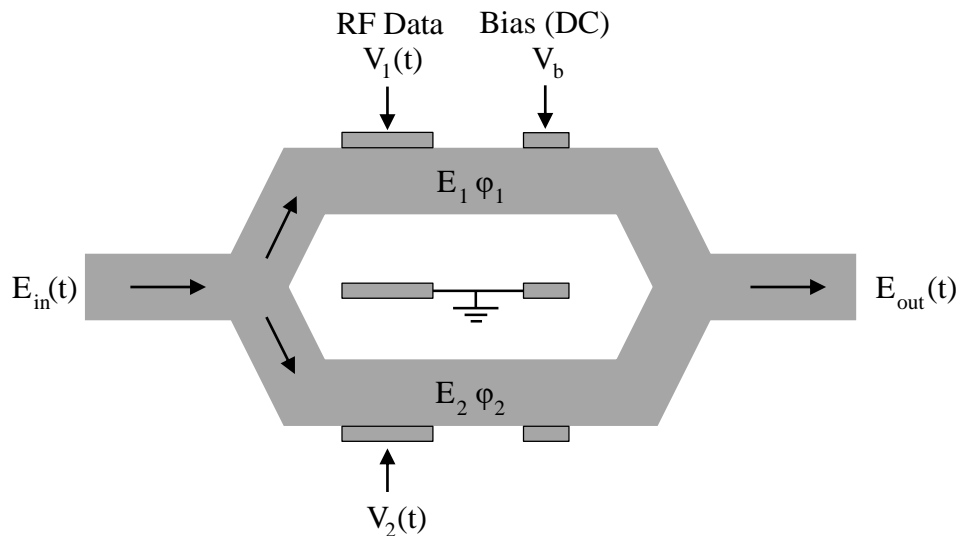


Figure 2 – Mach-Zehnder Modulator.

as [Dubovitsky et al. 2002]:

$$V_\pi = \frac{\lambda d_e}{2\Gamma n^3 r_{33} L}. \quad (3)$$

It is important to note that modulators contain a Bias Voltage Input as shown in 2 to define a point of operation. This voltage input (V_b) applies a constant shift in the phase that affects the signals directly. This characteristic permits the phase shift between the branches (Equation 2) to be rewritten as,

$$\Delta\phi = \frac{2\pi}{\lambda} \Delta n L + \frac{\pi V_b}{V_\pi}. \quad (4)$$

The transfer function of the device can then be obtained as a function of the applied voltage and phase shifts as [Dubovitsky et al. 2002],

$$\frac{E_o(t)}{E_i(t)} = \frac{1}{2} \left[1 + \cos \left(\frac{\pi V(t)}{V_\pi} + \Delta\phi \right) \right], \quad (5)$$

where E_i and E_o denote the input and output electrical fields respectively. This same equation can be rewritten to express the output power of the MZM as [Togneri 2005]:

$$\frac{P_o(t)}{P_i(t)} = \ell^2 \cos^2 \left(\frac{\pi V(t)}{4V_\pi} + \frac{\pi V_b}{2V_\pi} \right), \quad (6)$$

where P_o and P_i denote the output and input power respectively and ℓ is the insertion loss of the waveguides. Equation 6 demonstrates how the output power of the MZM relates to the voltage applied to the electrodes. The modulator is usually characterized through the bias voltage as this value defines the point of operation of the device. The output of transfer function, from Equation 6, with regard to the bias operation can be observed in Figure 3.

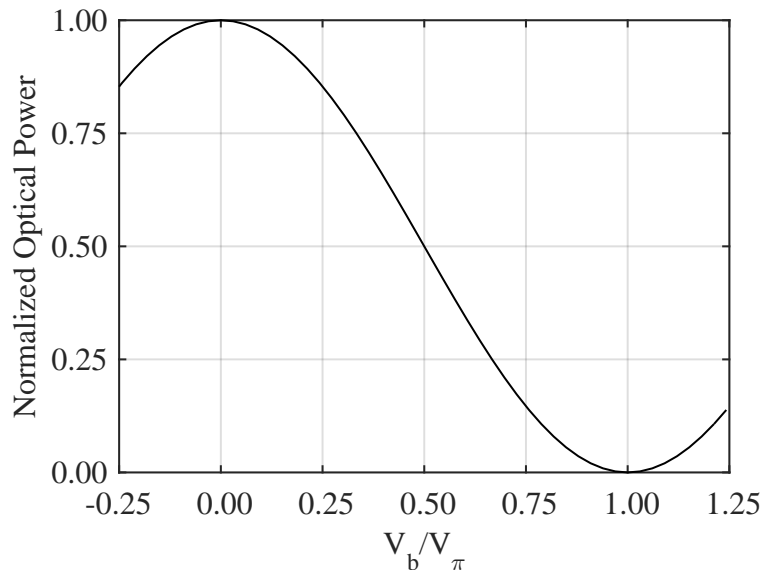


Figure 3 – Mach-Zehnder Modulator Transfer Function.

An alternative kind of modulator is the electro-absorption modulator (EAM). This modulator is created as a planar waveguide composed of multiple p-type and n-type layers. The structural composition makes it easier to integrate them on the same substrate as the light source. EAMs are comparable to MZMs when modulation speed is taken into account, on the other hand, they usually possess a lower extinction ratio [Djordjevic, Ryan e Vasic 2010].

2.1.2 Optical Channel

The optical channel is responsible for providing a connection between the transmitter and the receiver. This link is usually realized with a combination of optical fibers and amplifiers.

2.1.2.1 Optical Fibers

Optical fibers are waveguides, usually, composed mainly by some kind of glass with addition of dopants to improve desired properties. The most common type of optical fiber is made of silica (SiO_2) in pure form, with a common core dopant being *Ge*. Silica fibers dominate long-distance optical fiber communications especially due to the low losses in the near-infrared spectral region. Extremely low losses appear near the 1.5 μm region, reaching values as low as ≈ 0.20 dB/km at 1.55 μm [Photonics 2019]. These losses are limited by Rayleigh scattering and infrared absorption at short and long wavelengths respectively, as shown in Figure 4.

A principle known as total internal reflection is used to maintain the optical signal in the fiber. This works due to the way a step-index optical fiber is arranged as shown in

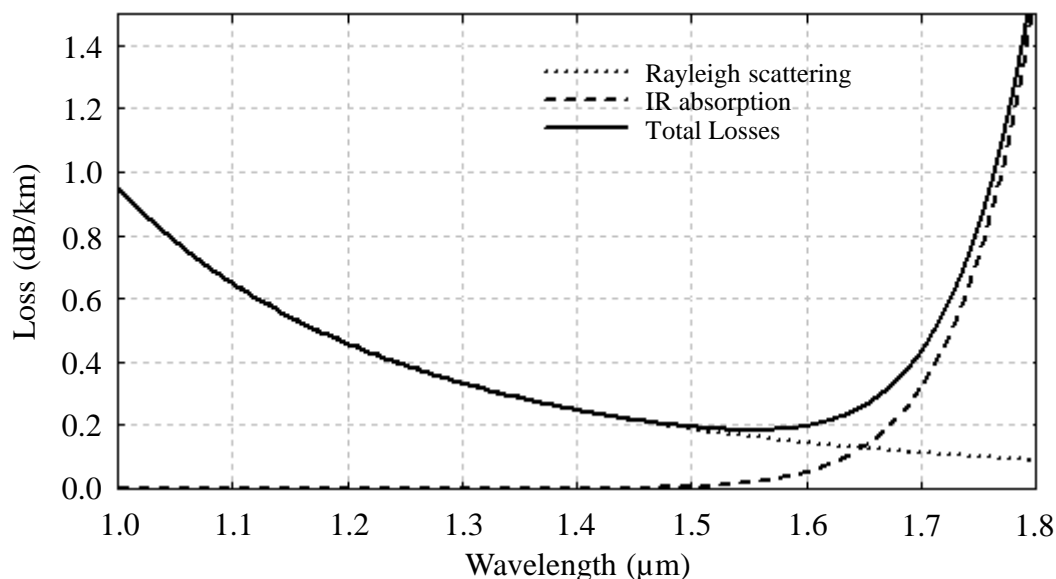


Figure 4 – Silica Fiber Losses. Source: [Photonics 2019] (Modified).

Figure 5. The two layers of glass have slightly different refractive indexes, with the core presenting a higher value than the cladding. Noting the refractive index difference, Snell's law can be applied to an incident ray of light, obtaining a condition for total internal reflection to occur [Smith, King e Wilkins 2007]:

$$n_0 \sin \theta_i < \sqrt{n_1^2 - n_2^2}, \quad (7)$$

where θ_i denotes the angle of incidence, n_0 is the refractive index outside the fiber, n_1 and n_2 are the core and cladding refractive indexes respectively. This condition is obtained from a side view of the optical fiber, but it can be extended to characterize a cone of rays incident to the fiber core. The acceptance cone can be expressed in terms of the numerical aperture:

$$NA = \frac{\sqrt{n_1^2 - n_2^2}}{n_0} \approx n_1 \sqrt{2\Delta}, \quad (8)$$

where Δ is the relative refractive index. A useful simplification of the equation can be used when $\Delta = (n_1 - n_2)/n_1$ is small (as occurs in most optical fibers) [Smith, King e Wilkins 2007].

A parameter known as normalized frequency can be defined by realizing a more complicated analysis of the fiber as a cylindrical waveguide. This parameter is given by,

$$V = \frac{2\pi a}{\lambda} NA, \quad (9)$$

where a denotes the fiber core radius. This is also known as the V parameter or V number. The usefulness of the parameter appears in the multimode analysis of optical fibers. By analyzing the solution of a wave equation for the fundamental mode, the first zero of the Bessel function occurs at 2.405. This means that if the V number is less than 2.405, only one mode can propagate in the fiber. For large values of V, the number of modes, in a step-index fiber, can be defined by [Smith, King e Wilkins 2007]:

$$M \simeq \frac{\pi^2}{2} \left(\frac{2a}{\lambda} \right)^2 (n_1^2 - n_2^2) = \frac{V^2}{2}. \quad (10)$$

Attenuation is not the only problem faced when transmitting data through an optical channel. Short pulses are spread out into a broader temporal distribution due to intermodal and chromatic effects. In singlemode fibers, only chromatic dispersion is available due to difference in velocities among different spectral components. This difference mainly occurs due to waveguide physical design and material dispersion caused by refractive index variation along different wavelengths, as defined by the Sellmeier equation [Djordjevic, Ryan e Vasic 2010]:

$$n(\lambda) = 1 + \sum_{i=1}^M \frac{B_i \lambda^2}{\lambda^2 - \lambda_i^2}, \quad (11)$$

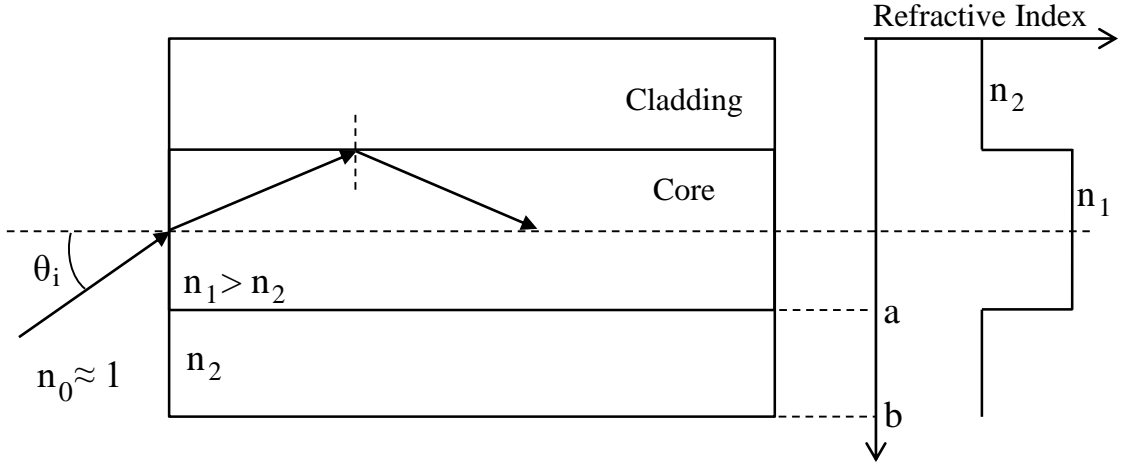


Figure 5 – Side view of an optical fiber, with light confinement demonstration through total internal reflection and step-index refractive profile.

where B_i is the intensity of the resonance points at the resonance wavelengths λ_i . The multiple wavelengths induce different velocities, generating a delay τ_g at a specific spectral component after a fiber length of L . This delay is known as the group delay, defined as,

$$\tau_g = \frac{L}{\nu_g} = L \frac{d\beta}{d\omega} = -L \frac{\lambda^2}{2\pi c} \frac{d\beta}{d\lambda}, \quad (12)$$

where β denotes the propagation constant, ω the angular frequency and ν_g the group velocity. Through this parameter, it is possible to obtain the difference in time delays between wavelengths, characterizing the pulse broadening, given by

$$\Delta\tau_g = \frac{d\tau_g}{d\lambda} \Delta\lambda = L \frac{d^2\beta}{d\omega^2} \left(-\frac{2\pi c}{\lambda^2} \Delta\lambda \right) = LD\Delta\lambda, \quad (13)$$

where D denotes the chromatic dispersion parameter defined as,

$$D = -\frac{2\pi c}{\lambda^2} \frac{d^2\beta}{d\omega^2} = -\frac{2\pi c}{\lambda^2} \beta_2, \quad (14)$$

where β_2 is the group-velocity dispersion (GVD) parameter. The dispersion parameter (D) is usually expressed in $ps/(nm \cdot km)$. Through the product LD , the system designer can easily estimate the total dispersion of the system and work to overcome signal distortions [Togneri 2005]. As the polarization vectors do not maintain constant in optical fibers, it is also common for different polarizations to arrive at different times leading to polarization mode dispersion (PMD). This difference, for two orthogonal polarization modes, is known as the differential group delay (DGD), defined as [Djordjevic, Ryan e Vasic 2010],

$$\Delta\tau = \left| \frac{L}{\nu_{gx}} - \frac{L}{\nu_{gy}} \right| = L\Delta\beta_1, \quad (15)$$

where β_1 denotes the propagation constant given by $1/v_g$.

The basic principles discussed beforehand assume a linear operation of the optical fiber; however, this is only valid for optical launch powers below several mW. At high powers,

two major nonlinear effects are considered due to nonlinear refractive index (Kerr effect) or nonlinear optical scattering. These effects lead to numerous different phenomena such as Self-Phase Modulation (SPM), Four-Wave Mixing (FWM), Stimulated Raman Scattering (SRS), etc. A vast number of applications take advantage of these properties, but for optical communications they should be avoided due to unwanted signal degradation [Djordjevic, Ryan e Vasic 2010].

2.1.2.2 Optical Amplifiers

Over long distances, the signal becomes attenuated and needs to be amplified. Before optical amplifiers, the signal was taken to the electrical domain, amplified and transformed back to the optical domain. This was a costly method which limited the system due to the electronics involved. Optical amplifiers eliminated such needs, as the signal is amplified optically.

In 1987, erbium-doped fiber amplifiers (EDFAs) were presented, demonstrating efficient amplification in the 1.5 μm spectral region. Other types of amplifiers were also developed, containing rare earth dopants such as ytterbium, neodymium, praseodymium, thulium and others. With the development of lasers with high output power, new techniques of optical amplification were also achieved mainly utilizing optical fiber nonlinear effects, such as Raman and Brillouin scattering. EDFAs are considered one of the most important amplifiers in optical communications due to characteristics such as high gain and high optical power, while having a low noise figure, when compared to other optical amplifiers. The relative simplicity of the amplifier is also taken into account [Freitas 2006].

The main components of fiber amplifiers are doped fibers and pump lasers. Pumping light into the doped fiber excites the ions to a higher energetic state. At higher states, two things may occur: spontaneous emission or stimulated emission. The first occurs spontaneously as the ions transit to lower states, emitting photons with random phase, frequency and polarization characteristics. This arbitrary light characterizes a phenomenon known as amplified spontaneous emission (ASE). Stimulated emission occurs when a signal transits through the doped fiber, inducing ion transitions to lower states while generating photons with the same optical characteristics of the signal [Becker, Olsson e Simpson 1999]. This process is illustrated in Figure 6, for two of the most commonly used pumping wavelengths in EDFAs. The three Erbium states involved are $^4I_{11/2}$, $^4I_{13/2}$ (metastable state) and $^4I_{15/2}$ (stable or ground state). The transition from $^4I_{11/2}$ to $^4I_{13/2}$ is very fast and non-radiative, in other words, no photon is generated during this transition. On the other hand, from the metastable to the ground state, stimulated and spontaneous emissions occur, generating light and contributing to the amplification process.

It is important to note that fiber amplifiers are limited by saturation, originated from the fact that the power propagation depends on the gain coefficient g_0 of the doped

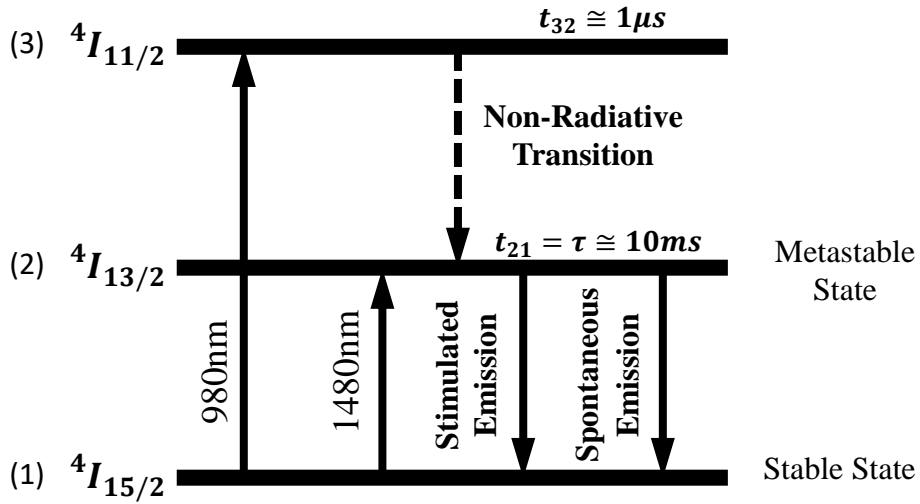


Figure 6 – Erbium transitions and energetic states for 980 and 1480 nm pumping.

fiber. Solving the propagation differential equation of the doped fiber, provides [Djordjevic, Ryan e Vasic 2010]:

$$G = G_0 \exp \left[-\frac{G - 1}{G} \frac{P_{out}}{P_{sat}} \right], \quad (16)$$

where G is the amplifier gain, P_{out} is the output power, P_{sat} is the saturation power and $G_0 = \exp(g_0 L)$, where L is the length of the doped fiber. P_{sat} represents the power required to energize the doped fiber sufficiently to obtain optical transparency, also known as zero gain. As the amplifier saturates the gain, the output power also saturates. The definition for output saturation power is established as the optical power at which the gain is reduced to $G_0/2$ (-3 dB). Applying this condition to Equation 16, it is possible to obtain:

$$P_{sat}^{out} = \frac{G_0 \ln 2}{G_0 - 2} P_{sat} \approx (\ln 2) P_{sat} \approx 0.69 P_{sat}. \quad (17)$$

Equations 16 and 17 define the saturation of the amplifier without ASE. When considering ASE in the equations, the ASE power should be deducted from the actual output power. This will lower the actual gain of the amplifier, defining how ASE can affect amplifier performance, as can be observed in Figure 7.

Three important parameters characterize an optical amplifier: output power (P_{out}), gain (G) and noise figure (NF). The output power helps the system designer understand how much power will be available at the output of the amplifier. The gain is useful for understanding chains of amplifiers or to define, easily, how much loss an amplifier can overcome. Noise Figure provides an idea of the signal degradation after passing through amplifiers.

These parameters can be obtained by realizing a spectral analysis of the signal before and after the amplifier, as shown in Figure 8. The gain is defined as the ratio between the signal input and output power. To obtain the signal output power, the ASE

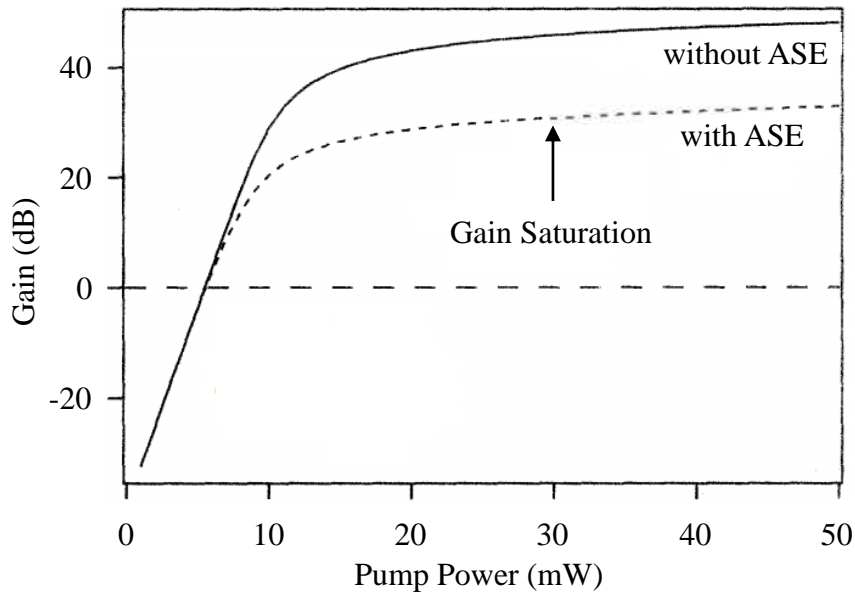


Figure 7 – EDFA typical Gain Saturation. Source: [Becker, Olsson e Simpson 1999] (Modified).

power P_{ASE} must be subtracted from the total output power P_{out} . An EDFA's gain can then be defined as,

$$G_{dB} = 10\log_{10}(G) = 10\log_{10}\left(\frac{P_{out} - P_{ASE}}{P_{in}}\right). \quad (18)$$

The noise figure is obtained from the ratio between the SNRs at the input and output of the amplifier. Another possibility is obtaining the noise figure from the gain and ASE power, defining it as,

$$NF = 10\log_{10}\left(\frac{SNR_{in}}{SNR_{out}}\right) = 10\log_{10}\left(\left[\frac{P_{ASE}}{h\nu\Delta\nu} + 1\right]\frac{1}{G}\right). \quad (19)$$

Three common configurations of optical amplifiers are usually used in optical communications: booster amplifiers, in-line amplifiers and preamplifiers. The first is used after the transmitter to compensate for losses of the transmitting elements, the second is placed along the optical links to compensate propagation losses and the third is used to increase the signal power before photodetection. Each of these can be identified in Figure 1.

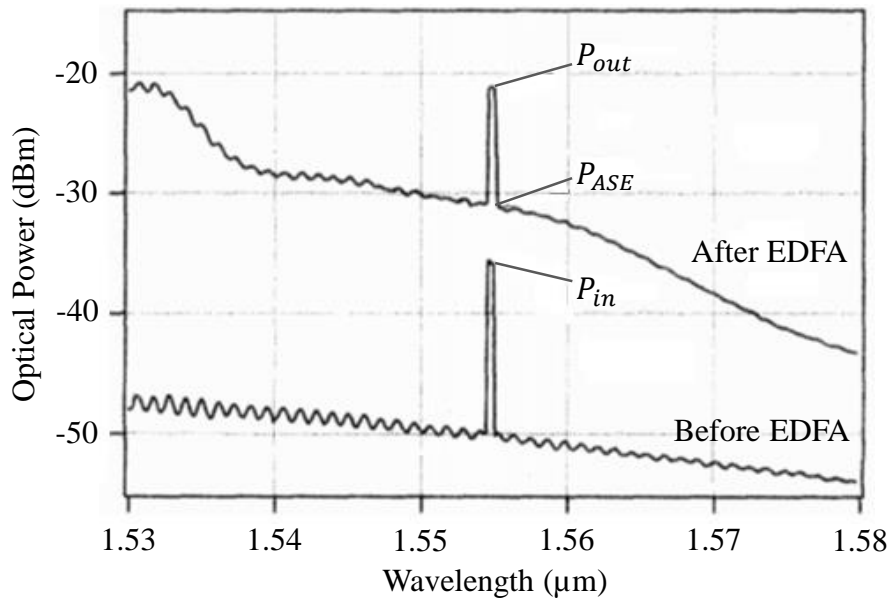


Figure 8 – Optical spectrum before and after an EDFA. Source: [Derickson 1998] (Modified).

2.1.3 Receiver

The main purpose of the receiver is to convert the optical signal into an electric signal that will be used to recover the transmitted data. This conversion is done by using photodetectors and RF amplifiers. There are many types of photodetectors such as p-n photodiode, p-i-n photodiode, avalanche photodiode (APD) and others not so commonly used. The name of these devices are references to the doping of the structural layer. Since the p-i-n photodetectors are the most common, this type of structure will be discussed in detail.

Figure 9a shows the composition of a typical p-i-n photodiode. This device consists of an intrinsic layer situated between p- and n-type layers. The intrinsic layer is chosen to be a material that absorbs photons that are then converted to electrons by the p-i-n structure. This process is repeated as the signal arrives, generating a photocurrent proportional to the incoming optical signal [Derickson 1998].

An equivalent model of the p-i-n photodiode is demonstrated in Figure 9b. The internal series resistance R_s is usually low, while the shunt resistance R_{sh} is high, so that the junction capacitance C_p dominates, guaranteeing a very high internal impedance. The photocurrent generated i_{ph} is proportional to the power of incident light P_{inc} . A relation can be established as $i_{ph}(t) = RP_{inc}(t)$, where R is the photodiode responsivity given by $R = \eta q / h\nu$ and η is the quantum efficiency, q is an electron charge and $h\nu$ is the photon energy [Djordjevic, Ryan e Vasic 2010].

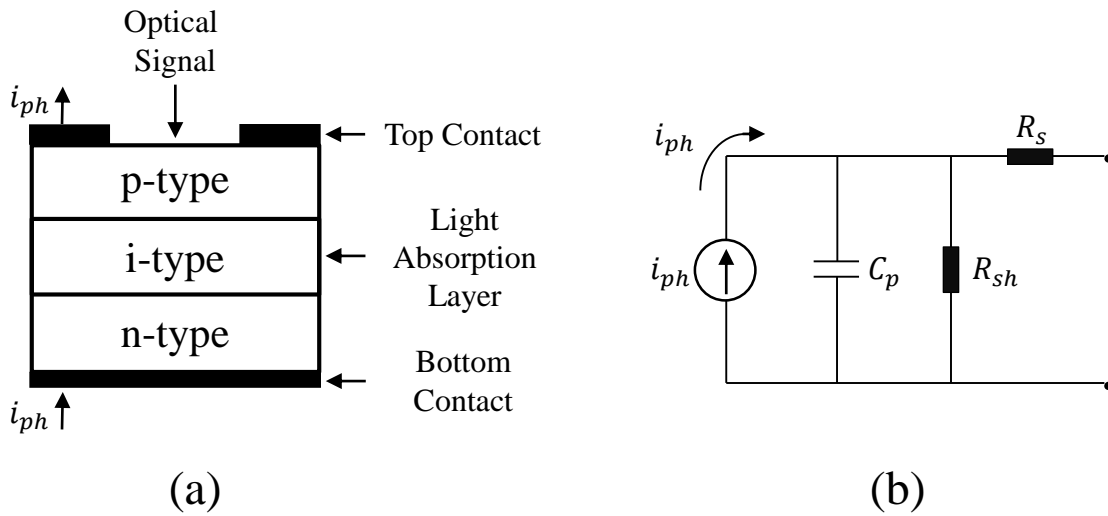


Figure 9 – Typical p-i-n photodiode: a) structure and b) equivalent model.

2.1.4 Other Optical Components

2.1.4.1 Polarization Controller

Some optical components are affected by the state of polarization of light during propagation, with MZMs and EDFAs being great examples of such components. For this purpose polarization controllers (PC) can be used to obtain the desired results. A common type of PC has a mechanical structure that permits the user to slightly rotate and squeeze a length of fiber around its axis. This results in a variation of the state of polarization at the output of the device. Other types of PCs exist, giving more control of the movements to achieve a better control of the polarization variation, but mainly serving the same purpose [Photonics 2019].

2.1.4.2 Optical Switch

Optical switches are used for enabling or disabling the passage of light in an optical link. Another possibility is switching the signal between different links. An optical modulator functions as an optical switch, but can only be applied as an ON/OFF switch. For other applications, technologies such as solid-state crystals or magneto-optic switches may be used to redirect signals to other links. These switches can be used in a wide variety of applications such as link protection, signal modulation, remote reconfiguration, etc.

2.1.4.3 Optical Couplers

Optical couplers allow light to be branched into other links, operating on the principle of coupled mode theory. This can be obtained by removing the cladding of two fibers and bringing their cores together, allowing light to couple from one core to the other, as shown in Figure 10a. By controlling the parameters of such technique, the coupling coefficient C can be varied to apply the desired coupling ratios. The example cited would create a 2x2 coupler, in which the outputs would be $P_{out1} = P_{in} \cos^2(CL)$ and $P_{out2} = P_{in} \sin^2(CL)$, with L being the length of the coupling section [Shaim e Khan 2011]. Different coupling ratios are obtained, simply, by varying the coupling length, as shown in Figure 10b. If only one input is used, the coupler is known as an optical tap coupler (1x2). However, if both inputs are used, the device is known as a directional coupler (2x2).

It is also useful to model these devices using a simple scattering matrix \mathbf{S} , assuming that the coupler is lossless and reciprocal:

$$\begin{aligned} \begin{pmatrix} E_{out1} \\ E_{out2} \end{pmatrix} &= \mathbf{S} \begin{pmatrix} E_{in1} \\ E_{in2} \end{pmatrix} = \begin{pmatrix} s_{11} & s_{12} \\ s_{21} & s_{22} \end{pmatrix} \begin{pmatrix} E_{in1} \\ E_{in2} \end{pmatrix} \\ &= e^{-j\beta L} \begin{pmatrix} \cos(CL) & j \sin(CL) \\ j \sin(CL) & \cos(CL) \end{pmatrix} \begin{pmatrix} E_{in1} \\ E_{in2} \end{pmatrix}, \end{aligned} \quad (20)$$

where E_{out} and E_{in} denotes the output and input electrical fields respectively. Scattering matrix elements are represented by s_{ij} and β is the propagation constant [Djordjevic, Ryan e Vasic 2010]. Keep in mind that this same technique may be extended to MxN couplers.

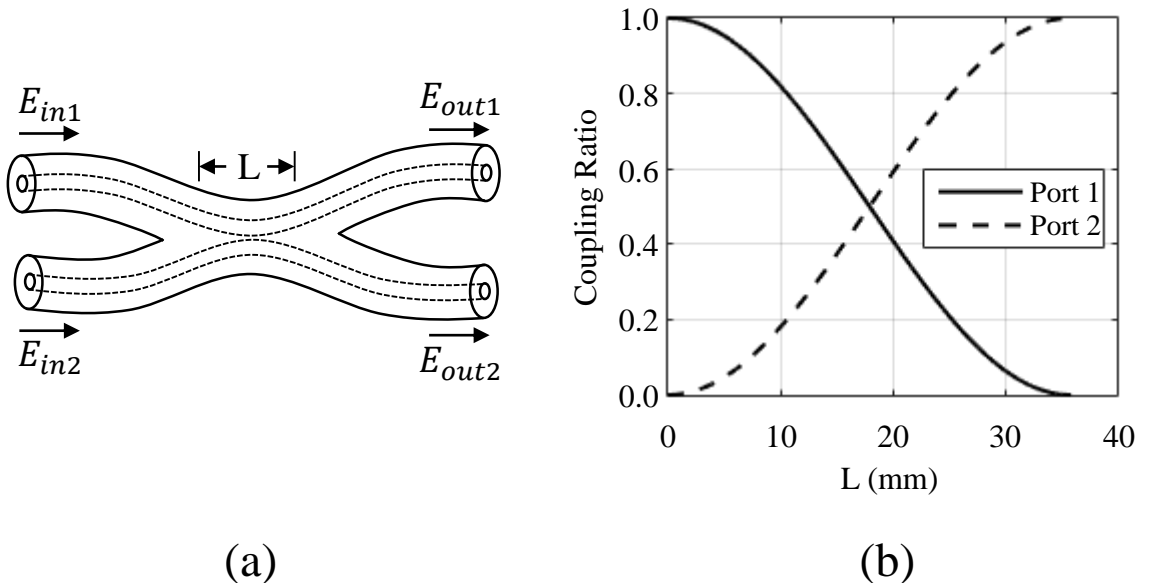


Figure 10 – Typical fiber coupler: a) fiber fusing based and b) coupling ratio example.

2.1.4.4 Optical Attenuator

Optical attenuators are devices used to weaken the optical power of the signal. They can be used in a fixed or variable configuration. Fixed optical attenuators have fixed losses and are usually used to protect equipment during high power measurements. Variable optical attenuators (VOA) are devices that allow changes in the signal attenuation. VOAs are desired either for tests, protection and/or power matching along optical links.

2.1.4.5 Optical Filter

Optical filters are devices that modify the spectrum of the signal directly. They are usually based on interferometry, having a wavelength-dependent transmission and reflection pattern. The most common types of filters are Fabry-Perot and Bragg gratings due to their relative simplicity. They can be mathematically described as:

$$E_{out}(t) = \frac{1}{2\pi} \int_{-\infty}^{\infty} E_{in}(\omega) H(\omega) e^{j\omega t} d\omega, \quad (21)$$

where $H(\omega)$ denotes the transfer function of the filter and $E_{in}(\omega)$ is the Fourier Transform (FT) of the input electrical field [Djordjevic, Ryan e Vasic 2010].

The FP filter consists, basically, of a cavity between two mirrors separated by a distance L . By controlling this distance, it is possible to adjust the frequency of the filter, creating a tunable optical filter. These filters can be made using fibers, crystals, semiconductor waveguides, etc. Their transfer function is defined as:

$$H_{FP}(\omega) = \frac{(1-r)e^{j\pi}}{1-re^{j\omega\tau}}, \quad \tau = 2L/\nu_g, \quad (22)$$

where r denotes the reflectivity of the mirrors, τ is the round-trip time within the cavity and ν_g is the group velocity. This transfer function is periodic with a period of $\Delta\nu = 1/\tau$, also known as the free spectral range (FSR). From this, it is possible to define an important parameter of FP filters, known as finesse [Djordjevic, Ryan e Vasic 2010]:

$$F = \Delta\nu/\Delta\nu_{FP} \cong \frac{\pi\sqrt{r}}{1-r}, \quad (23)$$

where $\Delta\nu_{FP}$ denotes the FP transmission peak width.

2.1.4.6 Isolators

Isolators are devices that allow light to travel in one direction, while attenuating light that travels in the opposite direction. They usually operate based on devices that rotate the polarization of light, also known as Faraday rotators. Isolators are usually used to protect sensitive optical components from optical reflections and back-propagating sources such as ASE.

2.2 Recirculating Fiber Loop

Optical telecommunications systems strive to achieve long distance communications, reaching thousands of kilometers. Such systems are expensive and require delicate study before implementation. For this purpose, in 1977 loop experiments started being performed to study pulse propagation in long distance transmissions. These experiments aimed to show the feasibility of long-haul systems using EDFA chains, without committing to the vast resources necessary to actually build such systems. It was only in 1991 that a BER lower than 10^{-9} was demonstrated for a 2.5 Gb/s NRZ signal over 9,000 km transmission distance, using a recirculating loop [Bergano et al. 1991] [Bergano e Davidson 1995] [Mazzali e Fragnito 1998].

For this technique to work, the signal is launched into the optical channel through an optical switch. After the signal is sent, the switch isolates the transmitter, leaving the signal to circulate in the loop. The signal can be monitored after every trip around the loop or a switch can control the output to obtain the signal after a desired number of trips. A basic loop setup is shown in Figure 11; however, modifications may be made to adapt the functionality of the system.

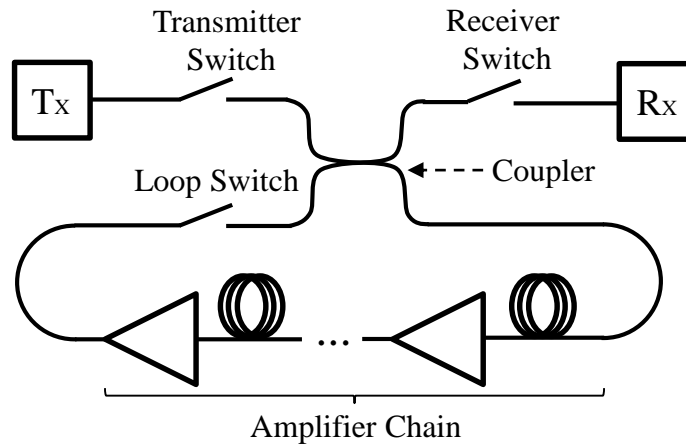


Figure 11 – Basic loop setup.

The timing of the transmitter switch needs to be carefully set so that the signal does not complete a trip around the loop and returns while the transmitter still feeds data to the optical channel. To prevent this, an important parameter known as the loop round trip time τ_{loop} needs to be defined as:

$$\tau_{loop} = \frac{n_1 L_{loop}}{c}, \quad (24)$$

where L_{loop} is the length of fiber in the loop, c is the speed of light in vacuum and n_1 is the core refractive index of the fiber. The transmitter switch must to be closed within a time limit defined by,

$$\tau_{data} < \tau_{loop}, \quad (25)$$

where τ_{data} denotes the total duration of the signal. The value of τ_{loop} may drift due to thermal and mechanical perturbations in the fiber, so this should be taken into account when defining switch timing [Bergano e Davidson 1995].

As can be seen by the timing diagram in Figure 12, the interval for loading data into the loop is known as the load state. As the transmitter completes the load state, the switch opens to isolate the loop from the transmitter. At this same moment, the loop switch closes and the signal is free to circulate through the amplifier chains. Every τ_{loop} the signal passes through the chain once. The receiver switch can then be timed to obtain the signal after a desired number of trips around the loop. Every trip corresponds to a distance of L_{loop} . As an example, in the timing diagram, the receiver switch is closed at the fourth trip, obtaining the signal after travelling a distance of $4 \times L_{loop}$.

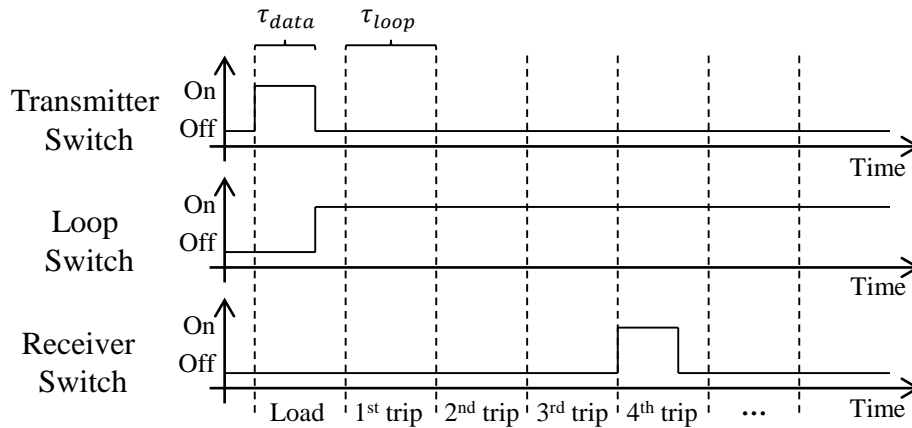


Figure 12 – Loop switch timing diagram, demonstrating how the switches should synchronize during operation.

Another important factor is the insertion loss introduced by additional hardware used to create the loop, such as the optical switches and couplers. These components would not be present in the real system and since this is a loop, their influences appear at every completed trip. For this reason, the transmitter switch should have a high extinction ratio and all loop specific equipment should have the lowest possible insertion loss.

By measuring the signal-to-noise ratio (SNR) after a single pass through the amplifier chain with and without the extra loss, an important characterization of the loop may be determined. The relative penalty factor is defined as the ratio of these SNRs, making it possible to understand how much the extra losses affect the looping technique. The value should be as close to one as possible [Bergano e Davidson 1995].

When transmitting signal over long distances, chromatic dispersion should be taken into account. This phenomenon broadens the optical spectrum, causing severe problems for receptions at long distances and high rates. Dispersion shifted fibers (DSF) may be added to the amplifier chain in the loop, compensating the dispersion caused by the standard fiber spans, reducing the effect significantly at each round trip.

2.3 OFDM

Orthogonal frequency division multiplexing (OFDM) is a type of modulation in which the information is carried over numerous lower rate subcarriers. The technique is inserted in the same context of multicarrier modulation (MCM) formats. It was first introduced in 1966 and remained underused until broadband applications became common in the early 1990s [Chang 1966]. From then on, it started to be incorporated in numerous telecommunications standards, such as wireless networks, power-line networks and long-term evolution. The use in these applications is mainly due to fundamental advantages of OFDM, for instance, the robustness against channel dispersion and the ease of phase and channel estimation in time-varying environments.

2.3.1 MCM Basics

To fully understand OFDM systems, it is essential to study in detail the concepts of MCM formats. Initially, a serial bitstream with a rate of R_b is converted into N parallel bitstreams with rate $R_n = R_b/N$. Each signal is then digitally mapped into complex symbols s_i and transformed from a discrete to a continuous signal by the transmission filter $g_{Tx}(t)$. The symbols are modulated by a subcarrier frequency of f_i and multiplexed into the channel, generating the signal $s(t)$, as depicted by Figure 13. The output signal can be defined as [Hanzo, Webb e Keller 2000] [Klenner 2004] [Silva 2011]:

$$s(t) = \sum_{i=0}^{N-1} s_i \cdot g_{Tx}(t) e^{j2\pi f_i t}. \quad (26)$$

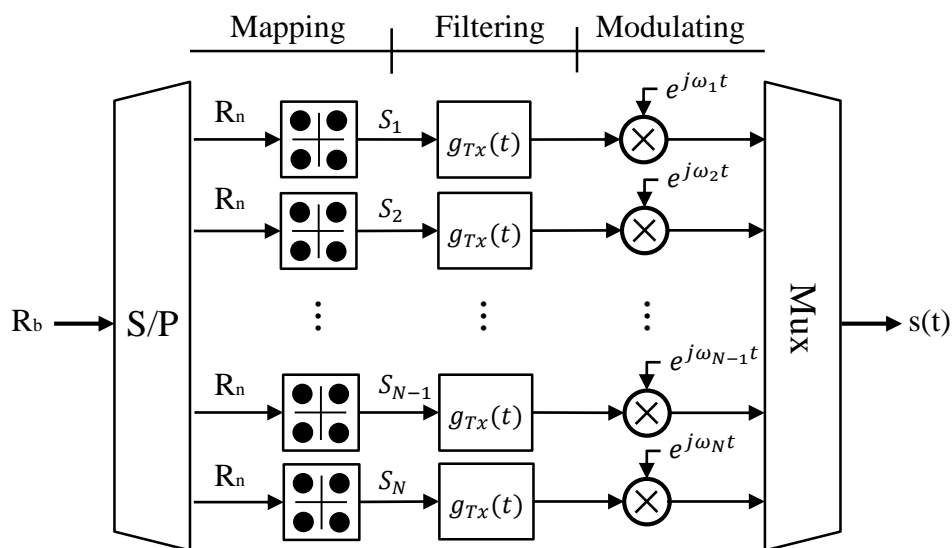


Figure 13 – Typical MCM Transmitter Diagram.

The reception is realized in a similar manner, demodulating the signals and digitizing them using a reception filter $g_{Rx}(t)$. The reception setup is shown in Figure 14. Each individual symbol duration in the parallel bitstream has a duration of T_s . When the signal is serialized, the total symbol duration becomes $T_N = NT_s$, since one symbol from each subcarrier is used. If the received signal has no noise or influence from the channel, it is possible to obtain the following [Klenner 2004] [Pinto e Albuquerque 2002] [Silva 2011],

$$\begin{aligned}
 \hat{s}_i &= \frac{1}{T_N} \int_0^{T_N} e^{-j2\pi f_i t} \times s_j(t) dt \\
 &= \frac{1}{T_N} \int_0^{T_N} e^{-j2\pi f_i t} \times \left(\sum_{j=0}^{N-1} s_j \cdot e^{j2\pi f_j t} \right) dt \\
 &= \frac{1}{T_N} \sum_{j=0}^{N-1} s_j \int_0^{T_N} e^{-j2\pi f_i t} \times e^{j2\pi f_j t} dt \\
 &= \frac{1}{T_N} \sum_{j=0}^{N-1} s_j \int_0^{T_N} e^{-j2\pi(f_i - f_j)t} dt \\
 &= \frac{1}{T_N} s_i \int_0^{T_N} 1 dt \\
 &= \frac{1}{T_N} s_i T_N \\
 &= s_i.
 \end{aligned} \tag{27}$$

Equation 27 proves that the received signal will be identical to the transmitted signal. However, the system requires many modulators and demodulators, making it extremely costly.

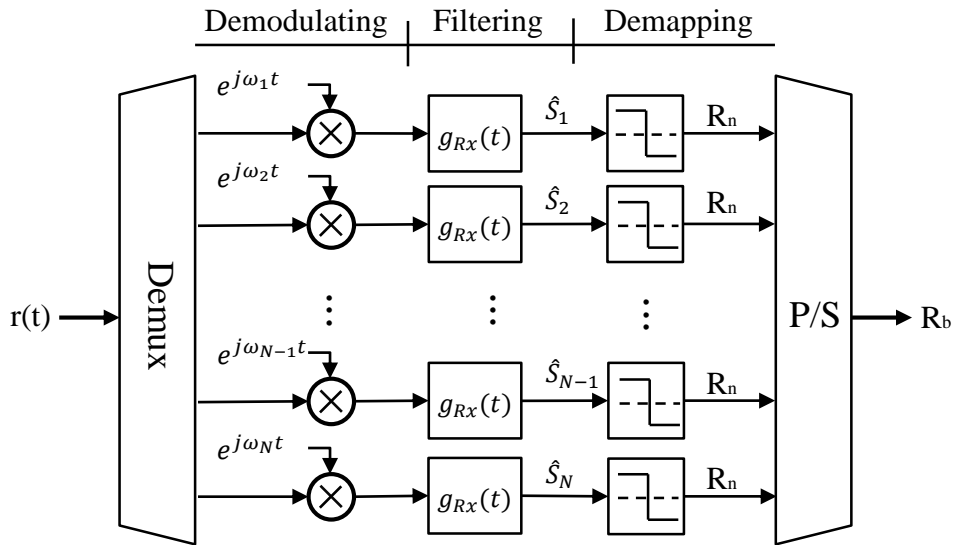


Figure 14 – Typical MCM Receiver Diagram.

2.3.2 OFDM Principles

The OFDM principle begins with a spectral separation of the subcarriers. To achieve this, cardinal functions, also known as sinc functions, are used to position each subcarrier at the desired frequency f_i . To avoid interchannel interference (ICI), guaranteeing orthogonality between subcarriers, each channel frequency is located at the spectral null point of adjacent subcarriers. For this to occur, the channel spacing is given by $\Delta f = 1/T_N$, thus positioning each channel at a frequency $f_i = i \cdot \Delta f$ [Silva 2011]. These functions are meant to replace the transmission and reception filters by a rectangular pulse that possesses the following equation in the time domain,

$$g_{Tx}(t) = g_{Rx}(t) = \text{rect}\left(\frac{t}{T_N}\right), \quad (28)$$

and in the frequency domain,

$$G_{Tx}(f) = G_{Rx}(f) = T_N \cdot \text{sinc}(\pi f T_N) \quad (29)$$

By joining equations 26 and 28, the OFDM transmitter can be defined as [Klenner 2004]

$$s(t) = \sum_{i=0}^{N-1} s_i \cdot \text{rect}\left(\frac{t}{T_N}\right) e^{j2\pi f_i t}. \quad (30)$$

Since the signal is sampled, the time variable can be rewritten as $t = n \frac{T_N}{N}$, for $0 \leq n \leq T_N$. By applying $f_i = i/T_N$ and $\text{rect}(t/T_N) = 1$, for an ideal case, equation 30 can be rewritten in a discrete form, as [Klenner 2004] [Shieh e Djordjevic 2010]:

$$s[n] = \sum_{i=0}^{N-1} s_i \cdot e^{j2\pi \frac{ni}{N}} = \mathfrak{F}^{-1}\{s_i\}, \quad (31)$$

where \mathfrak{F}^{-1} denotes the inverse discrete Fourier transform (IDFT). Equation 31 states that the OFDM transmitter can be implemented using an Inverse Fast Fourier Transform (IFFT), simplifying MCM systems. In a similar fashion it is possible to obtain the expression for the OFDM receptor [Klenner 2004] [Shieh e Djordjevic 2010]:

$$\hat{s}[i] = \frac{1}{N} \sum_{n=0}^{N-1} r[n] \cdot e^{j2\pi \frac{in}{N}} = \frac{1}{N} \mathfrak{F}\{r[n]\}, \quad (32)$$

with $0 \leq i \leq N - 1$ and \mathfrak{F} denoting the discrete Fourier transform (DFT). As opposed to the transmitter, the receiver is implemented using a Fast Fourier Transform (FFT).

2.3.3 Hermitian Symmetry

Some systems require real signals to be transmitted, such as visible light communications (VLC). The properties of the Fourier transform allow this with certain ease since the FT of a real signal $\mathfrak{F}\{s(t)\}$ has a Hermitian symmetry, in other words $S(f) = S^*(-f)$, where $*$ denotes the complex conjugate. This property can be used in the transmitter, inserting a signal with the following sequence [Ruiz, Cioffi e Kasturia 1992] [Proakis 1995],

$$s = [0, s_1, s_2, \dots, s_{N-1}, s_N, 0, s_N^*, s_{N-1}^*, \dots, s_1^*], \quad (33)$$

resulting in a real signal at the output of the IFFT. The main concern with this method is that at least $2N + 2$ inputs for the IFFT will be needed, but only N inputs are actually useful data, lowering the efficiency of the system. The real signal will transit through the optical channel and arrive at the receiver, where the property of the FT will return it to the Hermitian symmetry shown in Equation 33.

2.3.4 Cyclic Prefix

While passing through the optical channel, the signal will be affected by channel impairments, such as attenuation, dispersion and delay. If the signal is delayed and modified by a channel dispersion τ_{max} , the reception window that receives each symbol, may miss parts of the symbol. These missing parts affect the spectrum, afflicting the condition of orthogonality between subcarriers, resulting in inter-carrier interference (ICI). Furthermore, the delayed data may occupy part of the reception window of another symbol, leading to intersymbol-interference (ISI) [Shieh e Djordjevic 2010]. Figure 15 demonstrates how both these interferences occur.

To solve these problems, the cyclic prefix was proposed. This technique extends the symbol duration, by combining an identical copy of the end of the symbol to the beginning of the original symbol. The size of this copy is known as the guard interval T_g . As the channel delays the symbol, a part leaves the reception window and that same part reenters as the cyclic prefix, guaranteeing that the symbol is received wholly to avoid ICI. Separating the reception windows by a value of at least T_g averts ISI, as can be observed in Figure 15. The condition to avoid ICI and ISI is given by [Silva 2011],

$$\tau_{max} < T_g. \quad (34)$$

After implementing the Hermitian Symmetry and Cyclic Prefix, the basic OFDM setup is given by Figure 16. It is important to note how the IFFT and FFT eliminate the numerous modulators and demodulators shown in the MCM setups.

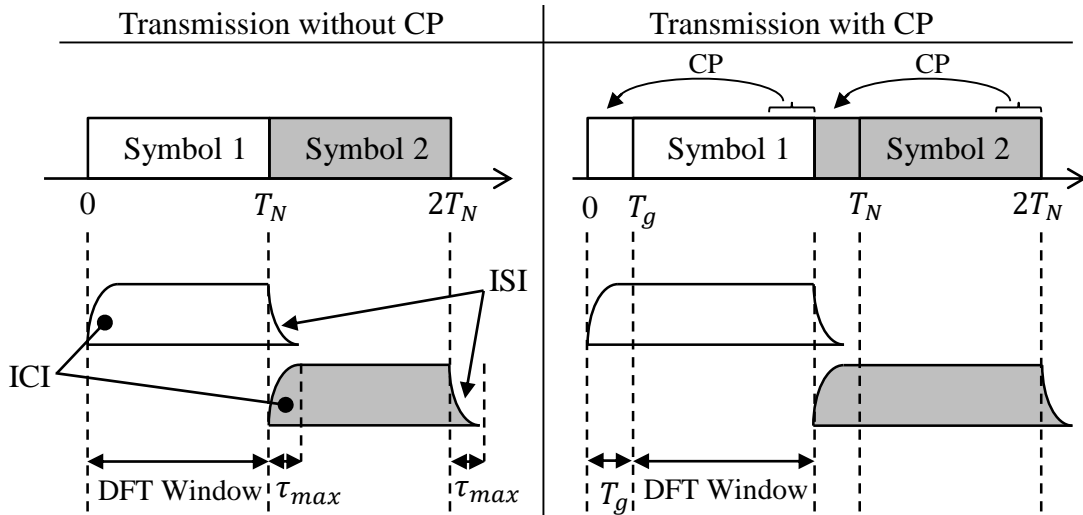


Figure 15 – Symbol transmission time diagram, with and without the CP. Modified: [Klenner 2004]

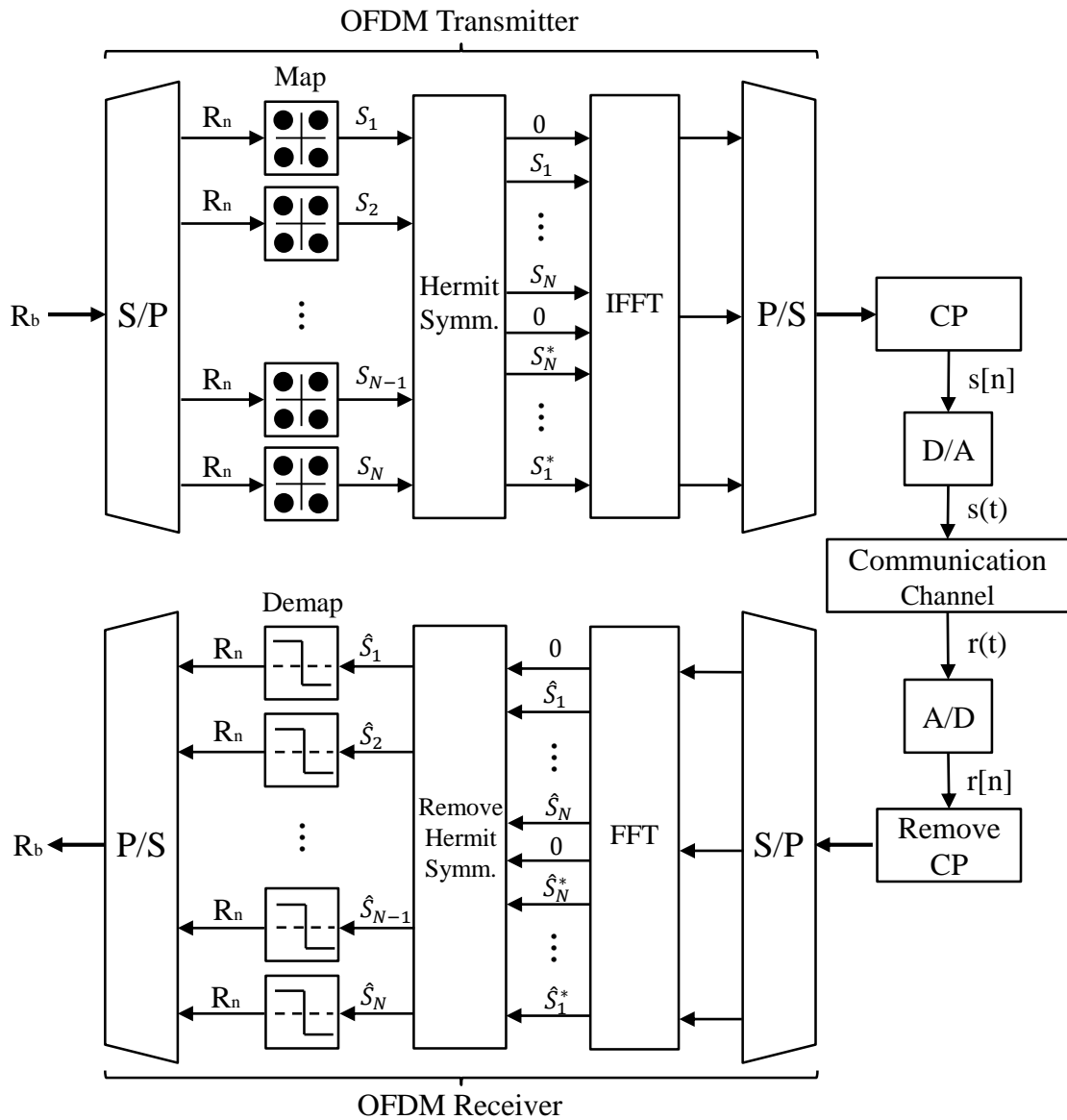


Figure 16 – Basic OFDM Setup.

2.3.5 Peak-to-Average Power Ratio of OFDM Signals

Despite the positive features of OFDM, high peak-to-average power ratio (PAPR) is cited as one of the main drawbacks in these systems. In the RF domain, power amplifiers saturate these high peaks, distorting the signal. As for optical OFDM, the amplifiers won't present a problem for fast transitioning peaks, but optical fiber nonlinearity may present a problem in this aspect.

The nature of this high PAPR can be easily understood by analyzing the multicarrier aspects of OFDM. The combination of the symbols in the time domain generates high values in some instants followed by lower values. This creates great differences between the peak and average values, that can be quantified as [Shieh e Djordjevic 2010],

$$PAPR = \frac{\max\{|s[n]|^2\}}{E\{|s[n]|^2\}}, \quad (35)$$

where E stands for the expected value. As can be observed, the definition of PAPR uses the expected value, making it a statistical parameter.

PAPR reduction is possible to achieve by simply clipping the OFDM signal, consequently increasing the BER of the system. Another possibility is achieved without distorting the signal. This is done by exchanging the original waveform to a set of waveforms that have a lower PAPR, increasing the computational complexity of the system. Both methods work towards PAPR reduction while presenting trade-offs for bandwidth efficiency and computational complexity. Another proposed technique attempts to apply a constant amplitude to the time-domain signal. This method is known as Constant Envelope OFDM (CE-OFDM) [Silva 2011].

2.4 CE-OFDM Principles

Constant Envelope OFDM was proposed by Steve Thompson in 2008 to reduce PAPR in wireless OFDM systems [Thompson et al. 2008]. The technique consists of modulating the phase of the OFDM signal, thus creating a signal with very moderate amplitude variations. PAPR is adequately reduced at the cost of computational efficiency and spectral broadening.

A great way of understanding this concept is by comparing amplitude and phase modulation techniques. A simple sinusoidal signal is shown in Figure 17a and this same signal modulated in amplitude and phase are shown in Figures 17b and 17c respectively. As can be observed, the outline of the amplitude modulation, takes the approximate shape of the original signal, causing it to have significant amplitude variations. When an amplitude modulation is applied to the conventional OFDM signal, the modulated signal will possess drastic amplitude variations, maintaining a high PAPR. However, if a phase modulation is

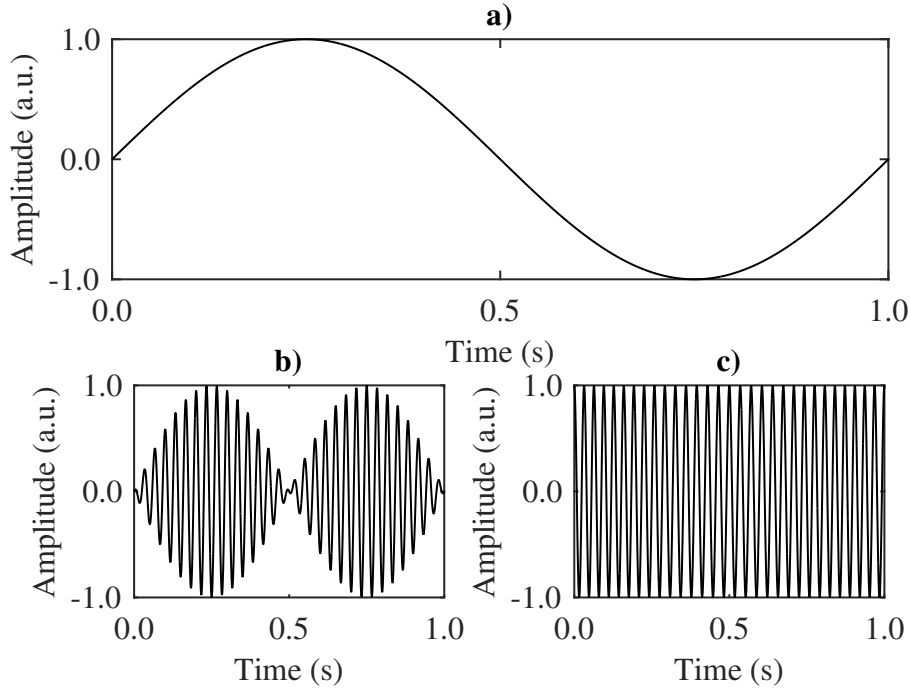


Figure 17 – Signal modulation example a) Sinusoidal signal, b) Amplitude modulated (AM) signal and c) Phase modulated (PM) signal.

applied to the signal, the amplitude of the signal tends to stay constant while the phase changes, creating a signal with a semi-constant amplitude, as shown in Figure 17c.

To understand the transformation from OFDM to CE-OFDM, the output from the conventional OFDM can be written as,

$$x(t) = |x(t)|\angle arg[x(t)] = A_x e^{j\phi_x(t)}, \quad (36)$$

where $x(t)$ denotes the conventional OFDM signal and $\phi_x(t)$ is the phase of that same signal. This signal is then transformed into $s(t) = A e^{j\alpha x(t)}$ and the resulting signal $y(t)$, modulated in phase, is given by,

$$\begin{aligned} y(t) &= \Re\{s(t)e^{j2\pi f_c t}\} \\ y(t) &= \Re\{A e^{j\alpha A_x(t) \exp[j\phi_x(t)]} e^{j2\pi f_c t}\} \\ y(t) &= A \cos 2\pi f_c t + \alpha x(t) \end{aligned} \quad (37)$$

where \Re denotes the real part of the signal, A is the amplitude of the signal, f_c is the central frequency, α is the constant for the phase shift. The signal from equation 37 will have significantly lower amplitude variations when compared to the original OFDM, thus being called a constant envelope signal [Thompson et al. 2004] [Thompson et al. 2008].

By using a phase modulation, concerns about spectral efficiency might arise. To study this aspect of the signal, it is useful to define the phase shift constant as $\alpha = 2\pi h C_N$, where h is the phase modulation index and C_N is a variance normalization constant. Now, equation 37 can be rewritten as,

$$y(t) = A \cos 2\pi f_c t + 2\pi h C_N x(t). \quad (38)$$

The modulation index is responsible for spectral scattering in CE-OFDM, making it an essential parameter when considering spectral efficiency. As higher values of h are used, a broader spectrum output is obtained, possibly interfering with adjacent channels [Silva 2011]. It is recommended to define h as to guarantee at least the same spectral efficiency as the conventional OFDM system. Spectral efficiency of CE-OFDM can be defined as,

$$\eta = \frac{R_b}{B_{RMS}}, \quad (39)$$

where R_b denotes the transmission rate and B_{RMS} the root-mean-square (RMS) value of the CE-OFDM bandwidth. The transmission rate is give by $R_b = B_W \log_2(M)$, where B_W is the signal badwidth and M is the number of points in the constellation diagram. B_{RMS} is the best form to establish CE-OFDM bandwidth since it considers the spectral broadening of the phase modulation index. This is obtained as $B_{RMS} = \max(2\pi h, 1) B_W$, guaranteeing that the signal will have at least the same bandwidth of the original OFDM signal that generated it [Silva 2011].

Since CE-OFDM is obtained by modulating the phase of a conventional OFDM signal, the same setup from Figure 16 can be used, with the addition of the phase modulator and demodulator, as depicted by Figure 18.

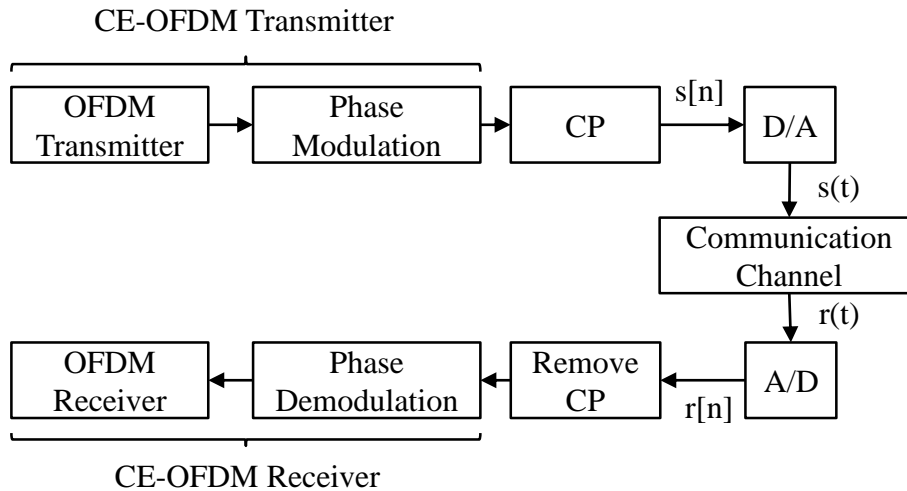


Figure 18 – Basic CE-OFDM Setup.

2.5 Evaluation Parameters

A comparison between the transmitted and received data is necessary in order to adequately evaluate the system. This comparison will be realized in two different manners during this text: bit error rate (BER) and error vector magnitude (EVM). Both may be used simultaneously; however, in some cases one might be preferable instead of the other requiring a careful analysis of the measurement parameters to correctly evaluate the system.

2.5.1 BER

One of the most important evaluation parameters is the bit error rate (BER), a technique that consists of comparing the input and output bits of the system in order to count the number of errors. The BER measurement is usually understood as:

$$BER = \frac{N_{err}}{N_{bits}}, \quad (40)$$

where N_{err} is the number of incorrect bit measurements and N_{bits} is the number of compared bits. During this measurement there are two possible outcomes: an erroneous or a correct bit, meaning that this is a binominal process. Assuming that the errors are independent of each other and that conditions do not change over time, the BER can be modeled using a binomial distribution. However, an accurate and considerably easier manner of evaluating the BER is through usage of the Poisson distribution with only one governing parameter μ , given by:

$$\mu = BER \cdot N_{bits}, \quad (41)$$

The probability density function for the BER measurement experiments can then be written as:

$$P(N_{err}, \mu) = e^{-\mu} \cdot \frac{1}{N_{err}!} \cdot \mu^{N_{err}}, \quad (42)$$

This equation demonstrates the probability of bit error occurrences for different values of μ . It is important to note that better results are obtained for higher values of μ , demonstrating the importance of choosing a correct number of bits to be compared during experiments [Muller, Stephens e McHugh 2005].

To simplify the analysis, the problem is then modified as the tester must know the number of bits to be compared in order to achieve a BER below a desired value. Equation 42 can then be used to establish a confidence level for the measurements as follows:

$$CL = 1 - e^{-\mu} \cdot \frac{1}{N_{err}!} \cdot \mu^{N_{err}}. \quad (43)$$

The tester can then numerically solve Equation 43 to verify if the number of bits compared is statistically sufficient for the desired BER.

2.5.2 EVM

Another form of evaluating system performance is through the analysis of constellation diagrams. The EVM is calculated by measuring the distance from the position of each received complex symbol to its ideal position in the diagram. The equation for calculating EVM is given by [Schmogrow et al. 2012] [Pereira et al. 2015],

$$EVM(dB) = 20 \cdot \log_{10} \sqrt{\frac{\frac{1}{N_s} \sum_{k=0}^{N_s-1} |Y_k - X_k|^2}{\frac{1}{N_s} \sum_{k=0}^{N_s-1} |X_k|^2}}, \quad (44)$$

where N_s is the number of analyzed symbols, $X_k = X_{Ik} + X_{Qk}$ and $Y_k = Y_{Ik} + Y_{Qk}$ are the received and transmitted symbols respectively with in-phase and quadrature components. This technique translates the spreading of the constellation diagram into a numerical parameter for system evaluation.

3 Design and Characterization

For an optical communications system to function as desired, all components must be studied thoroughly. The previous chapter laid out the foundations required to understand the key components of the system. This chapter displays the chosen elements of the system and characterizes them experimentally. The characterization is just as important as the theoretical background since these devices might present different characteristics than the ones displayed in the technical specification, leading to unexpected functionality of the devices. Since measurements will be realized during this chapter, it is important for the tester to be aware of laboratory safety measures shown in Appendix A before attempting to replicate these results. Every measurement procedure used in this chapter is also presented in Appendix B in order to guide future testers. These appendixes aim to be an educational document for future testers of the laboratory.

The chapter begins by displaying the characterization of the key optical components present in the transmitter, optical channel and receiver. Then, the elements inserted for the recirculating fiber loop are tested. Finally, the parameters of the OFDM and CE-OFDM systems are discussed individually.

3.1 Main Optical Components

3.1.1 Transmitter

A simplified setup was adopted for the transmitter, containing a light source for signal generation, a polarization controller (PC) to adjust polarization along the fiber, an MZM for electro-optical conversion and a booster EDFA for loss compensation and power amplification. The whole transmitter setup can be observed in Figure 19. As can be observed, a blue line is used for the electric signals and a black line for the optic signals, defining a convention for the following figures in this chapter. All components must be studied separately in order to understand eventual limitations of the system.

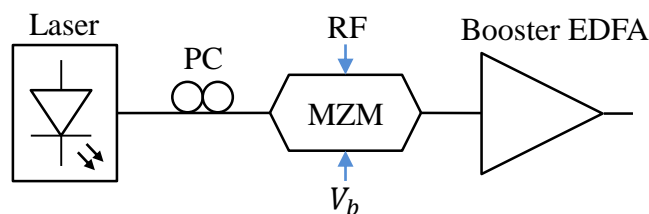


Figure 19 – Basic Transmitter Setup.

3.1.1.1 Light Source

For an ideal optical transmission, the light source should be as stable as possible to avoid frequency drifts that can lead to ICI. The spectral width should also be thin to improve spectral efficiency. High power is desirable to overcome system losses, but not necessary since optical amplifiers help in this sense.

To obtain these characteristics, a THORLABS TXP 5000 Series modular system was used. Various laser modules in the C-Band (1530–1565 nm) and L-Band (1565–1625 nm) are available. The chosen light source is a DFB laser diode with an isolator, at a wavelength of 1550.12 nm and spectral width below 10 MHz (Thorlabs LS5-C-25A-20-NM Module). Table 1 shows the specified and measured technical data, while Figure 20 presents the spectrum of the laser, measured with an APEX Optical Complex Spectrum Analyzer (OCSA) AP2683A. The output power was fixed to +5 dBm, to guarantee the desired power at the output of the modulator at the point of operation. The center wavelength and spectral width of the laser are not in agreement with the specified data. For the experiments in this work, the characteristics are still acceptable, but this could prove to be a problem in more complex WDM systems.

Table 1 – LS5-C-25A-20-NM DFB Laser Module Technical Data.

Type	Specified	Measured
Center wavelength (nm)	1550.12	1550.15
Spectral linewidth (MHz)	< 10	29.3
SMSR ¹ (dB)	> 40	53.3
Optical Power (dBm)	0-13	0-13

¹SMSR: Side Mode Suppression Ratio

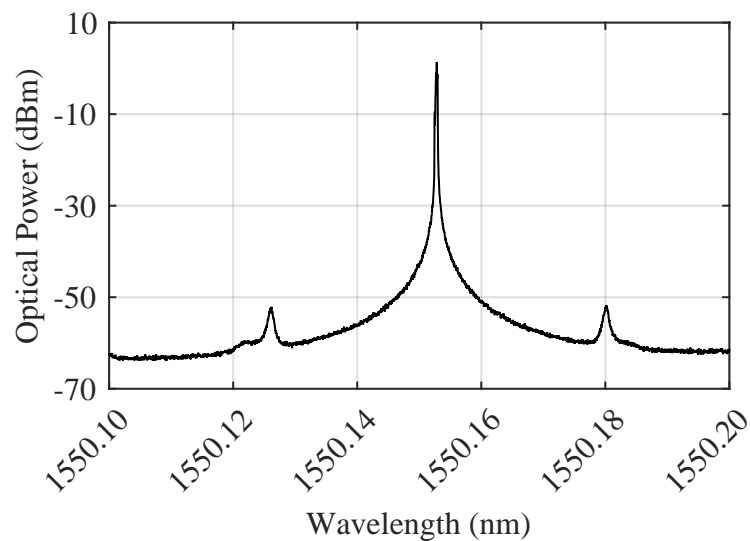


Figure 20 – LS5-C-25A-20-NM DFB Laser Measured Optical Spectrum ($P_{out} = +5$ dBm).

3.1.1.2 Optical Modulator

To avoid transmitter instability issues, external modulation was chosen for the optical communication system. The modulator should have a higher bandwidth than the optical signal and support the data rates of the transmission. For this application, the modulator Covega Mach-10 081-10-S-S-S-NS-STL (or, to simplify, Mach-10 081) was chosen. This model is based on Titanium-indiffused x-cut Lithium Niobate and uses a Mach-Zehnder interferometric architecture. With a bandwidth of 10 GHz, this modulator supports data rates from 10 to 12.5 Gb/s.

It is important to characterize the transfer function of the MZM to fully understand how the optical signal will react to the electric signals. A relatively simple setup, using only a power meter (PM) as a measuring instrument can be setup to realize this characterization, as shown in Figure 21. Before initializing the measurement it is important to set the PC as to obtain the maximum possible output power after the MZM, guaranteeing the lowest possible loss from the device. The data was obtained by sweeping the bias voltage V_b from -5 to 5V in steps of 0.2V and measuring the output power at each step, while no RF data is inserted into the MZM ($V(t) = 0$). The difference between V_b at the peak and valley of the curve was obtained from the characterization, defining a V_π of 6.6V. Figure 22 compares the measured transfer function to the analytical model from equation 6. The measured linear region is slightly deformed, demonstrating that a careful analysis of the operation point of this device should be realized.

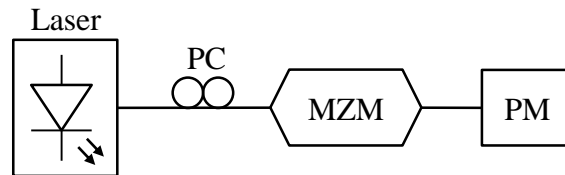


Figure 21 – Optical Modulator Characterization Setup.

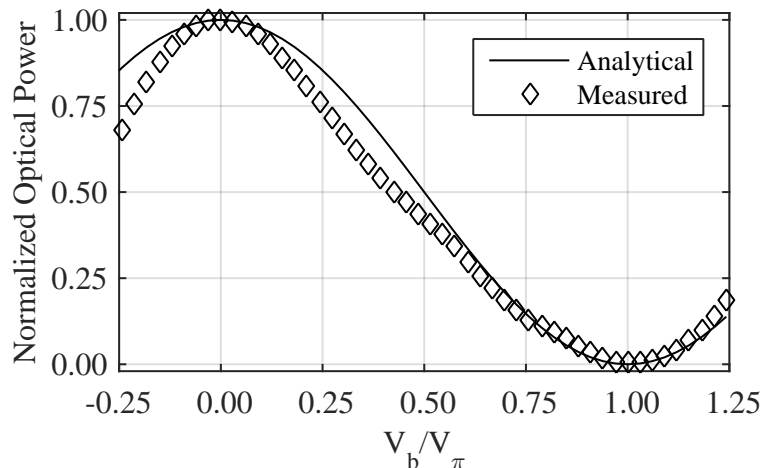


Figure 22 – Mach-10 081 Characterization: Analytical and Measured Transfer Function.

3.1.1.3 Optical Amplifier (Booster)

To compensate for losses of the transmitting equipment, an optical amplifier contributes to the system. An EDFA with Booster configuration was chosen for this task due to high gain supplied at moderate input powers. As the signal needs to have a stable output from the transmitter, the optical amplifier must have an automatic control feature for the output power. For this reason, the best option was the AP3370A Booster Amplifier module, from the APEX Optical MultiTest Platform (AP1000-8).

The characterization of these devices is realized by applying an input signal and attenuating it with a VOA, while monitoring the power before and after the amplifier, as can be seen in Figures 23a and 23b respectively. It is useful to monitor the signals with an Optical Spectrum Analyzer (OSA) so that the spectral difference before and after the amplifier can be observed to calculate gain and ASE power.

For the AP3370A Booster EDFA, the input signal was swept from -30 to 0 dBm in steps of 1 dBm, by using an Apex AP3364A Variable Optical Attenuator with the Thorlabs laser. The signals were measured using an Anritsu MS9740A OSA, obtaining the curves shown in Figure 24. The specified and measured technical data can be observed in Table 2, showing that the amplifier is in compliance with the specified data. It is possible to observe by Figure 24a that the output power saturates at around +10.5 dBm for input signals between -5 and 0 dBm. This point of operation was chosen for the amplifier since small fluctuations in the input power would not affect the output significantly. The high output power is also meaningful for overcoming insertion losses of the optical devices.

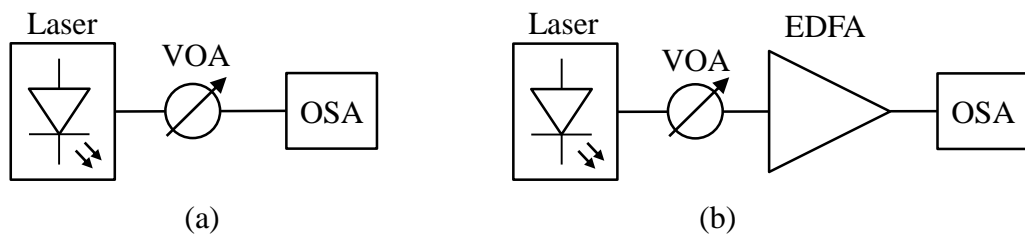


Figure 23 – EDFA Characterization Setup: (a) input signal measurement and (b) output signal measurement.

Table 2 – AP3370A Booster EDFA Module Technical Data.

Type	Specified	Measured
Output Power ¹ (dBm)	+13.0	+10.6
Noise Figure ² (dB)	4.5-5.0	5.4

¹ $P_{in} = 0$ dBm

² $P_{in} = -6$ dBm

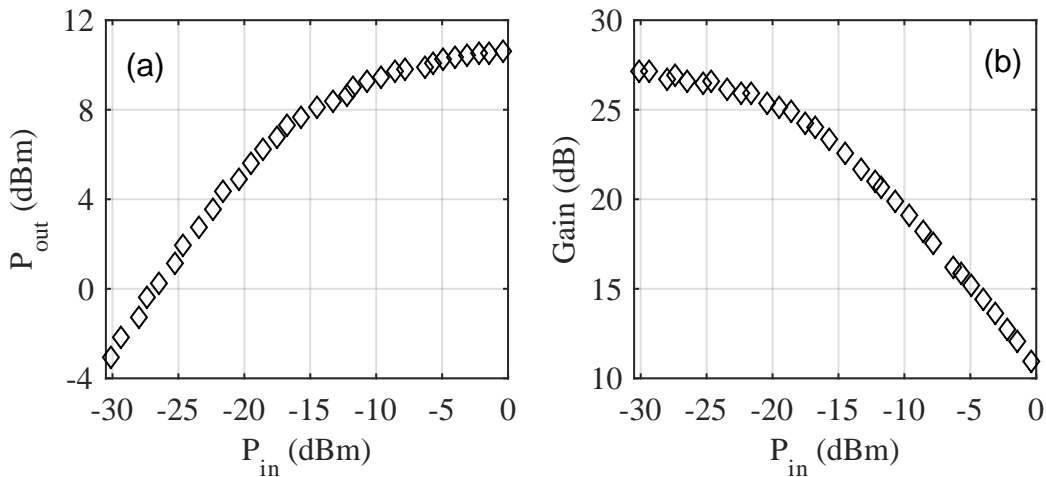


Figure 24 – AP3370A Booster EDFA Module Characterization: (a) Output Power and (b) Amplifier Gain.

3.1.2 Optical Channel

3.1.2.1 Optical Fiber

A standard was established, in 1984, with recommendations for geometrical, mechanical and transmission attributes of standard single-mode fibers (SSMF). This standard is known as Recommendation ITU-T G.652, updated regularly by the International Telecommunication Union (ITU) with the latest revision being released in 2016 [ITU-T 2016].

For the optical channel, Corning[®] SMF-28e+[®] fibers were used. These fibers are ITU-T G.652-compliant, guaranteeing at least the standard characteristics for the optical communication system, as can be observed by Table 3. The attenuation of the fiber is obtained by applying a known signal to the input and measuring it at the output. The penalty in power, divided by the length of the fiber span, is known as the attenuation at the wavelength of the measured signal, given in dB/km.

Table 3 – Corning[®] SMF-28e+[®] Technical Data.

Type	Specified	Measured
Attenuation (dB/km)	≤ 0.20	0.18
Dispersion (ps/[nm · km])	≤ 18.0	-
PMD (ps/ $\sqrt{\text{km}}$)	≤ 0.06	-
Numerical Aperture	0.14	-
Cladding Diameter (μm)	125.0	-
Core Diameter (μm)	8.2	-

3.1.2.2 Optical Amplifier (In-Line)

An In-Line amplifier is needed to overcome the fiber losses introduced in the optical channel. Since one of these amplifiers was not available, the closest match was an AP3370C Pre-Amplifier EDFA module, from the APEX Optical MultiTest Platform (AP1000-8). This EDFA has a high gain to overcome the loss of the fiber spans. It is also important to note that this amplifier will be inserted in the recirculating loop, so the automatic control feature for the output power will contribute for loop stability, maintaining the power level at the desired state.

The characterization was realized accordingly to the typical characterization setup shown in Figure 23. The specified and measured technical data can be observed in Table 4, demonstrating compliance with the specified data. Figures 25a and 25b, demonstrate the output power and amplifier gain characterization of the AP3370C Pre-Amplifier respectively. As can be observed, there is a saturation of the output power for values of input in the range of -20 to -10 dBm. Even though this region does not offer the highest gain, it was chosen as the point of operation since small fluctuations in the input power do not affect the output significantly. It is also a considerable region for compensating 50 to 100 km fiber spans (10 – 20 dB losses).

Table 4 – AP3370C Pre-Amplifier EDFA Module Technical Data.

Type	Specified	Measured
Signal Gain ¹ (dB)	20-40	35.6
Noise Figure ² (dB)	5.0-5.5	4.9

¹ $P_{in} = -30$ dBm

² $P_{in} = -6$ dBm

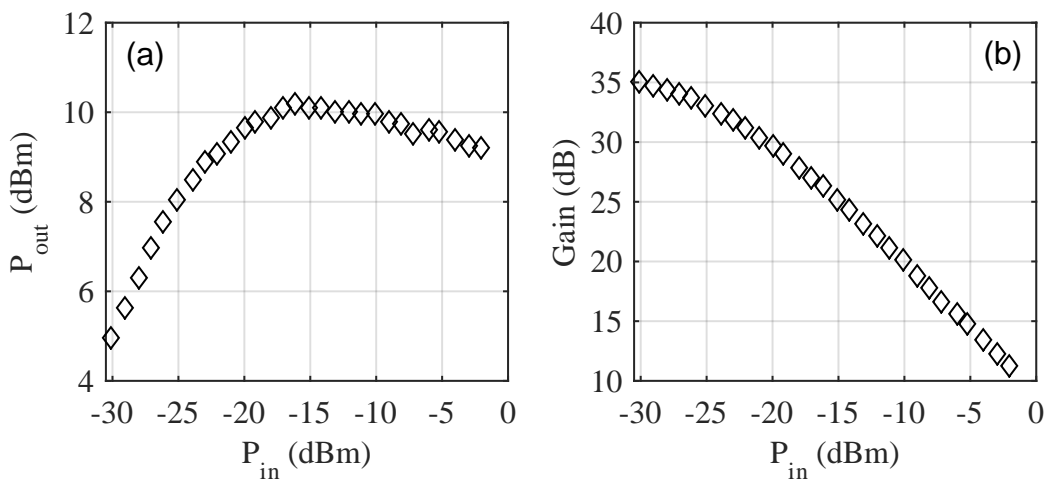


Figure 25 – AP3370C Pre-Amplifier EDFA Module Characterization: (a) Output Power and (b) Amplifier Gain.

3.1.3 Receiver

An amplified receiver is employed to improve the sensitivity of reception. This is realized by using a Pre-Amplifier EDFA, followed by an optical filter to limit ASE power and a photodetector for signal reception. The basic setup of this configuration is depicted in Figure 26.

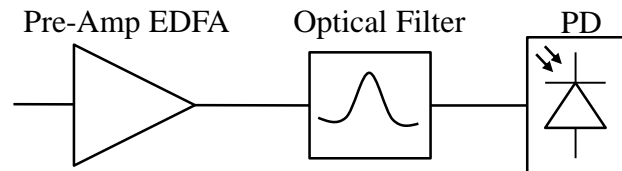


Figure 26 – Basic Receiver Setup.

3.1.3.1 Photodetector

The receiver stage should match or overcome the characteristics of the transceiver, such as signal wavelength, signal bandwidth and transmission rate. The chosen photodetector was a Thorlabs PDA8GS, which is an InGaAs Pin type fiber coupled detector. This device has a bandwidth of 9.5 GHz, while supporting 12.5 Gb/s transmission rates. A smaller bandwidth than the transmitter is not the ideal case, but as long as signals do not reach this value, the transmission will not be affected by this characteristic. When analyzing the electronic signals, the DC is unimportant since it does not carry information. The output of the detector is DC coupled, so a 11742A Blocking Capacitor was attached to the output in order to remove the DC from the signal. The main technical data of the detector is summarized in Table 5.

It is important to characterize the modulator and photodetector, regarding bandwidth, to truly obtain the limiting bandwidth of the transmission system. For this, a Vector Network Analyzer (VNA) may be used to input a signal on the modulator and then sweep the frequency of the signal while the photodetector receives the output signal from the modulator, as depicted by Figure 27.

For the measurement, an Anritsu VNA Master MS2038C/11 was used. The typical S-parameter for this characterization is the S₂₁, which expresses the transmission transfer function of the devices under test. As can be observed in Figure 28, the transfer function starts to decline at approximately 7.0 GHz, with the 3 dB compression point occurring at 9.2 GHz. Through this information, the actual maximum bandwidth of the system is defined as 9.2 GHz.

Table 5 – PDA8GS Technical Data.

Type	Specified
Max Input Power (dBm)	0.0
Sensitivity (dBm)	-20.0
Bandwidth (GHz)	DC - 9.5

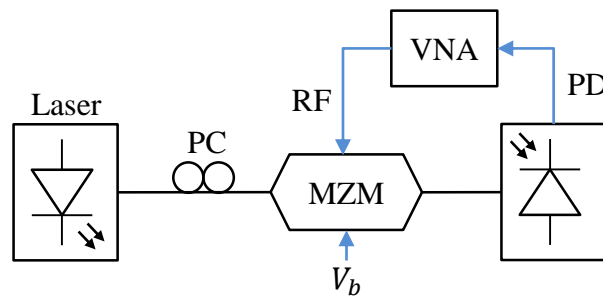


Figure 27 – Mach-10 081 and PDA8GS Frequency Response Characterization Setup.

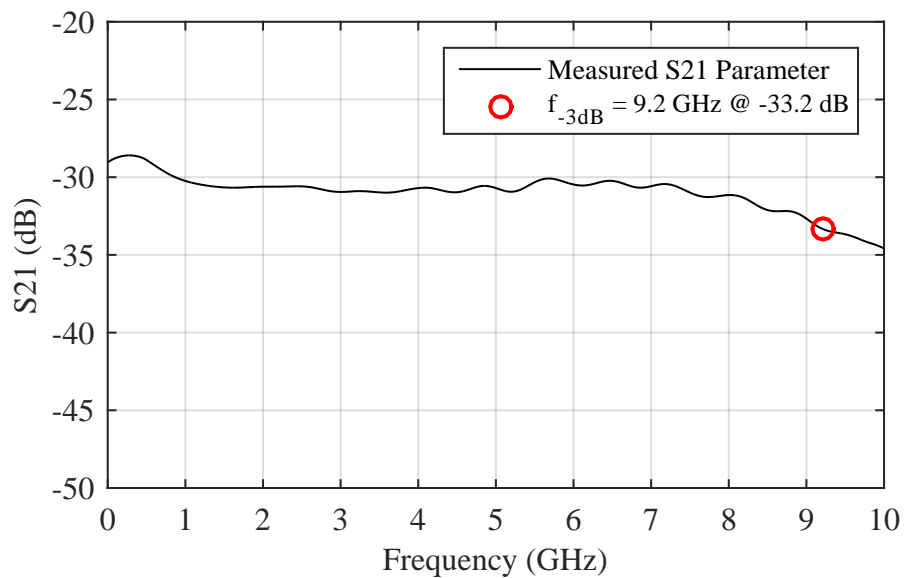


Figure 28 – Mach-10 081 and PDA8GS Frequency Response Characterization.

3.1.3.2 Optical Amplifier (Pre-Amplifier)

After passing through the optical channel, the signal usually arrives at the receiver at low power values. For this reason it is useful to amplify the signal before it reaches the detector. The power should respect two characteristics of the photodetector: the sensitivity and the maximum input power, so as to not damage the device. The amplifier chosen for this task was a Lightwave 2020 Compact Low Cost Pre-Amplifier EDFA (NOAPF251R000112, or simply NOAPF25).

The same setup from Figure 23 was used to characterize the amplifier. The data obtained from the measurements are presented in Figure 29 and the specified and measured parameters are disposed in Table 6. As can be observed, the gain of the amplifier saturates near 17 dB, a value significantly below the specified gain (25 dB). It is still possible to use the device since the signal is amplified by an In-Line Amplifier before leaving the optical channel, guaranteeing that the power level will not be significantly low. However, it is important to note how the characterization phase is essential to the design of the system. The point of operation for this device is chosen after the optical filter characterization, since the output power after the filter should not exceed the maximum input power of the photodetector (0 dBm - Table 5).

Table 6 – NOAPF25 Pre-Amplifier EDFA Technical Data.

Type	Specified	Measured
Signal Gain ¹ (dB)	25.0	16.9
Noise Figure ¹ (dB)	5.0-6.0	7.1

¹ $P_{in} = -30$ dBm

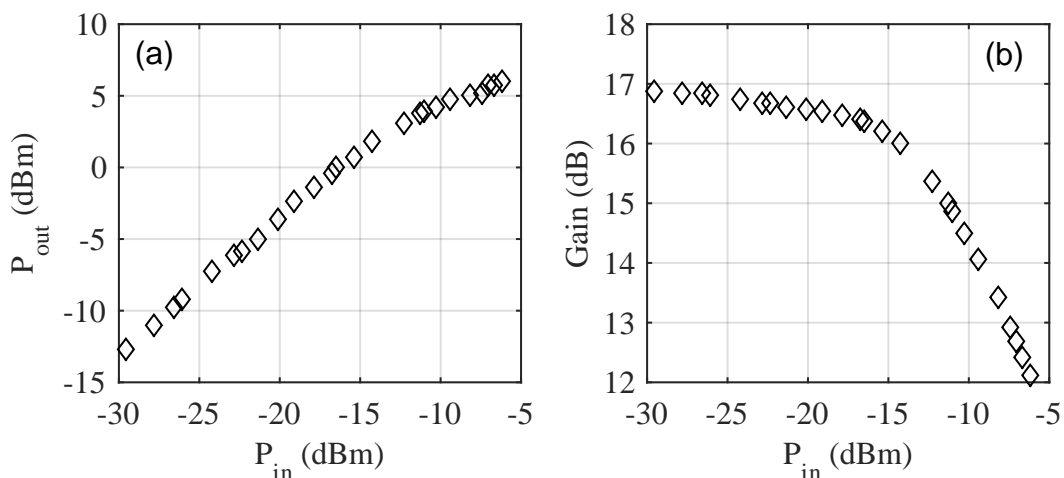


Figure 29 – NOAPF25 Pre-Amplifier EDFA Characterization: a) Output Power and b) Amplifier Gain.

3.1.3.3 Optical Filter

During the amplification process, the EDFA generates ASE that will enter the detector with the signal. An optical filter can be used to limit the ASE, guaranteeing that most of the power entering the detector is concentrated near the signal wavelength. For this, an AP3380A Optical Tunable Filter module, from the APEX Optical MultiTest Platform (AP1000-8), was used. The filter allows tuning in the C-Band, with low insertion loss and a narrow bandwidth, as shown in Table 7.

To characterize an optical filter it is necessary to use a broadband light source as the input signal. First, the broadband spectrum is measured (Figure 30a), followed by the filter being applied to the source and the output measured (Figure 30b) and compared with the source spectrum. The insertion loss is measured as the difference between the source and filtered signal at the peak wavelength of the filter. On the other hand, the finesse is obtained by subtracting the wavelengths where the 3 dB compression points occur. For the AP3380A characterization, an Anritsu MS9740A OSA was used since it can measure the spectrum and generate a broadband source at the same time. The outcome of the characterization is presented in Figure 31.

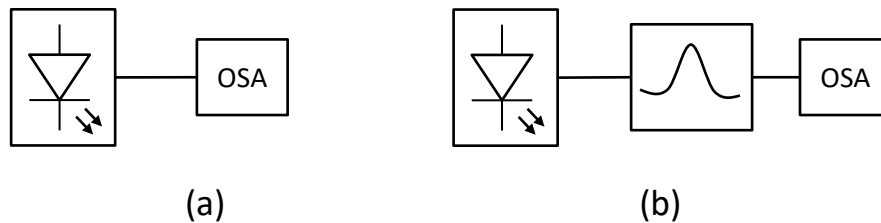


Figure 30 – AP3380A Optical Tunable Filter module Characterization Setup: a) Broadband source measurement and b) Filtered source measurement.

Table 7 – AP3380A Optical Tunable Filter module Technical Data.

Type	Specified	Measured
Tuning Range (nm)	1529-1564	1529-1564
IL @ Peak (dB)	<4.0	3.7
Finesse @ 3 dB (nm)	<0.15	0.23

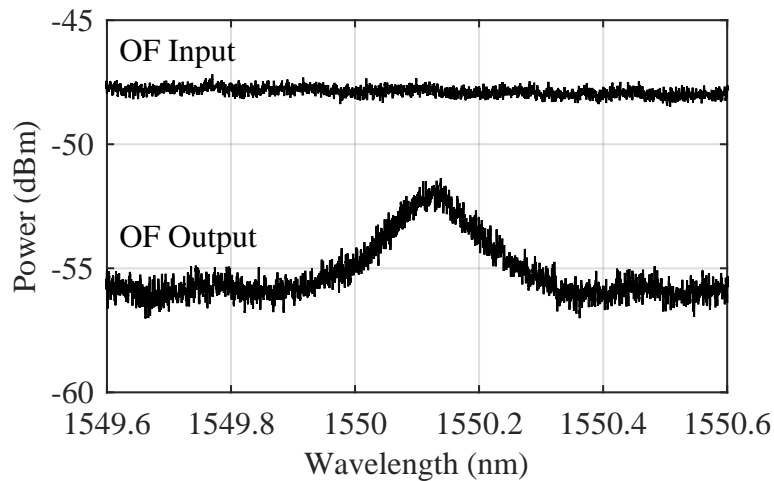


Figure 31 – AP3380A Optical Tunable Filter module Characterization.

3.2 Recirculating Fiber Loop

As discussed before, the loop technique requires additional equipment to be implemented. If the optical switch is slow (switching speed near τ_{loop} or greater) the technique will not work since the switch does not transit between the states fast enough. Only one adequate switch was available for this work, resulting in only one switch being used, transiting from the transmitter to the loop as can be observed in Figure 32. The 3 dB, or 50/50, coupler is responsible for feeding data to the loop and to the receiver. The receiver switch is not needed since the receiving equipment can trigger the signal at any desired time by using an external trigger signal. Before the amplifier chain, a coupler and a VOA are added to monitor and vary the fiber input power respectively. Monitoring the fiber input power will be important for analyzing OFDM and CE-OFDM with regard to fiber nonlinearity. This also requires that a high input power be available at the point of analysis. To solve this problem a compensator EDFA is introduced to compensate loop hardware losses, providing enough power at the fiber input.

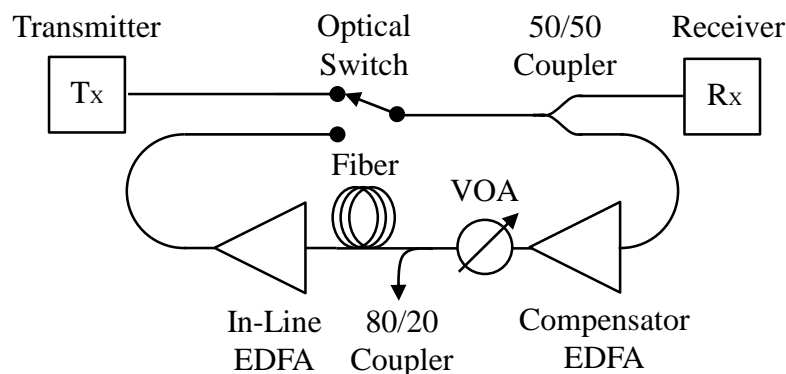


Figure 32 – Experimental Loop Setup.

3.2.1 Optical Switch

It is necessary to analyze τ_{loop} as this value defines the switching speed needed for the application. For SSMFs, the time in the closed loop is $4.89 \mu\text{s}/\text{km}$ of fiber [Mazzali e Fragnito 1998], as described by Equation 24. Since the chosen fibers usually come in spans of 50 km, the trip time will be approximately $244.5 \mu\text{s}$ per fiber span. Since a high gain amplifier is used for the In-Line EDFA, two fiber spans were used, for a total of 100 km and a trip time of approximately $489 \mu\text{s}$. Considering that a fast switch is needed, the chosen device was an Agiltron NanoSpeed™1x2 Series Fiber Optical Switch with a 5 kHz Repetition Rate NanoSpeed™Switch Driver.

The characterization of the optical switch is realized using a Tektronix Mixed Domain Oscilloscope (MDO) 3000 Series to analyze the signals and a PM to measure the insertion loss. The electric signal used to activate the switch is measured in conjunction with the signal generated by the photodetector, as shown by the setup in Figure 33a. These signals are compared in order to obtain the response times of the switch. The method of obtaining each characteristic of the response time is demonstrated in Figure 33b. Table 8 presents the specified and measured technical data. As can be observed, the measured response time and insertion loss of the switch is not in compliance with the specified data. However, since the response time values are still considerably smaller than the trip around both 50 km spans, it is still possible to use this switch.

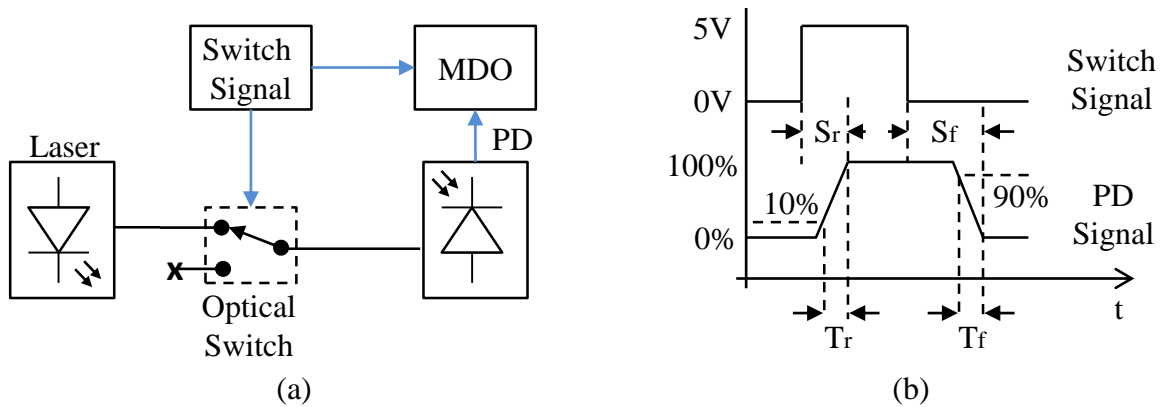


Figure 33 – Optical switch characterization: a) Measurement setup and b) Response Time diagram.

Table 8 – Agiltron NanoSpeed™ Technical Data.

Type	Specified	Measured
Insertion Loss (dB)	0.6-1.0	2.3
Extinction Ratio (dB)	-	26.2
Rise Time T_r (ns)	85-100	532
Fall Time T_f (ns)	85-100	1060
Switch Speed (Rise) S_r (ns)	315-350	888
Switch Speed (Fall) S_f (ns)	315-350	1112

3.2.2 Couplers

Two 1x2 couplers are used in the setup: one to feed the loop/receiver and another for monitoring the fiber input power. Since the signal is split, the insertion loss of these devices are essential for the loop technique. For this reason each device is characterized individually. The chosen couplers are Go4Fiber Singlemode 1x2 Couplers: SSD-1X2-35-50/50-R-2-1 and SSD-1X2-35-80/20-R-2-1.

The setup for this characterization is realized, simply, by measuring input and output powers and subtracting them to obtain the insertion loss. On the other hand, the excess loss is obtained by subtracting the total input power from the total output power. A full spectral characterization can be realized by using a broadband light source and an OSA, as depicted by Figure 34.

The full spectrum characterization of the 50/50 coupler is shown in Figure 35a. It is possible to observe that the insertion loss of the coupler is not symmetric, with more power exiting through port B. Table 9 expresses the specified and measured results at 1550 nm, demonstrating that the coupler does not deviate much from the specified data. A lower insertion loss is interesting for the looping technique, as it states that more power will be entering the loop. For this reason, port B was chosen for the loop input and port A for the receiver input.

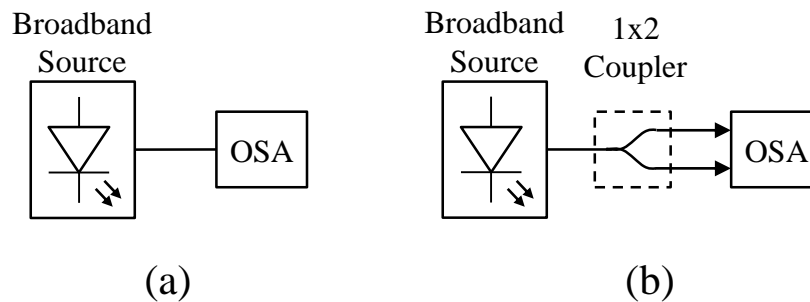


Figure 34 – Singlemode 1x2 Coupler Characterization Setup: a) Broadband source measurement and b) Coupler output measurement.

Similarly, the 80/20 coupler was characterized, with the spectral measurement demonstrated in Figure 35b. It is clearly possible to observe that port B is the tap port, since port A has the lesser insertion loss meaning that most of the power flows through it. Table 10 summarizes the specified and measured results at 1550 nm, demonstrating that the coupler is in compliance with the specified data.

Table 9 – SSD-1X2-35-50/50-R-2-1 Technical Data @ 1550 nm.

Type	Specified	Measured
Excess Loss (dB)	0.10	0.22
Insertion Loss [1 → A] (dB)	3.50	3.78
Insertion Loss [1 → B] (dB)	3.50	2.74
Coupling Ratio [A] (%)	50.0	44.1
Coupling Ratio [B] (%)	50.0	55.9

Table 10 – SSD-1X2-35-80/20-R-2-1 Technical Data @ 1550 nm.

Type	Specified	Measured
Excess Loss (dB)	0.10	0.21
Insertion Loss [1 → A] (dB)	7.80	7.53
Insertion Loss [1 → B] (dB)	1.30	1.59
Coupling Ratio [A] (%)	20.0	20.3
Coupling Ratio [B] (%)	80.0	79.7

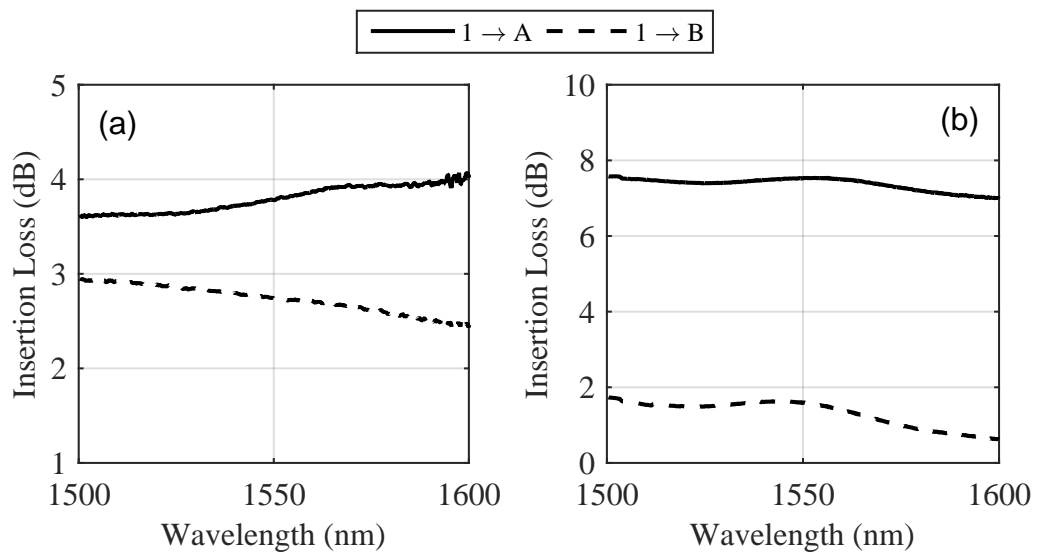


Figure 35 – Singlemode 1x2 Coupler Insertion Loss Characterization: a) 50/50 coupler and b) 80/20 coupler.

3.2.3 Optical Amplifier (Compensator)

As loop hardware adds losses to the system, it might be necessary to use an EDFA to compensate the losses of these devices. However, in every loop trip, the signal will acquire additional noise due to the Compensator EDFA. Since fiber nonlinearity requires high fiber input power, this amplifier is required in the experimental setup. For this application, a Lightwave 2020 Compact Low Cost Booster EDFA (NOABF101R000112, or simply, NOABF10) was chosen.

The same setup from Figure 23 was used to characterize the amplifier. The data obtained from the measurements are presented in Figure 36 and the specified and measured parameters are disposed in Table 11. As can be observed, the output power at $P_{in} = -6$ dBm is near 10 dBm indicating that the amplifier is in agreement with the specified technical data. However, the experimental input of this amplifier will be considerably high since it is placed after the 50/50 coupler, as shown by Figure 32. The output power at port B of this coupler is 4.96 dBm, leading to an output of 12.10 dBm at the amplifier output and consequently a gain of approximately 7 dB. The insertion losses of all loop specific hardware (switch, couplers and VOA) add up to a total of 6.6 dB, demonstrating that the EDFA compensates for losses of loop specific hardware in this point of operation.

Table 11 – NOABF10 Booster EDFA Technical Data.

Type	Specified	Measured
Output Power ¹	10.0	9.9
Noise ¹ (dB)	6.0-7.0	6.7

¹ $P_{in} = -6$ dBm

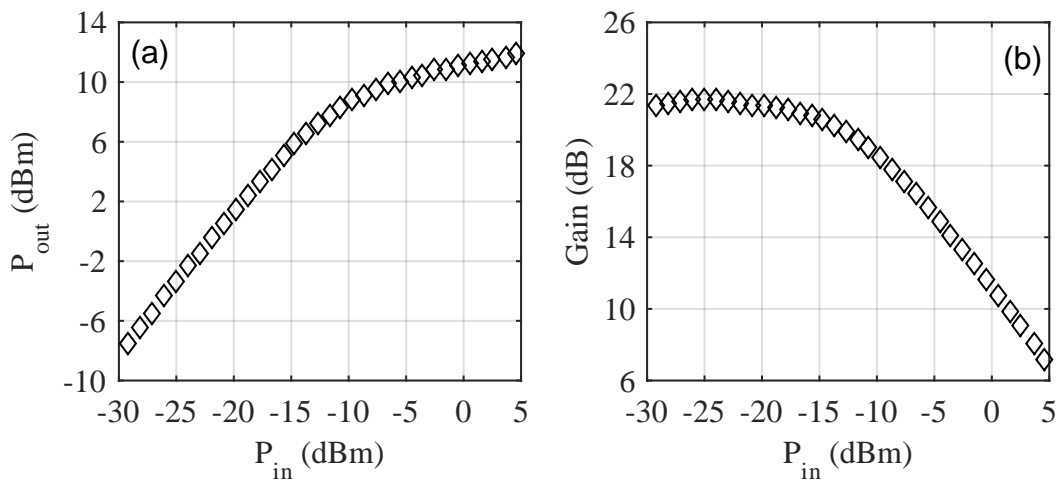


Figure 36 – NOABF10 Booster EDFA Characterization: a) Output Power and b) Amplifier Gain.

3.2.4 Loop Control Hardware

As discussed before, the switch needs to be carefully controlled in order to adequately implement the loop technique. Since the optical switch and both Lightwave2020 EDFAs were not ready to use, these devices required hardware designing before usage. A control setup for all devices was developed using a development board Freedom-K64F as shown in Figure 37. The development board controls both EDFAs, enabling pump power control in order to vary the gain and output power of these devices. An L298 H-Bridge is also controlled in order to generate two pulsed signals: the switch control signal and the triggering signal.

Figure 38 demonstrates how these signals control the loop. The switch signal is responsible for controlling the optical switch, feeding the transmitted data to the loop at high voltage (load state) and isolating the transmitter circuit by switching to the a low voltage (loop state). At the same time the trigger signal is sent to two devices: the signal generator and the oscilloscope. The pulse transition from high to low will active the signal generator (Tx Trigger), ordering the signal to be sent at the same time that the switch is on the load state. As can be observed, when the switch signal is in the high state and the Tx trigger occurs, the optical signal is sent into the loop adequately. To receive the signal at any desired time, the transition from low to high (Rx Trigger) of the trigger signal can be set by the user manually. Since the trigger signal was also sent to the oscilloscope, this device can use the Rx Trigger transition to obtain the signal at the desired time instance, acquiring the signal after numerous loop trips, consequently obtaining the signal at different transmission distances.

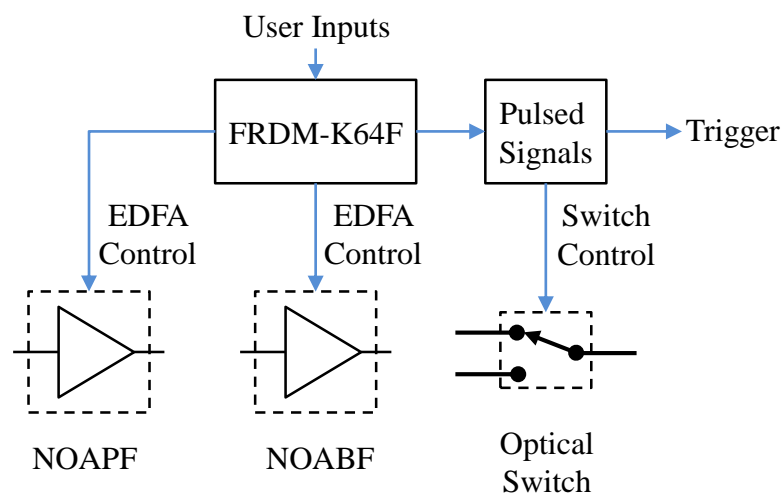


Figure 37 – Optical Switch and Amplifiers Hardware Design Setup.

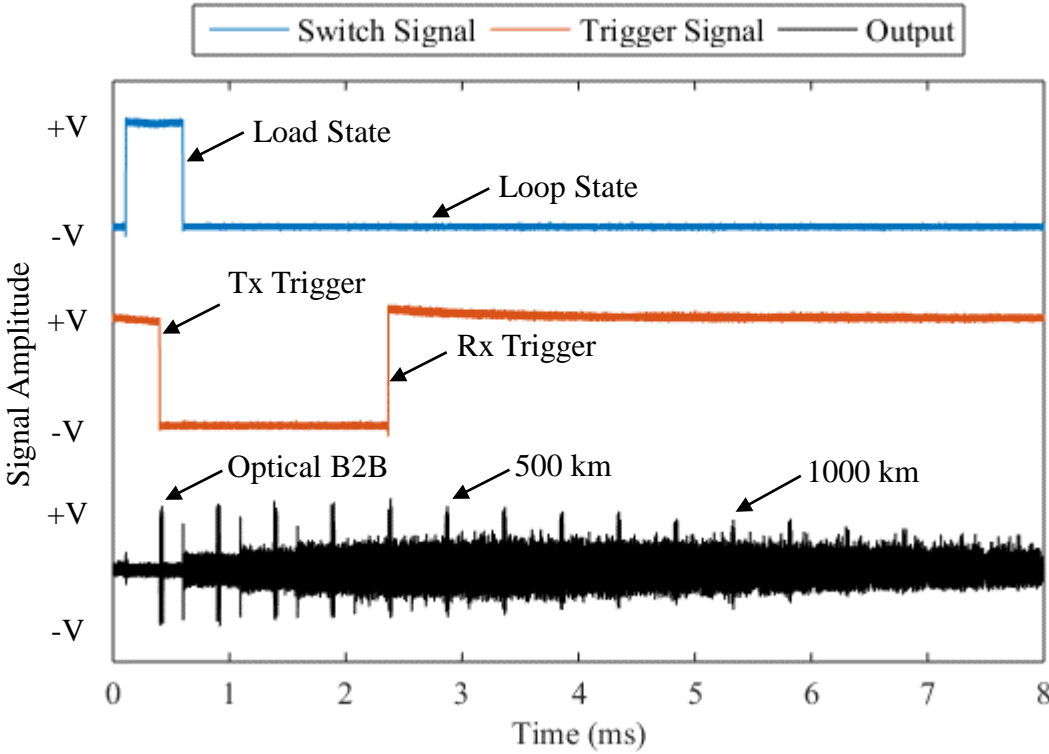


Figure 38 – Adopted switching and triggering diagrams for the loop technique.

3.3 OFDM

3.3.1 Signal Generation and Reception

To generate the electric signal, an Analog-to-Digital (A/D) converter is necessary. For this application, a Tektronix AWG7122C (Arbitrary Waveform Generator) was used. This device can generate two signals with a maximum of 12 GS/s or one single signal up to 24 GS/s by interleaving the two output channels. To recover the the signal, a Digital-to-Analog (D/A) converter must be employed. The Tektronix DPO71604C (Digital Phosphor Oscilloscope) was used for this task, having a maximum sampling frequency of 100 GS/s.

The Nyquist-Shannon sampling theorem states that receiving a signal with bandwidth B , requires a sampling frequency of at least $F_s \geq 2B$. By this theorem, the DPO can receive any signal generated by the AWG, stating the generator as the limiting factor for the transmission, in this case. The generator is also limited in frequency, since higher frequencies mean lower samples per cycle. For example, a 12 GHz signal, generated at 24 GS/s, would mean only 2 samples per cycle. To demonstrate this effect, a test can be realized by generating a sine wave and sweeping the frequency to higher values, while using a spectrum analyzer to measure the power of the signal at each frequency. For the AWG7122C, the frequency was swept from DC to 2.4 GHz in steps of 100 MHz, resulting in a 2 dB power penalty, as displayed in Figure 39. For this reason, a maximum frequency of 2 GHz was chosen for the experiments.

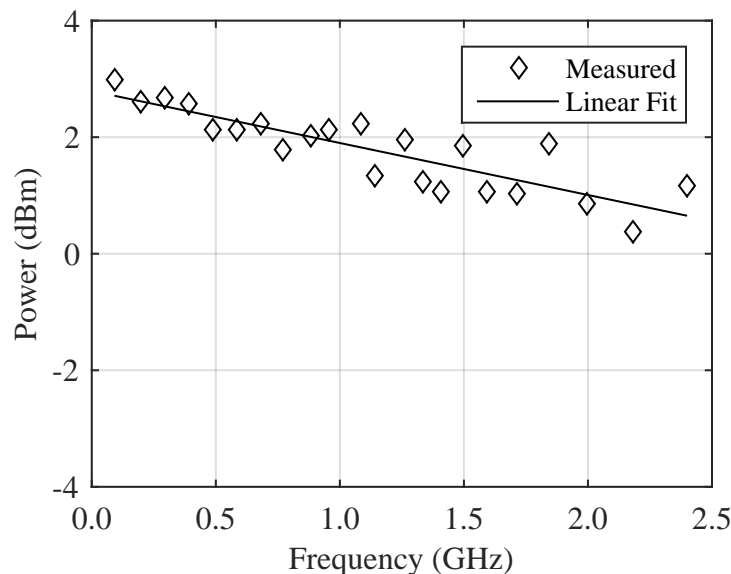


Figure 39 – Tektronix AWG7122C Frequency Characterization for signals generated at 24 GS/s.

3.3.2 OFDM System Design

Since the optical channel has amplifier chains (generated by the looping technique), this channel tends to be very noisy. For this reason, the initial modulation format chosen was 4-QAM with the possibility of expanding to higher values such as 16-QAM or even 64-QAM, depending on system performance. For a 1.5 GHz bandwidth signal, the sampling rate (F_s) should be at least 3 GS/s. Since the AWG can sample up to 24 GS/s, the signal can be generated at 3 GS/s and then be oversampled by a factor of 8, achieving the maximum sampling capacity of the generator, while improving system performance.

The size of the FFT determines the number of subcarriers of the system, making it an important parameter. If the OFDM system is complex-valued, the number of subcarriers equals the size of the FFT, while in real-valued OFDM systems, the number of subcarriers is half the FFT size as a result of the Hermitian symmetry. Higher values of FFT, improve system performance at the cost of system complexity. To avoid excessive complexity at the receiver and transmitter, values of FFT between 128 and 1024 are usually used, keeping in mind that this value is usually defined as a power of two. For this system, an FFT size of 512 was chosen. The OFDM system is real-valued, so the number of useful subcarriers N_c is equal to $\frac{N_{FFT}-2}{2}$, or 255, due to the Hermitian symmetry.

The subcarrier channel spacing Δf can be obtained from the signal bandwidth BW and the FFT size, as equated by $\Delta f = BW/N_{FFT}$. From the sample rate, it is possible to determine the useful OFDM symbol duration as $T_u = N_{FFT}/F_s$. The sample size of the useful OFDM symbol is equal to the FFT size, or $N_u = N_{FFT}$. Knowing the duration and size of the symbols, it is possible to establish the overheads that need to be inserted to improve the quality of transmission.

The cyclic prefix must also be carefully adjusted since it is composed of redundant information. Therefore, the main tradeoff when choosing the ideal guard time is between ISI robustness and the system net data rate. The guard time T_g can then be defined by rewriting Equation 34 as [Jansen et al. 2007],

$$\frac{c}{f_c^2} \cdot |D_L| \cdot N_{FFT} \cdot \Delta f + DGD_{MAX} \leq T_g, \quad (45)$$

where f_c is the optical carrier frequency, c is the speed of light, D_L is the total amount of chromatic dispersion, Δf is the subcarrier channel spacing and DGD_{MAX} is the maximum differential group delay (DGD). The value of DGD_{MAX} can be approximated by about 3.5 times the mean PMD of the optical link. The link PMD and total chromatic dispersion D_L can be extracted by using the values from the optical fiber, obtained in Table 3. From these parameters, Equation 45 can be rewritten as [Jansen et al. 2007],

$$\frac{c}{f_c^2} \cdot |D_f| \cdot L \cdot N_{FFT} \cdot \Delta f + 3.5 \cdot PMD_f \cdot \sqrt{L} \leq T_g, \quad (46)$$

where D_f is the dispersion value of the fiber, PMD_f is the PMD link design value of the fiber and L is the total link length. From Equation 46 it is possible to establish a relation between the guard time and the total length of the link. Aiming for a low overhead, a cyclic prefix sample size N_g of $1/128$ ($\approx 0.8\%$) of the signal samples ($N_g = N_u/128$) was chosen. This translates to a guard time of $T_g = N_g \cdot T_u/N_u = 1.33$ ns. The left side of the inequality (Equation 46) will only be greater than the chosen guard time for link lengths higher than 12,000 km. Therefore, if the link length remains well below 12,000 km, it is realistic to assume that the influence of chromatic dispersion is negligible during the experiments.

As the optical switch opens after the transmission of the signal is realized, there is no need for the AWG to keep sending the signal at this point. For this reason, a trigger is used to send the signal at the point where the switch is active for transmission. When the trigger signal reaches the AWG, the first few samples are distorted by the triggering process. For this reason, zeroes are inserted in the time domain before the signal. These zeroes can also be used to synchronize the received signal, using correlation. The sample size of these zeroes was found empirically by testing different sampling lengths and verifying how the transmission was affected. It was established that a preamble with a sample size N_{pr} of 5% of the signal ($N_{pr} = 0.05 \cdot n_{fr} \cdot N_u$) was enough to avoid triggering interference, while still synchronizing properly at the receiver. To define the number of OFDM frames (n_{fr}), the loop time should also be taken into account.

Since the loop trip time is defined by the fiber spans as 489 μ s, numerous data frames can be sent in order to maximize data transmission. Each frame will contain the cyclic prefix and the data, while all preambles are inserted at the beginning of the signal to avoid switching interference. The number of chosen frames sent will define the maximum signal time. However, it is important to note that the observed time window is limited to the maximum number of points displayed by the DPO. The AWG generates the signals at 24 GS/s so the reception was set to 50 GS/s to guarantee a well sampled received signal. The maximum points displayed by the DPO is $12.5 \cdot 10^6$ points, translating to a maximum time window of 250 μ s. However, a time window of 50 μ s was chosen to reduce computational complexity, receiving a reduced number of points from the DPO ($2.5 \cdot 10^6$ samples). A single symbol duration is 170.7 ns and the guard time duration is 1.3 ns. For 200 frames, the total useful symbol duration is 34.14 μ s and the total guard time is 0.26 μ s. The preamble is defined as 5% of the useful symbol duration, or 1.70 μ s. The total time signal with the preamble leads to a duration of 36.1 μ s, staying below the chosen time window, as shown in Figure 40a.

After defining the overheads, the rate of the system can be clearly determined. Each subcarrier will transport a number of bits n , that can be equated by $n = \log_2 M$, where M is the number of points in the constellation diagram of an M-QAM modulation. Without

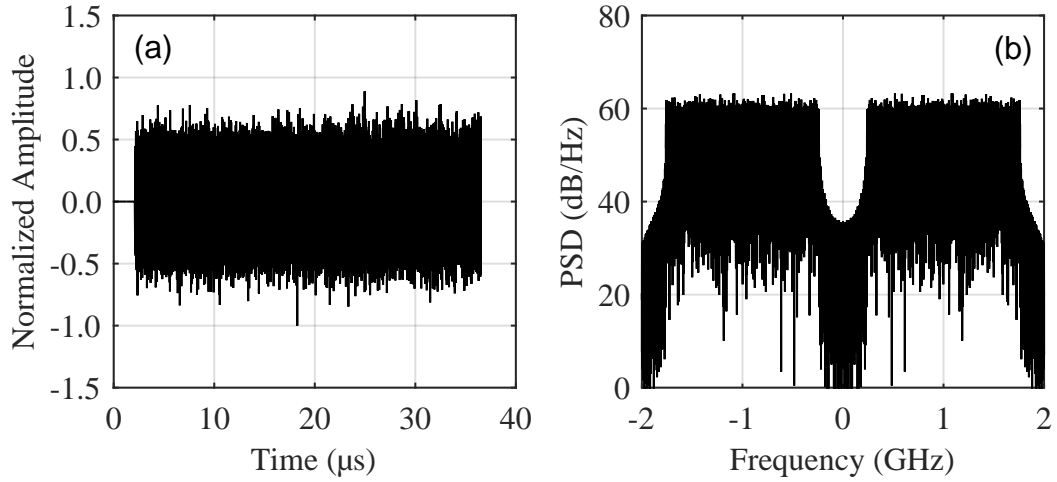


Figure 40 – Designed OFDM system: a) Time domain signal and b) Power Spectral Density (PSD).

the overhead, the total rate should be the number of bits per subcarrier multiplied by the total number of subcarriers, or $R_{total} = n \cdot \Delta f \cdot N_{FFT} = 3$ Gb/s. Since the Hermitian symmetry reduces the number of useful subcarriers, the nominal rate of the system reduces to: $R_{nominal} = n \cdot \Delta f \cdot N_c = 1.49$ Gb/s. The raw rate is obtained by taking the overheads into account, reducing the nominal rate and being expressed as,

$$R_{raw} = R_{nominal} \cdot \frac{1}{1 + \varepsilon_{pr}} \cdot \frac{1}{1 + \varepsilon_{cp}}, \quad (47)$$

where ε_{pr} represents the preamble overhead given by $\varepsilon_{pr} = N_{pr}/N_u$ and ε_{cp} defines the cyclic prefix overhead given by $\varepsilon_{cp} = N_g/N_u$. Since forward error correction (FEC) is not being used, Equation 47 defines the actual data rate of the system: $R_{raw} = 1.41$ Gb/s. All previously discussed parameters of the system are summarized and quantified in Table 12.

Table 12 – OFDM System Parameters.

Parameter	Symbol	Designed
Modulation		4-QAM
Bandwidth (GHz)	BW	1.5
FFT Size	N_{FFT}	512
Useful Subcarriers	N_c	255
Subcarrier Spacing (MHz)	Δf	2.93
Symbol Sample Size	N_u	512
Cyclic Prefix Sample Size	N_g	4
Symbol Duration (ns)	T_u	170.7
Guard Time (ns)	T_g	1.3
Preamble Duration (μ s)	τ_{pr}	1.70
Signal Duration (μ s)	τ_{data}	36.1
Raw Rate (Gb/s)	R_{raw}	1.41

3.4 CE-OFDM

Since CE-OFDM consists of modulating the phase of conventional OFDM, all parameters from Table 12 will remain the same. However, the time domain signal changes due to the modulation. The amplitude is constant, lowering the PAPR of the system as can be seen in Figure 41b. While CE-OFDM exhibits a PAPR of 2.2 dB, the OFDM system presents 8.4 dB, demonstrating the main difference between both techniques as shown in Figure 41a.

The phase modulation index should be studied thoroughly since it is the main parameter of this technique. Figure 42 demonstrates the CE-OFDM spectrums for different phase modulation indexes. As can be seen, increasing the phase modulation index also increases the power of the signal components, however, the power of unwanted components is also increased, reducing spectral efficiency of the system. This parameter will be discussed in detail during the experimental results.

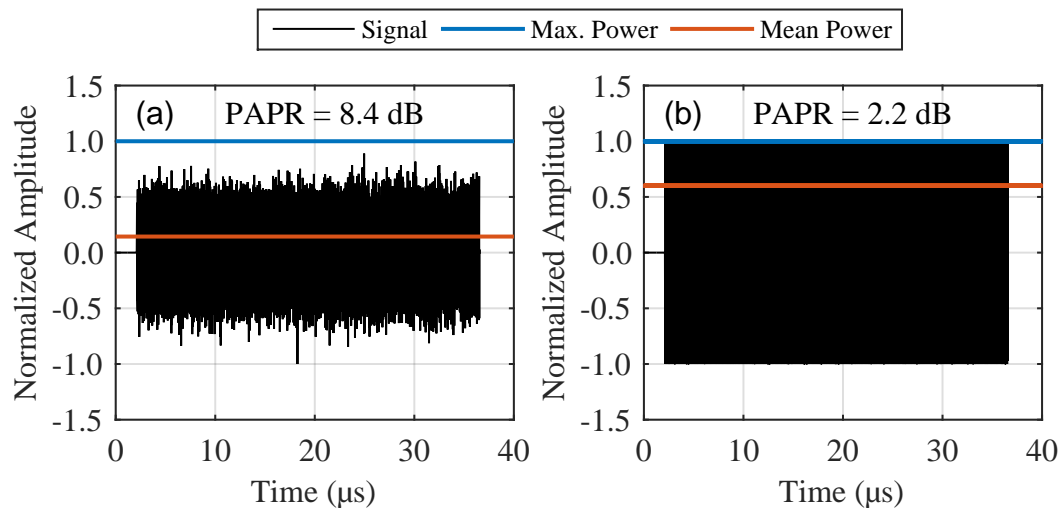


Figure 41 – PAPR Comparison between signals: a) OFDM and b) CE-OFDM.

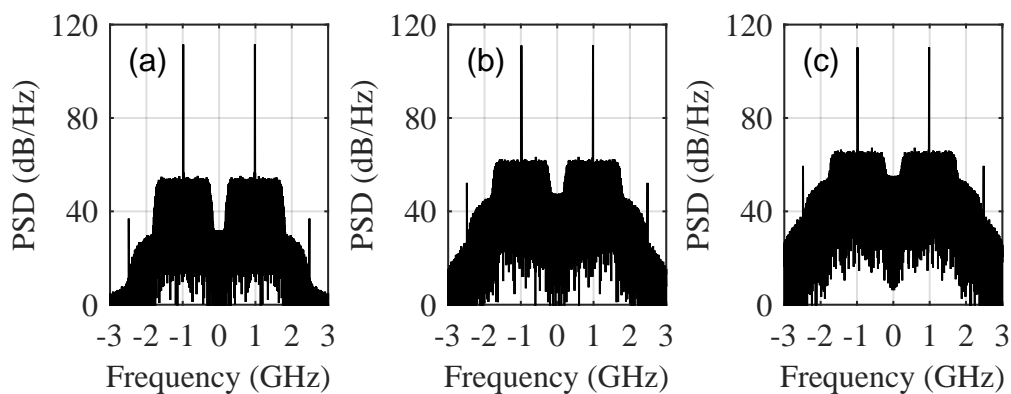


Figure 42 – CE-OFDM Spectrum for different phase modulation indexes: a) $h = 0.10$, b) $h = 0.25$ and c) $h = 0.40$.

4 Experimental Results

After laying the foundations of optical communications and characterizing all devices, the final setup can be built for experimenting. During most tests, OFDM and CE-OFDM are compared to understand how both techniques react to the system. The first test requires studying the best point of operation for the optical modulator over different distances. Then, the phase modulation index is discussed in more detail for various transmission distances. With these initial parameters defined, the optical fiber input power is studied and transmission distances are discussed for both OFDM and CE-OFDM. Finally, higher bit rates are studied, exposing limitations of the setup. Figure 43 demonstrates the complete setup used for all experiments.

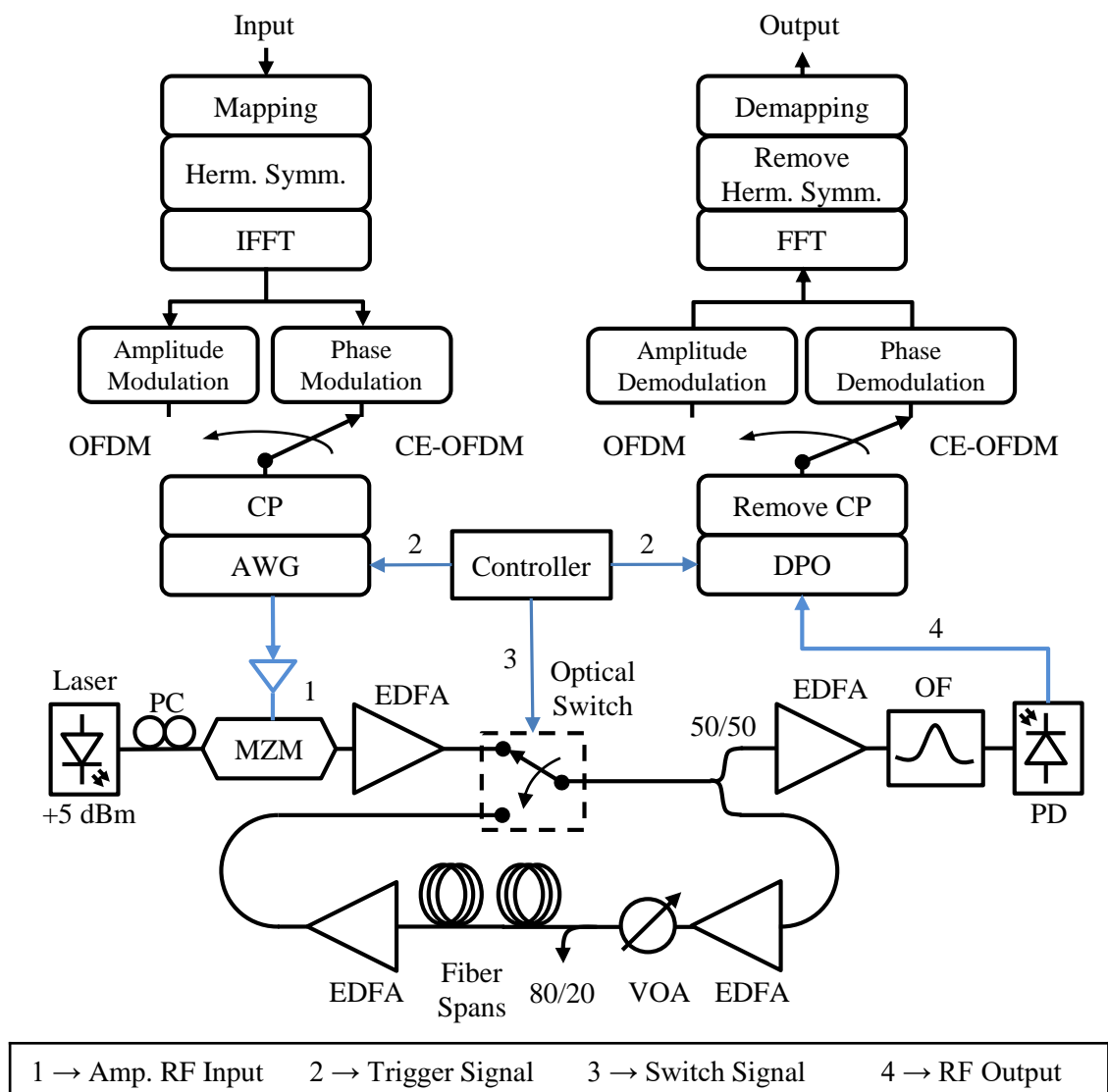


Figure 43 – Complete Experimental Setup.

4.1 Modulator's Point of Operation

Electro-optical conversion is one of the fundamental features of the transmitter, requiring a careful analysis to provide a high quality optical signal. In order to take advantage of the linearity of the MZM, the best point of operation for the bias seems to be $V_\pi/2$. However, Figure 22 demonstrates how the measured transfer function is not perfectly linear, affecting the overall result of the electro-optical conversion. It is also important to note that as the bias approaches V_π , the carrier power reduces, affecting the direct detection at the reception. For these reasons, the bias should be studied thoroughly before a point of operation can be chosen.

For this test, the bias voltage was swept from -3V to 3V in steps of 0.5V. At each step, the signal is measured at the output and compared with the input signal. The test is repeated for numerous distances in order to observe the relation between the bias and the transmission distance. The fiber input power is maintained at 10 dBm for this test, so as to induce nonlinearities in the fiber and characterize the point of operation for the worse case scenario.

The test results for OFDM signals are demonstrated in Figure 44a. It is easily observed that the outcome has a quadratic shape, exposing a minimum point for each curve. These valleys indicate the best point of operation at each transmission distance. For the optical back-to-back configuration, the best point of operation occurs at $0.56V_\pi$ for an EVM of approximately -27 dB. As the transmission distance is increased, the best point of operation shifts to $0.64V_\pi$, therefore defining the point of operation for long-haul systems. This shift originates from optical channel effects that were not present in the optical back-to-back configuration.

As for CE-OFDM, the curves are slightly different as shown by Figure 44b. The optical back-to-back configuration has a flatter valley due to the semi-constant amplitude of this signal. This characteristic of CE-OFDM signals allows it to fully take advantage of the linear region, whereas the performance of OFDM signals are quickly affected by bias changes due the clipping of high peaks at the nonlinear regions of the MZM. As the CE-OFDM signal passes through the optical channel, noise affects the signal, increasing the PAPR and consequently affecting the flatness of the valley. This can be easily observed in the 200, 400 and 600 km curves of Figure 44b, as the curve changes its shape as the distance increases. For the optical back-to-back configuration, an EVM of -26.1 dB is reached at the lowest point, for a bias of $0.64V_\pi$. As for higher distances, the best point of operation is shifted to $0.71V_\pi$.

A noteworthy feature of both signals is the performance decay as the bias tends to 0 or V_π , demonstrating how the signal reacts when the point of operation begins transiting the nonlinear regions of the MZM. The best point of operation of CE-OFDM is closer to

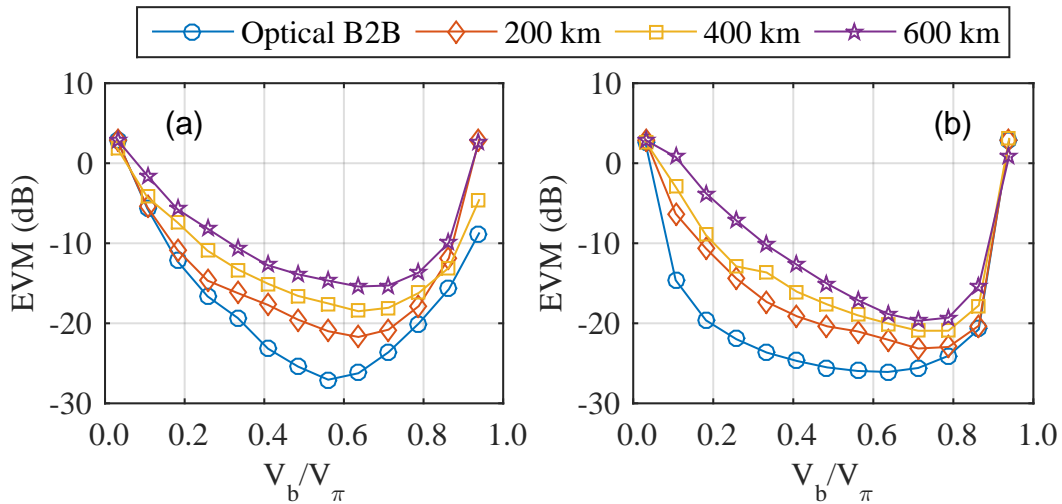


Figure 44 – MZM Point of Operation Analysis: a) OFDM signals and b) CE-OFDM signals.

the nonlinear region than for OFDM, demonstrating how the constant envelope improves the system in this sense. It is also possible to observe how CE-OFDM obtained a better performance than OFDM over long distances, for the best points of operation. This is due to the high input power of the optical fiber, inducing fiber nonlinearities in the system and consequently reducing the performance of high PAPR signals.

The optical spectrum was measured using the APEX OCSA (AP2683A) to observe the bias effects on the optical signal. The OFDM spectrum for a bias of $0.33V_\pi$ and $0.64V_\pi$ can be seen in Figures 45a and 45b respectively. The lower point of operation demonstrates how the optical carrier interacts with the subcarrier, affecting signal transmission negatively, whereas the higher point of operation clearly shows more power in the subcarriers, separating them efficiently from the optical carrier. The same effect is demonstrated in the CE-OFDM spectrums for $0.26V_\pi$ and $0.71V_\pi$, shown on Figures 46a and 46b respectively. At lower points of operations, the carrier dominates significantly over the signal, resulting in poor system performance since the power level of the subcarriers is closer to the optical noise. On the other hand, higher points of operations raise the overall optical power of the signal portion, while reducing carrier power, resulting in poor performance of the direct detection system since the carrier is required to acquire the signal efficiently at the PD. Higher points of operation are preferable, as demonstrated by Figure 44, since the signal presents more power, thus improving the SNR of each individual subcarrier. However, this point of operation should not be increased sufficiently as to affect the direct detection.

From the results it can be easily defined that for OFDM and CE-OFDM signals, the MZM should operate at $0.64V_\pi$ and $0.71V_\pi$ respectively. These values are maintained throughout the following tests, guaranteeing the best possible performance for transmission over long distances.

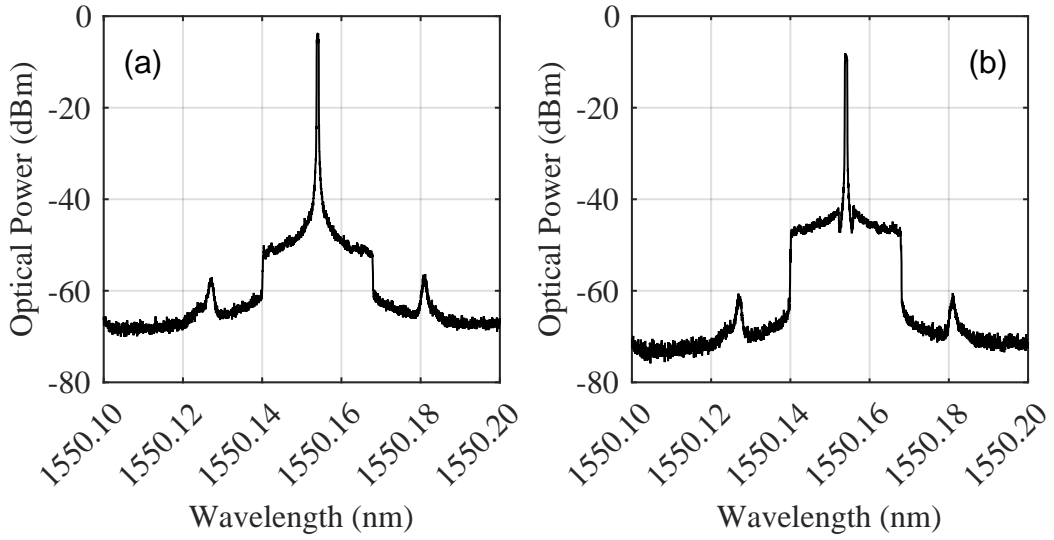


Figure 45 – Measured OFDM Optical Spectrum for a) $0.33V_\pi$ and b) $0.64V_\pi$.

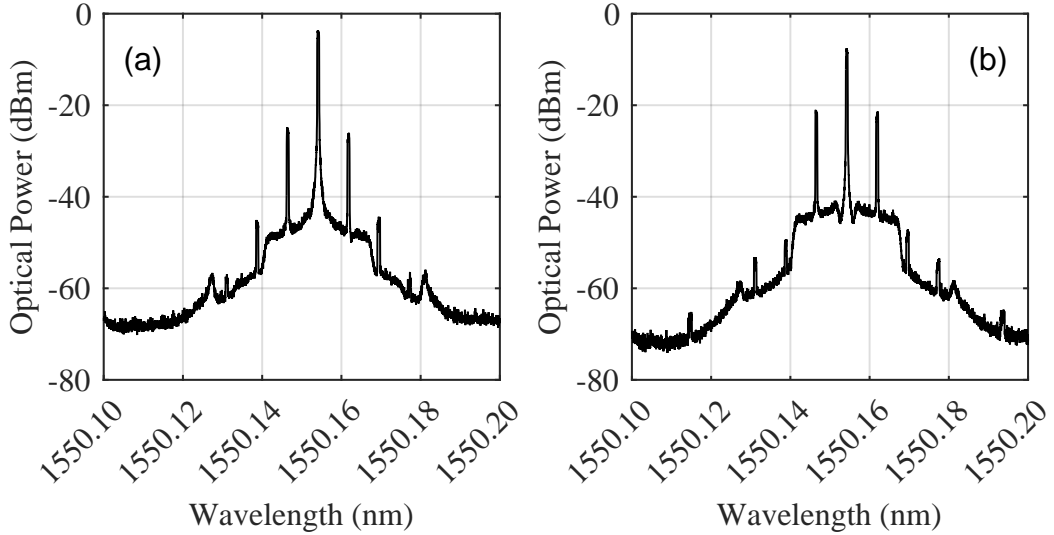


Figure 46 – Measured CE-OFDM Optical Spectrum for a) $0.26V_\pi$ and b) $0.71V_\pi$.

4.2 CE-OFDM Phase Modulation Index

With the modulator point of operation defined, it is important to evaluate the phase modulation index, h , with regard to system performance due to its importance to CE-OFDM signals. As discussed in previous sections, the phase modulation index is directly responsible for spectral scattering, affecting spectral efficiency as defined by Equation 39. Lower values of h limit the system due to noise sensitivity, whereas higher values limit it due to modulation nonlinearity [Rocha et al. 2019]. Therefore, the modulation index should be investigated to define clearly the best regions for improved system performance.

The test was realized by sweeping the modulation index from 0.1 to 0.5 in steps of 0.05. This was realized for numerous distances in order to observe the effects of the index in the system. The power at the input of the fiber was maintained at 10 dBm and the

modulator biased at $0.71V_{\pi}$.

In the optical back-to-back configuration, the regions are well defined with a decrease in performance for values below 0.15 and above 0.2, as shown in Figure 47. Indexes in this interval achieve EVM values near -27 dB, indicating an optimal region for the system. However, as the transmission distance rises, the system is increasingly limited due to noise, while the modulation nonlinearity seems to not affect the performance as much. This is clearly observable at distances over 1,000 km, where the phase modulation index needs to be above 0.35 for adequate system performance. The modulation nonlinearity region is also undefined for these distances since the curve appears to be nearly flat. Therefore, higher distances are only possible through the usage of higher phase modulation indexes, leading to spectral inefficiency.

As higher distances should be explored, the chosen phase modulation index is 0.40, as this value clearly allows for reaching distances above 1.200 km, as shown in Figure 47. Lower values will eventually limit the system at long distances due to noise. Therefore, this value is defined as the optimum point of operation for the CE-OFDM system during the experiments.

The spectral difference between the CE-OFDM phase modulation indexes were demonstrated in Figure 42. These same spectrums were measured using the APEX OCSA (AP2683A) to observe how the signal responds to the optical system. Figure 48 demonstrates the results, making it possible to observe how for higher phase modulation indexes, the spectrum is well defined with a higher power difference between the subcarrier frequencies and the optical noise.

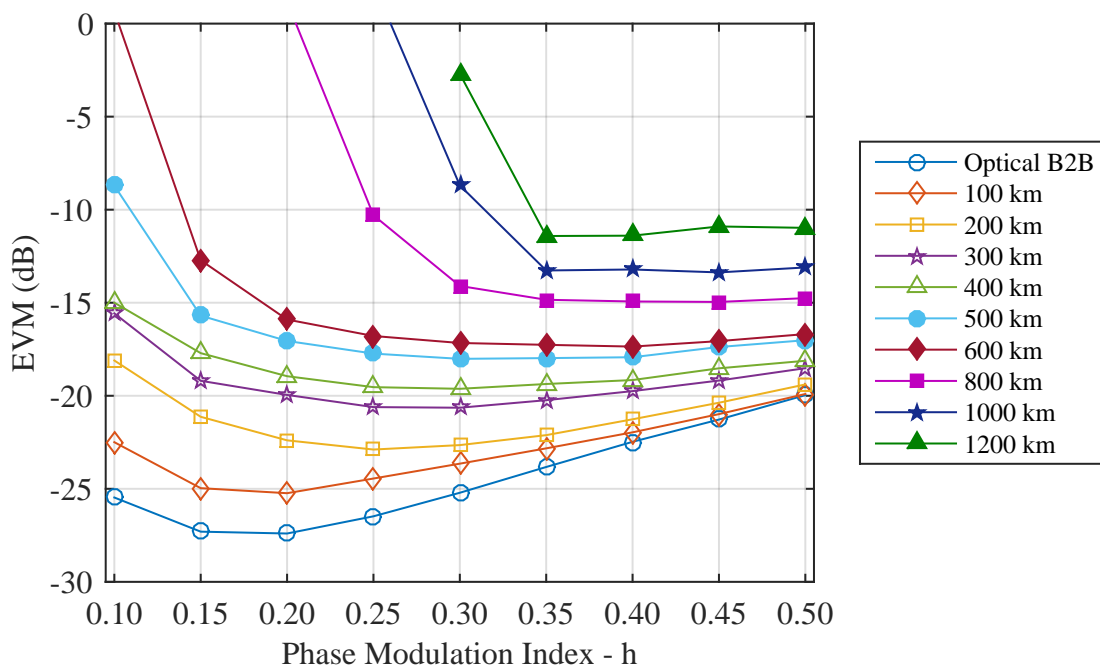


Figure 47 – CE-OFDM Phase Modulation Index Analysis.

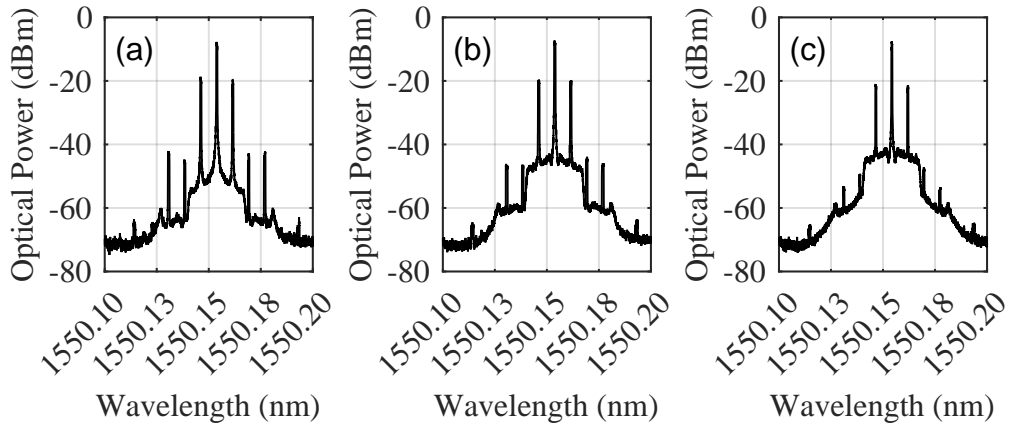


Figure 48 – Measured CE-OFDM Optical Spectrum for different phase modulation indexes: a) $h = 0.10$, b) $h = 0.25$ and c) $h = 0.40$.

4.3 Optimum Fiber Launch Power

Until this point, high fiber input power was used in order to stimulate fiber nonlinearities and characterize the systems parameters at the worst case scenario. However, fiber launch power should be studied carefully to improve system performance. For this reason, the loop setup presents additional equipment that allow for launch power variation and analysis (Compensator EDFA, VOA and coupler). The test was realized by attenuating the output of the EDFA while monitoring the power through the coupler until the desired fiber launch power was reached. A variation from 0 to 10 dBm in steps of 2 dBm was used for this experiment. At each step, performance measurements were taken for analysis. This was realized for numerous transmission distances in order to obtain the results shown in Figure 49.

From Figure 49a, it can easily be seen that the OFDM system has very poor performance at higher launch powers. This performance decay is aggravated at longer distances where noise build up is intensive, increasing the PAPR of the system, thus increasing fiber nonlinearity further. The performance penalty begins at a launch power of approximately 6 dBm, so anything past that is not recommended for this system. For values lower than 2 dBm, the performance seems to slowly degrade due to noise dominance over the signal. From 0 to 2 dBm the penalty in EVM is very small, however the tendency demonstrates that performance will worsen, and therefore it is not recommended to use a launch power inferior to 2 dBm.

On the other hand, Figure 49b demonstrates the performance of the CE-OFDM system. This result demonstrates flatter curves than the ones presented in the OFDM system. The system does not appear to present power penalty due to launch power variations until transmission distances as high as 600 km. After that, some fluctuations occur due to noise build up, but nothing as significant as presented in Figure 49a. This

clearly demonstrates the high fiber nonlinearity tolerance of CE-OFDM systems, where at 10 dBm launch power over 1,000 km, a difference of approximately 10 dB in EVM between the two techniques is measured (-10 dB for CE-OFDM and 0 dB for OFDM). However, it is important to note that this improvement is obtained at the cost of spectral efficiency. It is also noteworthy to mention that the performance difference between the two techniques at lower launch powers is not significantly high, with CE-OFDM having a slight lead. By observing the tendency of these curves around 900 and 1,000 km transmission distances, it is possible to assume that CE-OFDM will have approximately the same launch power considerations as OFDM, restricting these values between 2 and 6 dBm for improved system performance.

As both systems present performance penalty regions at long distances, it is possible to establish an optimal region for the fiber launch power. Any values from 2 to 6 dBm are considered adequate for transmission experiments.

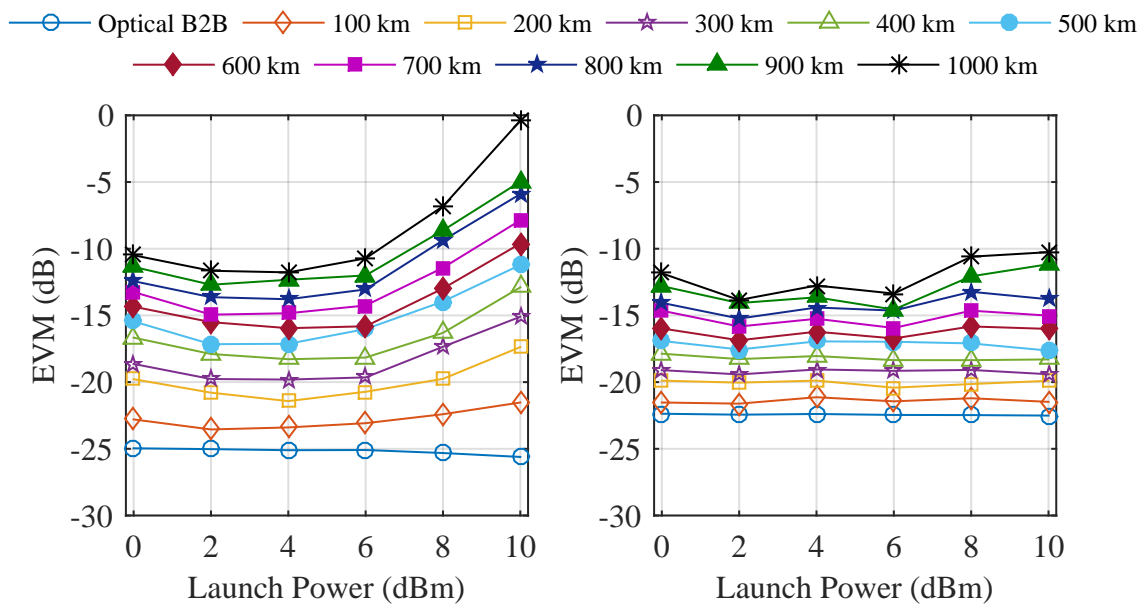


Figure 49 – Fiber Launch Power Analysis: a) OFDM and b) CE-OFDM.

4.4 Transmission Distance Analysis

As observed before, fiber launch power is essential to telecommunications transmission systems. Since values from 2 to 6 dBm were described as the best cases for the systems, these values were used to compare the systems in BER measurements. Due to hardware limitations, these measurements were realized in offline processing by acquiring data during experiments, saving and calculating the BER afterwards for each measurement. To establish a reference, it is considered that the signal can only be recovered for BER values lower than 3.8×10^{-3} , corresponding to the expected FEC Limit of a concatenated Reed-Solomon code with 7% redundancy.

The outcome of the experiment for the OFDM system is displayed in Figure 50a. For launch power of 4 and 6 dBm, the system demonstrates similar performance, achieving error free transmission until 700 km and staying just below the FEC limit at 1.100 km with a BER of 2.2×10^{-3} and 1.4×10^{-3} respectively. The curve for 2 dBm launch power is slightly shifted in comparison to the others, demonstrating superior performance. A BER of 9.1×10^{-4} was measured at 1.200 km, before surpassing the FEC limit. Similarly, the CE-OFDM system encountered zero bit errors until 700 km, obtaining similar performance as the OFDM system, as depicted by Figure 50b. This was expected since the EVM curves for both systems in Figure 49 were similar for the chosen region of analysis. A transmission distance of 1.200 km was achieved for 4 and 6 dBm launch powers, with BERs of 2.2×10^{-3} and 1.3×10^{-3} respectively. As for a 2 dBm launch power, a slightly improved performance was obtained at 1.300 km for a BER of 1.7×10^{-3} .

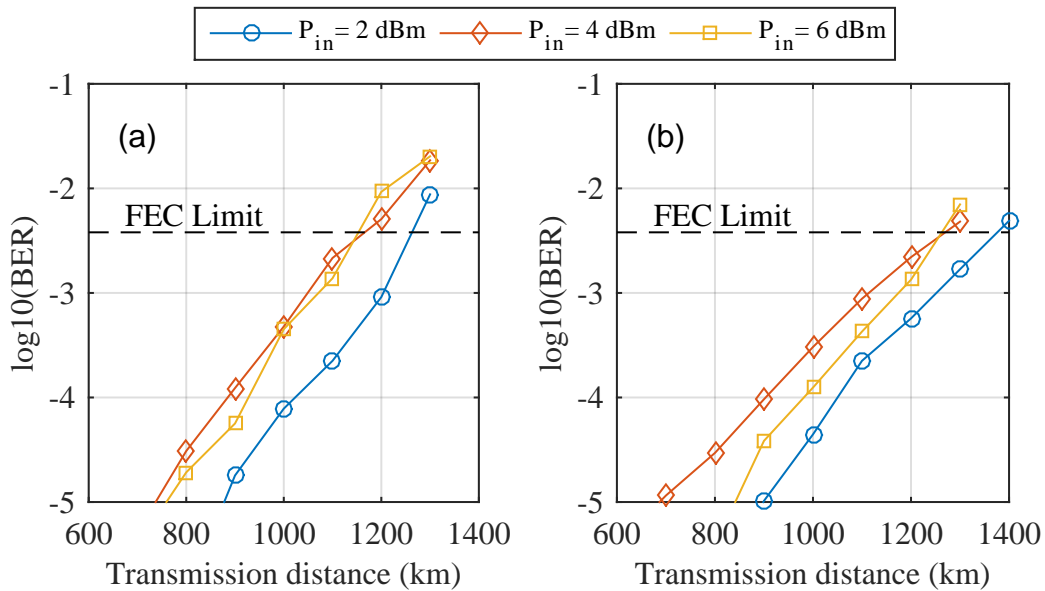


Figure 50 – BER as a function of transmission distance for different fiber launch powers (P_{in}) in the optimal region for: a) OFDM and b) CE-OFDM systems.

The slight performance gain is clearly seen in the constellation diagram shown in Figure 51. The color scheme of the diagram demonstrates the density of data in each parts of the constellation, with 0 being the least concentrated and 1 being the most concentrated spot. As can be seen, the OFDM system (Figure 51a) presents a slightly broader diagram than the CE-OFDM system (Figure 51b), clearly demonstrating how CE-OFDM possesses best performance at this point of analysis.

It is also possible to analyze these systems at high launch powers to observe the difference between them at regions where fiber nonlinearity begins to affect transmission. For this, launch powers of 8 and 10 dBm were analyzed, as shown in Figure 52. The OFDM system is shown in Figure 52a, demonstrating how increasing the power gravely affects the system, with the lower launch power presenting a significantly better performance. For 10

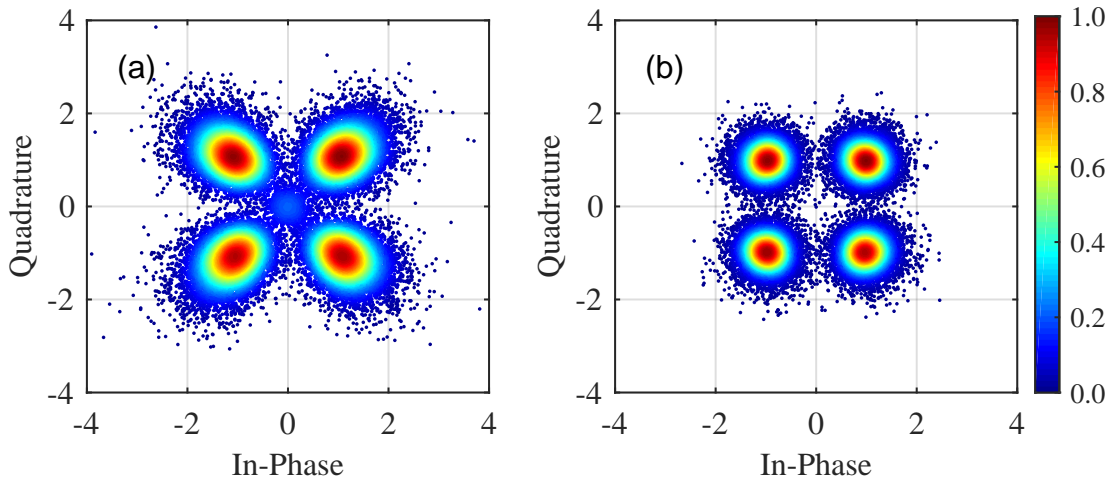


Figure 51 – 4-QAM constellation diagram for a transmission distance of 1.300 km at a fiber launch power of $P_{in} = 2$ dBm for a) OFDM and b) CE-OFDM.

dBm, the system achieves a BER below the FEC limit at 600 km, while for the 8 dBm test this distance was increased to 800 km. By comparing Figures 52a and 52b, it is clear that CE-OFDM has improved performance in this scenario, reaching higher distances for approximately the same values of BER. It is also easily seen how raising the launch power does not affect the system significantly as both CE-OFDM curves are similar. Distances of 900 and 1,000 km were achieved with for the 8 and 10 dBm launch powers respectively.

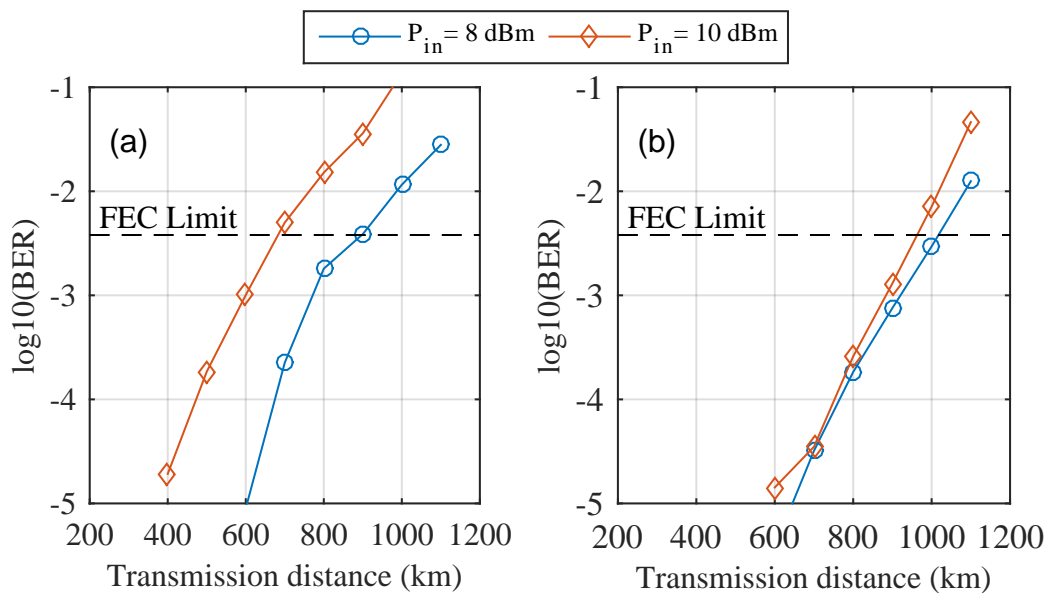


Figure 52 – BER as a function of transmission distance for different fiber launch powers (P_{in}) in the high fiber nonlinearity region for: a) OFDM and b) CE-OFDM systems.

By observing the constellation diagram of both systems at 1,000 km (53), it is possible to observe how OFDM tends to present many errors as the concentration of the data is clearly tending to the center point of the diagram, straying away from the ideal

symbol mapping points. On the other hand, the constellation diagram of the CE-OFDM system is clearly well behaved, with data well centered at the ideal points, tending to present less erroneous data measurements than the OFDM system.

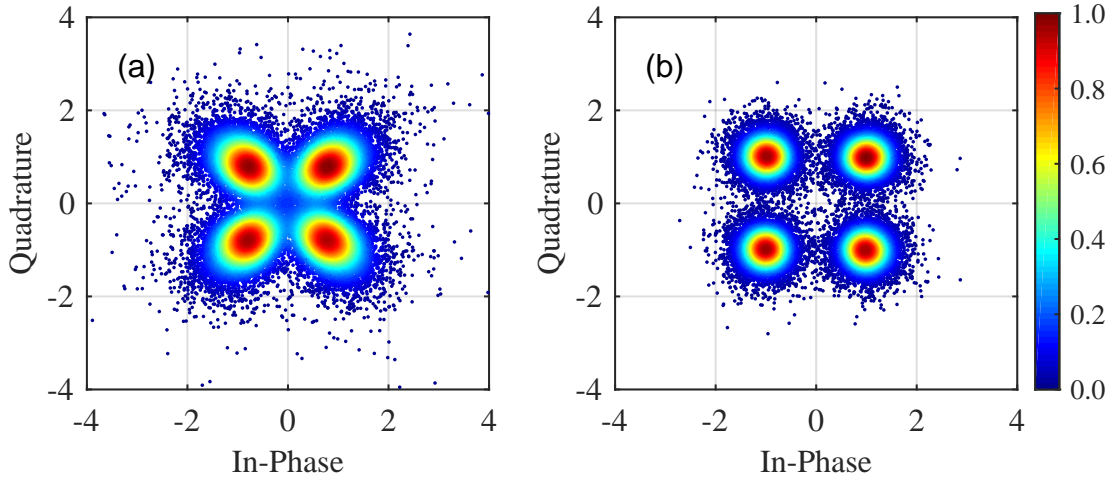


Figure 53 – 4-QAM constellation diagram for a transmission distance of 1,000 km at a fiber launch power of $P_{in} = 8$ dBm for a) OFDM and b) CE-OFDM.

Both experiments demonstrate how OFDM and CE-OFDM reacts to high transmission distances. While operating at optimal fiber launch power, both systems present similar performance, with CE-OFDM having a slight edge. However, when fiber nonlinearity is concerned, CE-OFDM clearly surpasses OFDM in terms of performance, achieving higher distances at the same BER values. This clearly demonstrates how PAPR reduction influences the system positively for high fiber launch powers.

4.5 16-QAM System Analysis

Until now, only 4-QAM was utilized during experiments with a raw rate of 1.41 Gb/s. One possibility for improving the rate of the system is increasing the number of bits contained in a symbol. However, with this, the points in the constellation diagram are also increased and the signal becomes more susceptible to noise since more constellation points can interfere with each other. In other words, a better EVM is needed to realize the same transmission. To demonstrate this and improve the rate of the system, 16-QAM was used during a experiments, doubling the number of bits per symbol from 2 to 4 ($n = \log_2(16) = 4$), resulting in a nominal transmission rate of 2.99 Gb/s and consequently a raw transmission rate of 2.82 Gb/s.

A fiber launch power of 2 dBm was used since this corresponded to the best point during transmission experiments with 4-QAM. The signal was transmitted and BER measurements were taken at numerous transmission distances. Figure 54 demonstrates the BER evolution for 16-QAM OFDM and CE-OFDM systems as the signal travels through

the spans of fibers. For these systems, bit errors start appearing after around 300 km of transmission with CE-OFDM presenting a slight edge over the OFDM system. The OFDM system reaches 600 km with a BER of 2.8×10^{-3} , while CE-OFDM reaches 700 km at a BER of 2.6×10^{-3} . As can be observed, a higher transmission rate was obtained at the cost of transmission distance. While 4-QAM achieved 1.200-1.300 km for 1.41 Gb/s transmission, 16-QAM doubles the rate for around half of that distance (600-700 km).

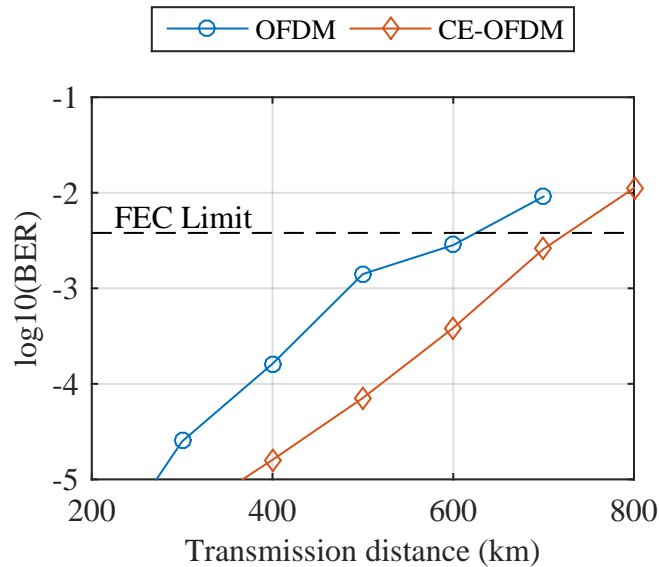


Figure 54 – BER as a function of transmission distance for 16-QAM the a) OFDM and b) CE-OFDM system.

By observing the constellation diagrams of these transmissions in Figure 55, the limitation of the system is clearly observed. For the outer points in the constellations, the data density is not as concentrated as the inner points, resulting in higher errors in the outer symbols. As more points interfere with each other, the EVM of the transmission tends to rise quickly and the system becomes more prone to errors, leading to lower transmission distances being reached. The CE-OFDM constellation shown in Figure 55a is slightly better than for the OFDM system, however both systems show similar performance at this point of analysis, as shown before.

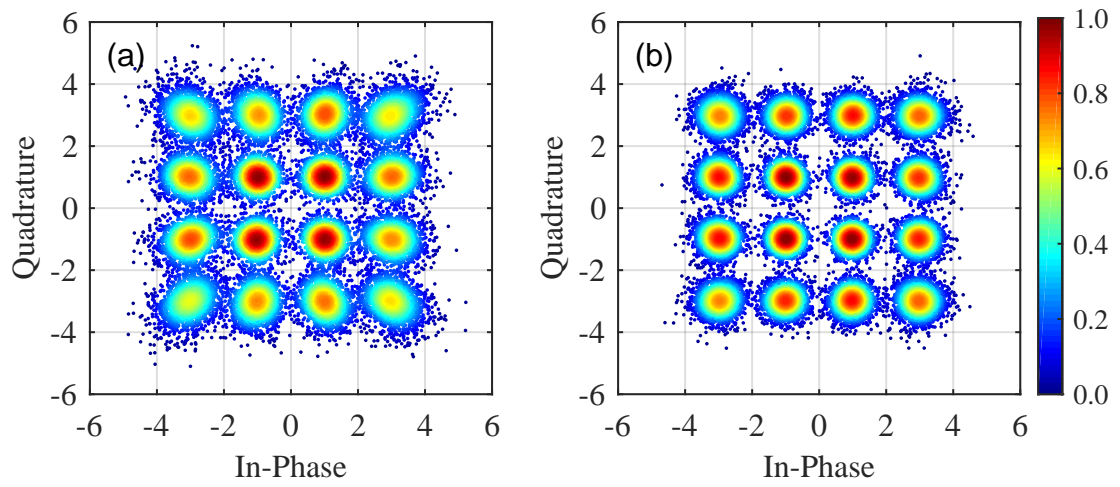


Figure 55 – 16-QAM constellation diagram for a transmission distance of 700 km at a fiber launch power of $P_{in} = 2$ dBm for a) OFDM and b) CE-OFDM.

5 Conclusion and Future Research

In this work, long-haul communications is broadly discussed using OFDM and CE-OFDM through a recirculating fiber loop. Initially, an extensive theoretical background is laid out in order to understand all fundamental features of the experimental setup. In sequence, every device was thoroughly characterized and discussed individually, guaranteeing that each apparatus functions as desired during experiments. The loop technique for achieving long distances is carefully considered, followed by the design of OFDM and CE-OFDM systems for long-haul transmission through the recirculating fiber loop. Such discussions assure that the experimental setup will provide high quality results for analysis, contributing to the overall quality of the work.

At first, the point of operation of the MZM was discussed. In the optical back-to-back configuration it is possible to observe how OFDM performance quickly decays as the point of operation deviates from the linear region, limiting the system at a very specific polarization point. On the other hand, CE-OFDM presents a higher tolerance to the nonlinear regions, demonstrating a broad range for the point of operation. However, as the signals transit through the optical channel, noise affects the systems severely, increasing the PAPR and making both systems have a similar curve, with an optimum point of operation clearly shifted when compared to the optical back-to-back configuration. The analysis provided operation points of $0.64V_\pi$ and $0.71V_\pi$ for OFDM and CE-OFDM respectively.

As CE-OFDM requires the phase modulation of the conventional OFDM signal, an important parameter arises, known as the phase modulation index. Such variable is directly related to the spectral efficiency of the technique, requiring careful attention to guarantee optimal performance. At shorter distances, it was easily observed how three regions were clearly defined: an optimum region, a noise limited region and a high modulation nonlinearity region. As transmission distances increase, higher values are needed for the phase modulation index to overcome the noise limited region, leading to spectral inefficiency of the system at such points of operation. Since long-haul transmissions are desired, a phase modulation index of 0.4 was chosen for the experiments.

Another important parameter of optical communication systems is the fiber launch power, leading to fiber nonlinearity at higher values. As OFDM presents a high PAPR, it is severely affected by nonlinear effects, causing distortion of the peaks and consequently reducing the overall performance of the system. CE-OFDM is implemented in order to reduce PAPR and avoid peak distortions of the conventional OFDM systems. Such characteristic enables a high nonlinear tolerance that was tested thoroughly. It was observed that OFDM was severely affected by high launch power, presenting an extreme performance

decay at such values over short and long transmission distances. On the other hand, CE-OFDM was only faintly affected at higher transmission distances, presenting a significantly higher performance than OFDM in all cases. The experiment clearly demonstrated the high CE-OFDM tolerance of fiber nonlinear effects over transmission distances. As for lower values of launch power, both systems presented similar performance with CE-OFDM presenting a slight edge over OFDM at the cost of a lower spectral efficiency. The optimal launch power for both techniques was defined as being any value in between 2 and 6 dBm.

In order to compare the systems more efficiently, BER measurements were taken over numerous transmission distances for both techniques under optimal launch power conditions and at high fiber nonlinearity regions. As stated before, under optimal conditions, both systems have similar performance, with OFDM reaching 1.100 – 1.200 km at just under the defined FEC limit, while CE-OFDM obtained nearly the same values at around 1.200 – 1.300 km. At the high fiber nonlinear region, with high fiber launch power, CE-OFDM obtained a significantly higher performance, reaching 900 – 1,000 km transmission distances just under the FEC limit, while OFDM reached 600 – 800 km under the same conditions.

All initial tests were realized considering the designed OFDM and CE-OFDM systems, with only two bits per symbol (4-QAM) and a raw rate of 1.41 Gb/s. The noisy characteristic of the optical channel makes it difficult to increase the order of the constellation diagram. Performance experiments were realized with 16-QAM at the optimal fiber launch power region, improving the raw rate to 2.82 Gb/s while maintaining the same hardware. The OFDM system reached 600 km with a BER just below the FEC limit, while CE-OFDM reached 700 km for approximately the same value of BER. As can be observed, a shorter distance is reached due to the noisiness of the channel, requiring significant space between the constellations for adequate transmission. Overall, the rate was doubled while the transmission distance reduced in nearly half, indicating a trade-off that might compensate for the system designer, depending on the application.

While carefully designing the OFDM system, the complexity of such technique becomes clear since a wide variety of parameters are available and decisions about each parameter are crucial. Testing each parameter separately is a possibility, but this consists in a very time-consuming method to acquire the desired results. A solution is to utilize optimization codes to encounter the best possible parameters for each system. Each optimized system can then be compared efficiently with regards to system performance. The optimized system should also present the best case scenario for the optical communication system, improving performance.

Only DDO systems were analyzed due to cost and simplicity, however CO systems have shown superior performance over long-haul communications. With this, longer distances and higher rates can be explored for a better comparison between both OFDM and

CE-OFDM techniques, possibly reaching transoceanic distances. For such distances, the loop should also be improved, exchanging the switch for another with a high extinction ratio, providing a deeper separation between the transmitter and the optical channel during the looping stage. Such hardware adaptations allow the looping technique to reach its full potential, simulating long distance communication systems more efficiently.

In conclusion, the contributions for the work were satisfactory. The loop technique was implemented and characterized entirely, permitting numerous analysis with different transmission distances. The tool may also be used by other testers of the laboratory to compliment further future research. Both OFDM and CE-OFDM systems were designed and implemented successfully in the loop, achieving distances as high as 1.300 km below the FEC limit. It was also possible to realize various comparisons between both techniques, demonstrating that CE-OFDM outperforms OFDM when fiber nonlinearities are introduced in the signals. The main contribution to date, in this scope, was:

- M. Santos, Caio & Nunes, Reginaldo & Lima Silva, Jair & Segatto, Marcelo & Pontes, Maria. (2018). Recirculating Loop for Experimental Transmission of DDO-OFDM Signals. Tu4A.7. 10.1364/LAOP.2018.Tu4A.7.

Bibliography

- AGRAWAL, G. P. *Lightwave technology: components and devices*. [S.l.]: Wiley, 2004. Cited in page 33.
- ALMEIDA, T. M. de. *Aumento da Eficiência Espectral de Sistemas DDO-OFDM Através de Otimização via Algoritmo Genético*. Dissertação (Mestrado) — Universidade Federal do Espírito Santo, 2014. Cited in page 29.
- ANRITSU. *MS9740A Optical Spectrum Analyzer Operation Manual*. [S.l.]. Cited in page 103.
- BECKER, P.; OLSSON, N.; SIMPSON, J. *Erbium-Doped Fiber Amplifiers: Fundamentals and Technology*. [S.l.]: Optics and Photonics, 1999. Cited 4 times on pages ix, 27, 38, and 40.
- BERGANO, N. S. et al. A 9000 km 5 Gb/s and 21,000 km 2.4 Gb/s Feasibility Demonstration of Transoceanic EDFA Systems using a Circulating Loop. *Optical Fiber Conference*, OSA, 1991. Cited 2 times on pages 27 and 45.
- BERGANO, N. S.; DAVIDSON, C. R. Circulating Loop Transmission Experiments for the Study of Long-Haul Transmission Systems Using Erbium-Doped Fiber Amplifiers. *Journal of Lightwave Technology*, IEEE, v. 13, n. 5, p. 879–888, 1995. Cited 3 times on pages 27, 45, and 46.
- CHANG, R. W. Synthesis of Band-Limited Orthogonal Signals for Multichannel Data Transmission. *The Bell System Technical Journal*, IEEE, v. 45, p. 1775–1796, 1966. Cited 2 times on pages 27 and 47.
- CHANG, R. W. *OFDM for Wireless Multimedia Communications*. Artech House, 2000. Cited in page 27.
- CHEMTRONICS. *How To Clean and How Not to Clean Fiber Optic Connectors*. 2019. <<https://www.chemtronics.com/how-to-clean-and-how-not-to-clean-fiber-optic-connectors>>. [Online; accessed on March 29, 2019]. Cited 2 times on pages xi and 99.
- DERICKSON, D. *Fiber Optic Test and Measurement*. [S.l.]: Prentice Hall Inc, 1998. Cited 4 times on pages ix, 32, 33, and 41.
- DJORDJEVIC, I.; RYAN, W.; VASIC, B. *Coding for Optical Channels*. [S.l.]: Springer, 2010. Cited 10 times on pages 32, 33, 35, 36, 37, 38, 39, 41, 43, and 44.
- DUBOVITSKY, S. et al. Analysis and Improvement of Mach–Zehnder Modulator Linearity Performance for Chirped and Tunable Optical Carriers. *Journal of Lightwave Technology*, IEEE, v. 20, n. 5, p. 886–891, 2002. Cited 2 times on pages 33 and 34.
- FREITAS, M. *Amplificadores Óticos a Fibra Sob um Ambiente Dinâmico*. Tese (Doutorado) — Universidade Federal do Espírito Santo, 2006. Cited 2 times on pages 27 and 38.

HANZO, L.; WEBB, W.; KELLER, T. Single- and Multi-carrier Quadrature Amplitude Modulation: Principles and Applications for Personal Communications, WLANs and Broadcasting. John Wiley and Sons, 2000. Cited 2 times on pages 27 and 47.

ITU-T. *Recommendation ITU-T G.652: Characteristics of a single-mode optical fibre and cable*. 2016. <<https://www.itu.int/itu-t/recommendations/rec.aspx?rec=13076>>. [Online; accessed on February 28, 2019]. Cited in page 61.

JANSEN, S. L. et al. Coherent Optical 25.8-Gb/s OFDM Transmission Over 4160-km SSMF. *Journal of Lightwave Technology*, IEEE, v. 26, p. 6–15, 2007. Cited 2 times on pages 28 and 75.

KLENNER, P. *Communications technology laboratory, The OFDM multi carrier system*. 2004. Unpublished notes. Cited 5 times on pages ix, 47, 48, 49, and 51.

MAZZALI, C.; FRAGNITO, H. L. Recirculating Loop for Experimental Evaluation of EDFA Saturated Regime Effects on Optical Communication Systems. *Transactions on Microwave Theory and Techniques*, IEEE, v. 46, n. 3, p. 253–256, 1998. Cited 2 times on pages 45 and 68.

MULLER, M.; STEPHENS, R.; MCHUGH, R. *Total Jitter Measurement at Low Probability Levels, Using Optimized BERT Scan Method*. 2005. White Paper, Agilent Technologies. Cited in page 55.

NUNES, R. B. *OFDMA PON - Arquitetura para Redes Ópticas Passivas com Acesso Múltiplo por Divisão de Frequências Ortogonais*. Tese (Doutorado) — Universidade Federal do Espírito Santo, 2016. Cited in page 29.

NUNES, R. B. et al. Experimental Validation of Constant-Envelope OFDM System for Optical Direct-Detection. *Optical Fiber Technology*, Elsevier, v. 20, p. 303–307, 2014. Cited in page 28.

PEREIRA, E. da V. *Transmissão de Sinais OFDM com Envoltória Constante em Sistemas Ópticos com Detecção Coerente*. Tese (Doutorado) — Universidade Federal do Espírito Santo, 2017. Cited in page 29.

PEREIRA, E. da V. et al. Impact of Optical Power in the Guard-Band Reduction of an Optimized DDO-OFDM System. *Journal of Lightwave Technology*, IEEE, v. 33, n. 23, p. 4717–4725, 2015. Cited in page 56.

PHOTONICS, R. *Fiber Polarization Controllers*. 2019. <https://www.rp-photonics.com/fiber_polarization_controllers.html>. [Online; accessed on February 25, 2019]. Cited in page 42.

PHOTONICS, R. *Silica Fibers*. 2019. <https://www.rp-photonics.com/silica_fibers.html>. [Online; accessed on February 14, 2019]. Cited 2 times on pages ix and 35.

PINTO, E. L.; ALBUQUERQUE, C. P. de. A técnica de transmissão OFDM. *Revista Científica Periódica - Telecomunicações*, IEEE, v. 2, n. 1, 2002. Cited in page 48.

PROAKIS, J. G. *Digital Communication*. [S.l.]: McGraw-Hill, 1995. Cited in page 50.

- ROCHA, H. R. de O. et al. Increasing the Spectral Efficiency of DDO-CE-OFDM Systems by Multi-Objective Optimization. *Journal of Lightwave Technology*, IEEE, 2019. Cited in page 82.
- RUIZ, A.; CIOFFI, J. M.; KASTURIA, S. Discrete Multiple Tone Modulation with Coset Coding for the Spectrally Shaped Channel. *IEEE Transactions on Communications*, IEEE, v. 40, n. 6, p. 1012–1029, 1992. Cited in page 50.
- SCHMOGROW, R. et al. Error Vector Magnitude as a Performance Measure for Advanced Modulation Formats. *IEEE Photonics Technology Letters*, IEEE, v. 24, n. 1, p. 61–63, 2012. Cited in page 56.
- SHAIM, M. H. A.; KHAN, M. R. H. Design and Simulation of a Low Loss Optical Fiber Coupler. *International Journal of Electronics and Communication Engineering*, IRPH, v. 4, n. 5, p. 473–482, 2011. Cited in page 43.
- SHIEH, W.; DJORDJEVIC, I. *OFDM for Optical Communications*. [S.l.]: Elsevier, 2010. Cited 4 times on pages 28, 49, 50, and 52.
- SILVA, J. A. L. *Transmissão de Sinais OFDM com Envelope Constante em Sistemas Ópticos IMDD*. Tese (Doutorado) — Universidade Federal do Espírito Santo, 2011. Cited 8 times on pages 28, 29, 47, 48, 49, 50, 52, and 54.
- SILVA, J. A. L.; CARTAXO, A. V. T.; SEGATTO, M. E. V. A PAPR Reduction Technique Based on a Constant Envelope OFDM Approach for Fiber Nonlinearity Mitigation in Optical Direct-Detection Systems. *Journal of Optical Communications and Networking*, IEEE, v. 4, p. 296–303, 2012. Cited in page 28.
- SMITH, F. G.; KING, T. A.; WILKINS, D. *Optics and Photonics: An Introduction*. [S.l.]: Wiley, 2007. Cited in page 36.
- THOMPSON, S. C. et al. Constant Envelope OFDM. *IEEE Transactions on Communications*, IEEE, v. 56, 2004. Cited 2 times on pages 28 and 53.
- THOMPSON, S. C. et al. Constant Envelope OFDM Phase Modulation: Spectral Containment, Signal Space Properties and Performance. *Military Communications Conference*, IEEE, v. 2, p. 1300–1312, 2008. Cited 3 times on pages 28, 52, and 53.
- TOGNERI, A. P. *Análise de Sistemas de Multiplexação por Subportadora - SCM*. Dissertação (Mestrado) — Universidade Federal do Espírito Santo, 2005. Cited 2 times on pages 34 and 37.

A Safety Considerations

A.1 Optical Safety Considerations

Before measuring any type of optical signal, safety considerations should be taken into account. It is noteworthy to mention that even relatively low powers can lead to permanent eye injuries, making it essential for the tester to know the devices under test. As most telecommunication wavelengths are inserted in the infrared region, the light is usually invisible to the human eye, making it extremely dangerous during operation. It is imperative that the tester stays aware of the symbols and labels indicating such light beams, in order to avoid direct exposure. A wide variety of labels are available, with some being more common than others, such as the labels demonstrated in Figure 56.

The light sources are classified according to the IEC 60825-1:2014 standard. These classes are summarized in Table 13. According to the standard, every equipment of class 2 or higher should contain the triangular label demonstrated in Figure 56a. These lasers in general should be handled by trained personnel, in order to avoid accidents. Other labels might be employed to demonstrate more specific information about the equipment, such as the the typical warning labels demonstrated in Figures 56a and 56b. These complementary labels usually show information such as laser class, power and risks.

For equipment classes above 3, always use appropriate handling equipment, such as laser safety glasses and interlocks. The power should always be measured with a power meter, as to guarantee that an adequate level of power is being injected into the system. It is also important to measure the power at each setup modification in order to maintain safe levels for optic devices and measurement equipment. Always keep the light source turned off during assembly of the optical setup to avoid direct or diffused beam exposure.

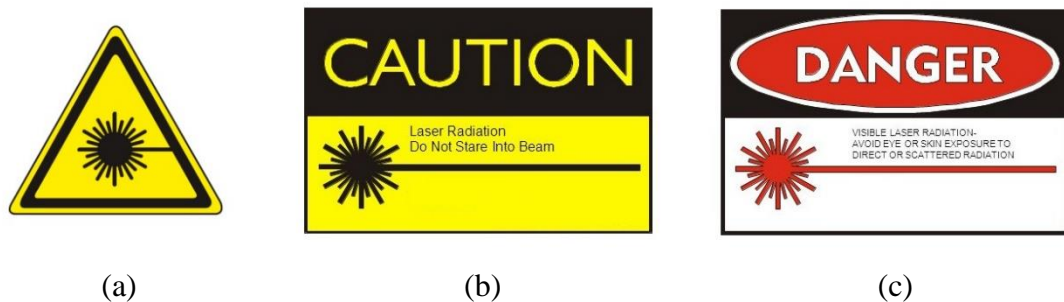


Figure 56 – Typical laser hazard labels.

Table 13 – Summarized IEC 60825-1:2014 standard light source classification.

Safety Class	Summary
Class 1	Inherently safe under conditions of normal use.
Class 1M	Inherently safe, unless optical instruments are used.
Class 2	Safe under limited exposure (<0.25 s) due to human blink reflex. Lasers limited to visible range (400-700 nm), with power inferior to 1 mW.
Class 2M	Safe under limited exposure (<0.25 s) due to human blink reflex, unless optical instruments are used. The power may be higher than 1 mW.
Class 3R	Safe if handled carefully. Lasers in the visible range are limited to 5 mW, while other wavelengths have variable limits.
Class 3B	Safe if handled carefully. Limits up to 0.5 W are applicable, requiring specific instruments for handling, such as protective eyewear and safety interlocks. Diffused radiation should normally be harmless.
Class 4	Most hazardous type of laser, requiring careful handling. They can cause damage to eyesight, skin and others as a result of direct, diffused and/or indirect beam viewing. They must be equipped with safety interlocks.

A.2 Inspection and Cleaning Procedures

While handling optical fibers, careful assembly should be taken into account due to the sensitivity of these devices with regards to dust particles and incorrect handling. Small particles stick to the connector's end face, causing performance loss in the optical link. Optical fibers can be severely affected by dust particles invisible to the human eye due to the small dimension of the core. For such reasons, inspection and cleaning procedures should be taken into account while setting up the system to avoid beam scattering and signal attenuation.

The inspection of an optical connector can be realized using an ordinary scope to carefully examine the connector's face. An example of such scope is the Thorlabs FS201. To operate the scope, the connector's point is inserted into the adapter and held firmly in place. A switch illuminates the the device under test, allowing for coaxial or oblique illumination, depending on the switch selection. To clearly observe the core, an adjustment of the focus knob might be necessary.

Important: Always guarantee that no power is being injected into the fiber while realizing an inspection!

The importance of inspection is demonstrated in Figure 57, where common connector contamination is demonstrated. When removing the protective end cap of a connector, it is common to think that the new connector will be perfectly clean, however, Figure 57a

demonstrates that contamination may occur nevertheless. While handling the connector, the tester must avoid any contact with the end face, as shown by Figure 57b, where a finger has touched the connector. Another common mistake is to couple a clean connector to and unclean one, causing cross-contamination, as demonstrated in Figure 57c. Another concern is that of dust particles, such as lint from clothing that attaches itself to the end face of the connector, causing contamination as shown in Figure 57d.

The most common method of cleaning a connector's end face is with a dry wipe or swab. Dry cleaning must be implemented with care since the act of cleaning may create a static charge that attracts contamination to the clean connector. However, hand-held dry cleaners are practical and easy to use, making them a common choice for optical fiber cleaning. An example is the fiber cleaning cloth spool shown in Figure 58a. To effectively clean the connector, the user must place the connector's end face firmly on the exposed cloth and carefully move the face along the cloth, causing any contamination to pass from the connector to the cloth. After a couple of usages, the cloth should be discarded and a new one placed in its place. The cloth spool allows disposing of used cloth easily, as you pull the used part and a new one comes into its place. Figure 58b demonstrates the inspection of a recently clean connector face, proving the efficiency of the cleaning process.

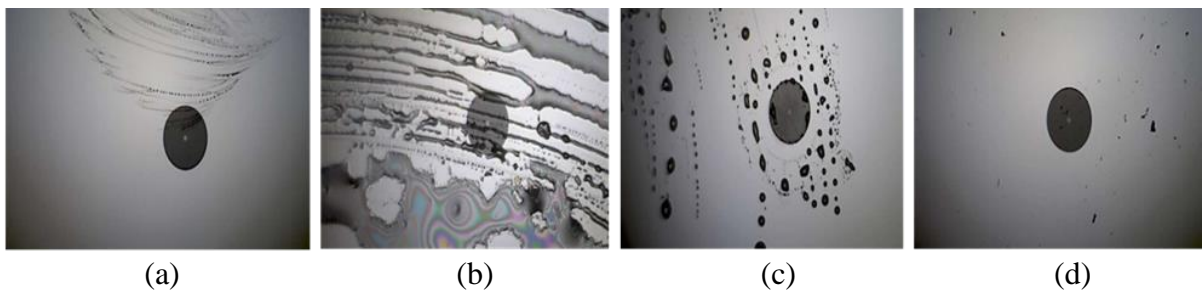


Figure 57 – Inspection of contaminated connector faces: a) protective end cap removal, b) fingerprint exposure, c) cross-contamination from unclean connector and d) lint from clothing. Source: [Chemtronics 2019].

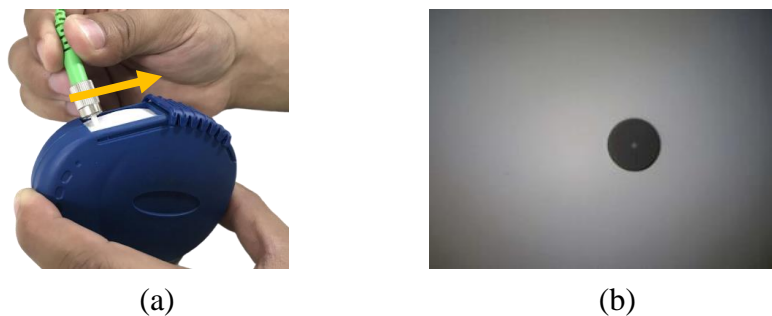


Figure 58 – Connector cleaning: a) fiber cleaning cloth spool usage example and b) clean connector inspection. Source: [Chemtronics 2019].

A.3 Electrostatic-sensitive Devices

Electrostatic-sensitive devices are components that can be easily damaged due to static charges that build up on static-accumulating materials. These components should be handled in static controlled locations to avoid component failure due to electrostatic discharge (ESD). Most optical component controller chips and RF components are ESD sensitive, requiring careful handling during operation. The testing area should have a grounded table, with most equipment being efficiently grounded to avoid static accumulation. The user should also wear a grounded wrist wrap to avoid user ESD. Figure 59 shows a DPO with ESD sensitivity label near the inputs. The tester should be aware of such symbols while handling equipment and components since this will indicate that the device is sensitive to ESD.



Figure 59 – DPO with ESD sensitive inputs. The wrist wrap grounds the user, protecting the equipment from ESD.

B Measurement Procedures

B.1 Light Source Measurement

The light source is usually evaluated for power levels and/or spectral shape. The first measurement is straightforward, using a simple power meter to obtain the power levels of the component. For a power measurement using a power meter, the following procedure may be adopted:

Power Measurements

1. Inspect and clean connectors with the light source turned off;
2. Connect the light source to the power meter;
3. Select the measuring wavelength;
4. Turn on the light source and measure the optical power.

If a spectral analysis is needed, an OSA will be used to measure the signal. It is wise to use the power measurement before inserting the signal into the OSA to guarantee that the power level is below the maximum admitted by the OSA. With this in mind, the following procedure may be adopted:

Spectral Measurement

1. Inspect and clean connectors with the light source turned off;
2. Measure the optical power using a power meter to guarantee that it is below the OSA's limit;
3. Connect the light source to the OSA;
4. Select the measuring wavelength interval;
5. Select the power interval;
6. Select the desired resolution;
7. Turn on the light source and measure the spectrum.

The optical spectrum can usually be extracted from the OSA for an offline processing of the signal. By following the steps above and extracting the data, a curve similar to Figure 20 is obtained. From the data it is possible to obtain all measurements presented in Table 1. Note that these measurements may also be taken directly from the OSA by using analysis tools. The center wavelength and optical power may be measured in any OSA, however, SMSR and spectral linewidth may require a more advanced equipment to measure. The measurements from Table 1 and Figure 20 were obtained from an APEX Optical Complex Spectrum Analyzer (OCSA) AP2683A, with a resolution of 10 fm. The other available OSA is an Anritsu MS9740A OSA with a minimum resolution of 30 pm, making it difficult to measure the SMSR, for example.

B.2 Optical Modulator Measurements

Optical Modulator characterization is usually realized by measuring the output power of the device. For this reason, it is possible to completely characterize the device with only a power meter. The measurement setup is displayed in Figure 21. The procedure for such measurement is the following:

Optical Modulator Characterization

1. Inspect and clean connectors with the light source turned off;
2. Assemble the setup from Figure 21;
3. Measure the input optical power using a power meter to guarantee that it is below the MZM's limit;
4. Measure the optical power at the output of the MZM while varying the polarization controller, slowly, until the maximum possible output power is obtained (optional);
5. Change the bias voltage;
6. Measure the output power;
7. Repeat steps 4 and 5 in desired voltage steps, until all values are gathered.

By following the procedures above, a curve similar to the one demonstrated in Figure 22 is obtained. Step 3 is realized to obtain the lowest possible loss from polarization effects. Since the characterization output is normalized, this step is optional for the characterization. However, step 3 is primordial for the use of the MZM in optical communication systems since it will reduce the device's overall insertion loss. If the tester desires to observe the spectral properties of the device, the same spectral measurement procedure realized in the Light Source Measurements may be employed.

B.3 Optical Amplifier Measurements

Optical amplifier measurements are usually realized to characterize gain and noise figure. The most precise way to acquire these measurements is using an OSA to obtain the optical power in all wavelengths involved in the amplification process. The analysis is realized with the input power spectrum and the output power spectrum, requiring a measurement before and after the amplifier, as shown in Figure 23. It is important to observe the dynamic of the gain and noise figure with respect to the input signal power, making it essential to include a VOA in the setup. Light sources usually allow for power variation, however this is usually accomplished by changing the bias current of the device, which can change the shape of the spectrum. By setting the light source power and varying the power using a VOA, it is possible guarantee that the spectrum will only attenuate and not change significantly in shape.

The Anritsu MS9740a OSA has built in functions to analyze gain and noise figure by using Spectrum Division, Polarization Nulling, Pulse or WDM methods [Anritsu]. The ASE power in the analysis window is measured and an interpolation is realized to efficiently estimate the noise at the signal wavelength. Two ASE fitting techniques are available: the Gaussian fitting and the Mean fitting, as demonstrated by Figure 60. The Gaussian fitting is realized by approximating the power value (dBm units) at λ_s through a second-order fitting of the power values (dBm units) from λ_1 to λ_4 (Figure 60a). On the other hand, the Mean fitting is realized by acquiring the mean power (mW units) between λ_2 and λ_3 (Figure 60b). The Fitting Span is the bandwidth of the data range used for the ASE Fitting methods, usually defined around the peak wavelength. The Masked Span is the bandwidth, around the peak wavelength, disregarded from the ASE fitting since it is the region where the power should be estimated.

While setting up the measurement, a test parameter window will require the user to select the main parameters, as demonstrated by Figure 61. Pin Loss and Pout Loss refers to the loss inserted when taking these signals to the OSA. The values inserted will compensate the signals in order to compensate these losses. The noise figure is multiplied by a factor, k , responsible for NF calculation calibration. This value is defined as the parameter "NF Cal" and should be set to adjust the NF values according to the users interest or setting 1 to disregard NF calibration. The parameters "O.BPF Lvl Cal" and "O.BPF BW" refer to the loss and bandwidth of the optical bandpass filter respectively. The first parameter should be set to 0 if no filter is inserted or if a built-in filter is being evaluated. Similarly, the filter bandwidth parameter should be set to 999 nm if a filter is not inserted.

The parameter "NF Select" refers to the NF calculation method. By choosing S-ASE, only the beat noise between the optical signal and the ASE is calculated, resulting in a calculation similar to Equation 19. Since the term $1/G$ is very small due to high

gain values, the OSA neglects this term, resulting in a simplified equation for the S-ASE calculation method:

$$NF = 10 \log_{10} \left(k \cdot \frac{P_{ASE}}{h\nu G \Delta\nu_{act}} \right), \quad (48)$$

where k denotes the correction value set by NF Calc and ν_{act} is the frequency bandwidth of actual resolution, defined by,

$$\nu_{act} = \left(\frac{1}{\lambda - RES_{real}/2} - \frac{1}{\lambda + RES_{real}/2} \right) \cdot c \cdot 10^9, \quad (49)$$

where λ_s denotes the signal wavelength and RES_{real} is the resolution calibrated by the OSA before the measurement is realized.

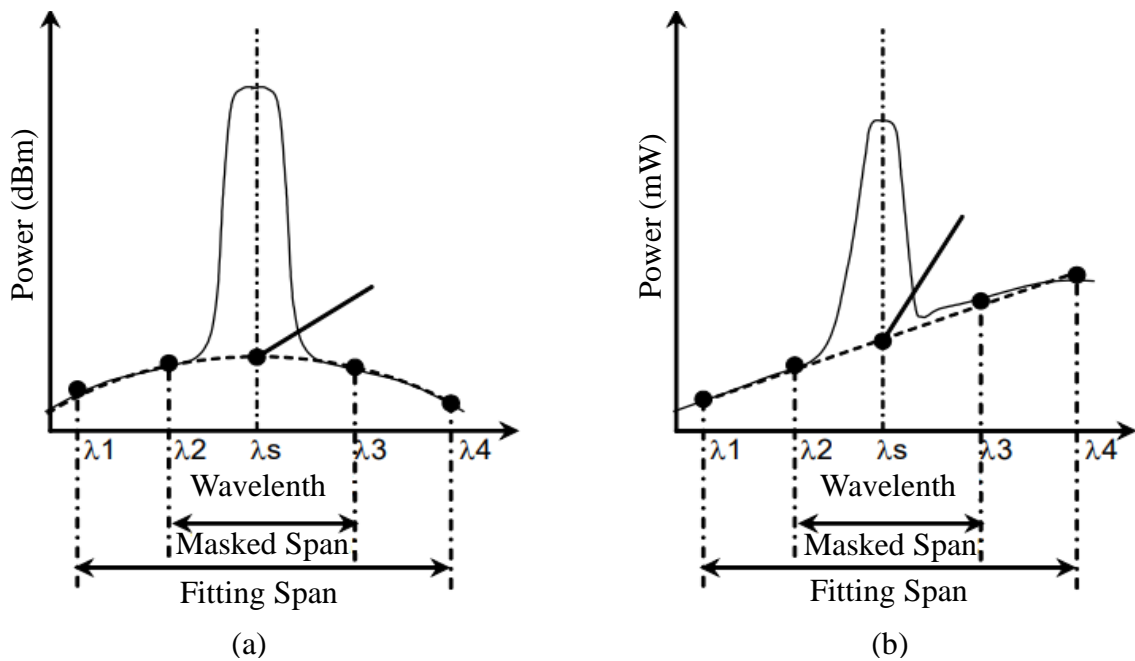


Figure 60 – ASE Fitting methods: a) Gaussian fitting and b) Mean Fitting.



Figure 61 – MS9740a Optical Amplifier Characterization Test Parameters Example.

If the Total calculation method is selected, all noise portions are calculated and summed to obtain the total NF. Therefore, the total NF can be defined as,

$$NF = 10\log_{10}(k \cdot (F_1 + F_2 + F_3 + F_4)), \quad (50)$$

where F_1 is the beat noise between optical signal and ASE, F_2 is the beat noise between ASE, F_3 is the optical signal shot noise and F_4 is the ASE shot noise. Each noise term can then be defined as,

$$F_1 = \frac{P_{ASE}}{h\nu G \Delta\nu_{act}}, \quad (51)$$

$$F_2 = \frac{P_{ASET}^2}{2h\nu G^2 P_{in}(\lambda) \Delta\nu_{act}}, \quad (52)$$

$$F_3 = \frac{1}{G}, \quad (53)$$

$$F_4 = \frac{P_{ASET}}{G^2 P_{in}(\lambda)}. \quad (54)$$

In the set of equations, $P_{ASET} = P_{ASE} \cdot (\Delta\nu_a / \Delta\nu_{act})$ and $\Delta\nu_a$ can be defined as,

$$\Delta\nu_a = \left(\frac{1}{\lambda - BPFBW/2} - \frac{1}{\lambda + BPFBW/2} \right) \cdot c \cdot 10^9, \quad (55)$$

where BPFBW denotes the bandpass filter bandwidth.

With all measurement parameters defined, the characterization can be realized by following the procedures below. Safety should be the number one concern during these measurements since high optical powers can be obtained during the amplification process. It is also important to carefully monitor the power in order to always work within the power limit of the measuring equipment.

Optical Amplifier Characterization

1. Inspect and clean connectors with the light source and amplifier turned off;
2. Assemble the setup from Figure 21;
3. Prepare the MS9740a OSA for Optical Amplifier Measurement by selecting the "Application" menu and choosing "Opt.AmpTest";
4. Choose the desired "Method" of amplifier testing;
5. Press "Res Cal" to calibrate the resolution before measurement;
6. Choose a trace to store the Pin data;
7. Measure the power with a power meter to guarantee that the power is below the OSA's limit;

8. Measure Pin using the setup shown in Figure 21a;
9. Choose a trace to store the Pout data;
10. Measure the power with a power meter to guarantee that the power is below the OSA's limit;
11. Measure Pout using the setup shown in Figure 21b;
12. Press "Parameter" to define all test parameters (Figure 61);
13. Press "Set" to calculate and display the results;

Figure 62 demonstrates a typical result of the Optical Amplifier Characterization procedure, with Trace A being Pin (yellow trace) and Trace B being Pout (blue trace). All parameters and results are displayed in the upper part of the screen.

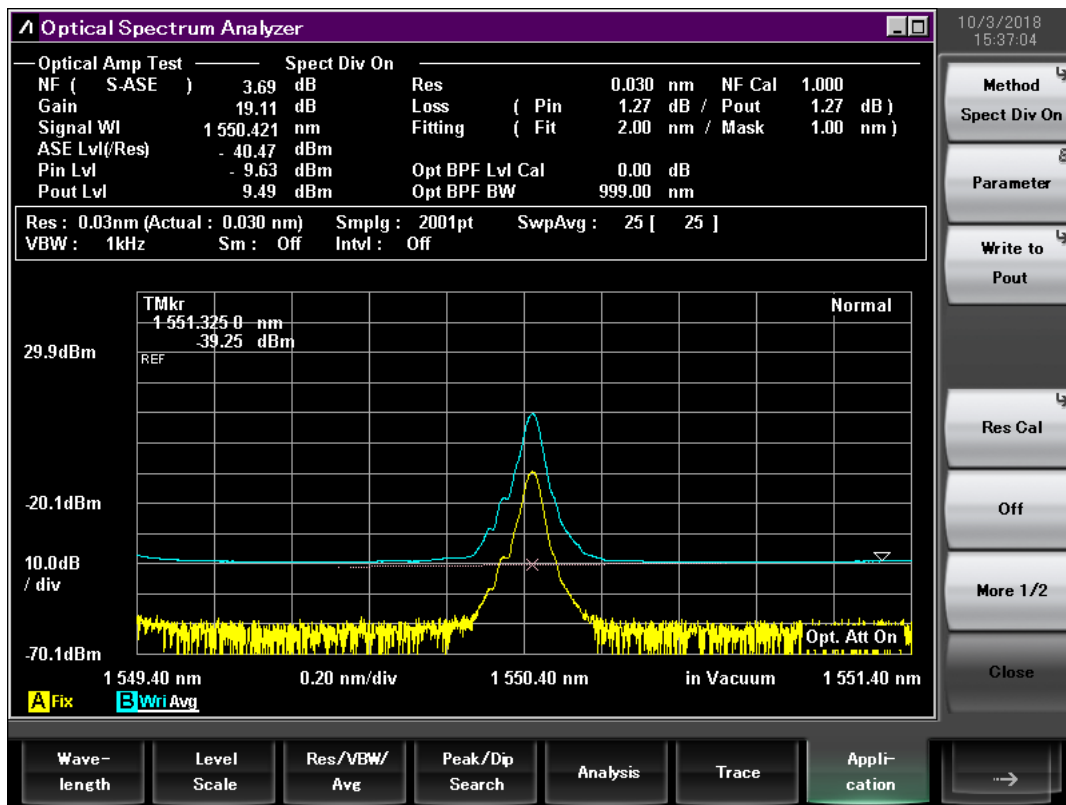


Figure 62 – MS9740a Optical Amplifier Characterization Test Example.

B.4 Optical Fiber Measurements

To characterize an optical fiber, simple power measurements may be realized with a power meter by inserting a light source in one end and computing the loss at the other end. This method is simple and effective, but does not allow for a precise measurement of the fiber distance. The power meter measurement can be realized as follows:

Optical Fiber Power Meter Measurement

1. Inspect and clean connectors with the light source turned off;
2. Select the wavelength for measurement;
3. Measure the power of the light source with the power meter;
4. Connect the light source to one end of the fiber;
5. Measure the power at the other end of the fiber;
6. Compute the cumulative loss by subtracting the power values;
7. Estimate the loss per km by dividing by the fiber length.

A more accurate characterization requires an optical time-domain reflectometer (OTDR) to send pulses in one end of the fiber and extract, from the same end, light that is reflected back from points along the fiber. In a typical OTDR, the following procedures may be adopted:

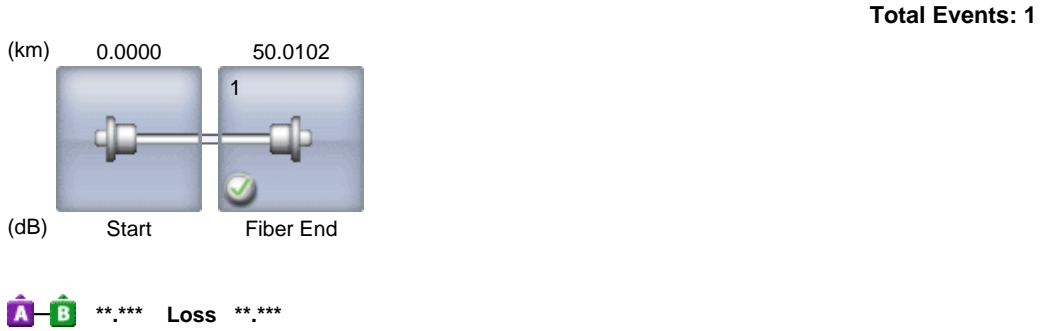
Optical Fiber OTDR Characterization

1. Inspect and clean connectors;
2. Connect any end of the fiber to the OTDR;
3. Set the wavelength for measurement;
4. Set the distance range for the measurement;
5. Set the pulse width for analysis;
6. Execute the measurement.

For the characterization of the Corning[®] SMF-28e+[®] fiber, an Anritsu MT9083A2 OTDR was used. The procedure above was used to obtain the results in Figures 63 and 64. The first figure demonstrates the graphical event of the analysis and a table with a summary of the detected measurements. With a power meter measurement, only the cumulative loss of the fiber would be achieved, whereas the event table of the OTDR

shows the distance of the fiber and the loss. A trace of the measurement is also available as shown in Figure 64. This trace demonstrates the pulse propagation along the fiber, making it possible to observe any failures in the optical fiber, such as severe bends or broken sections.

Graphical Events



Event Table

No	Dist (km)	Type	Loss (dB)	Reflect (dB)	dB/km	Cum. Loss (dB)
1	50.0102		Fiber End	**.*	0.179	8.976

Figure 63 – Anritsu MT9083A2 Graphical Events and Event Table for SSMF characterization.

OTDR Trace

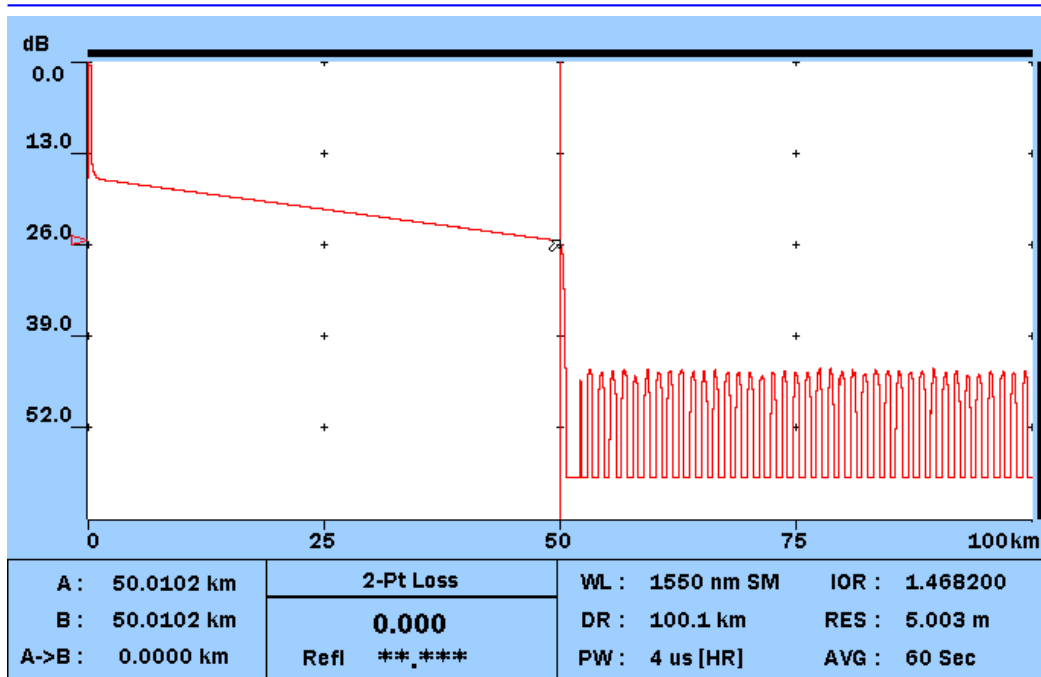


Figure 64 – Anritsu MT9083A2 SSMF characterization trace.

B.5 Optical Switch Measurements

Optical switches are usually characterized for insertion loss and response time. For the insertion loss, simple power measurements can be realized by inserting a light source in one end and measuring the output power in the other. The difference in power is the insertion loss of the equipment.

Optical Switch Insertion Loss Measurement

1. Inspect and clean connectors with the light source turned off;
2. Select the wavelength for measurement;
3. Measure the power of the light source with a power meter;
4. Connect the light source to one end of the switch;
5. Measure the power at the outputs;
6. Compute the insertion loss by subtracting the power values;
7. Change the state of the switch and remeasure, if necessary.

For the response time a slightly more complex setup must be employed, such as demonstrated in Figure 33a. An MDO and a PD must be used to obtain the correct measurements. It is wise to note that the PD must have a faster response time than the switch or the measurement will be limited by the PD. With that in mind the procedure for measuring the response time is:

Optical Switch Response Time Characterization

1. Inspect and clean connectors with the light source turned off;
2. Assemble the setup from Figure 33a;
3. Measure the power of the light source to guarantee that it is below the limit of the PD;
4. Set the appropriate voltage and time scales in the MDO;
5. Compare the switch and PD signals as shown in Figure 33b, to obtain the response times.

By applying both procedures demonstrated above, the Agiltron NanoSpeed™1x2 Series Fiber Optical Switch was characterized, obtaining the values presented in Table 8. The measurements for the response time characterization are demonstrated in Figures 65-68.

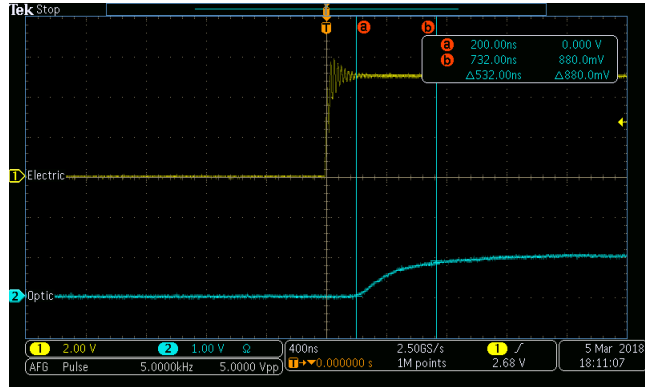


Figure 65 – Switch Rise Time (T_r) Measurement.

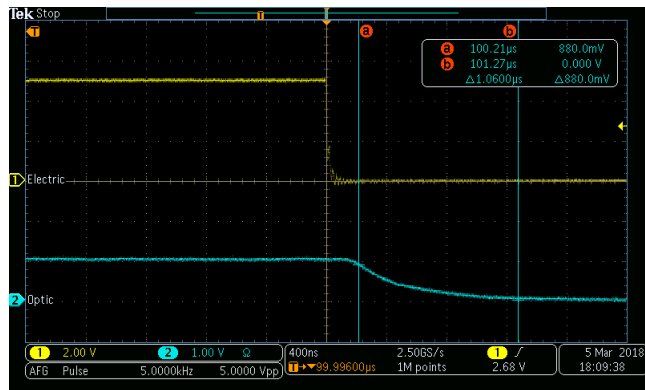


Figure 66 – Switch Fall Time (T_f) Measurement.

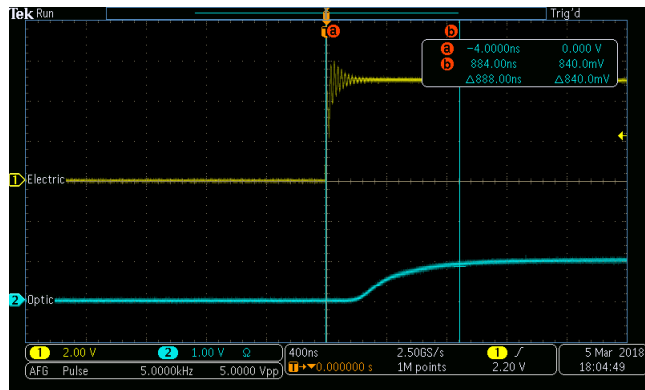


Figure 67 – Switch Rise Speed (S_r) Measurement.

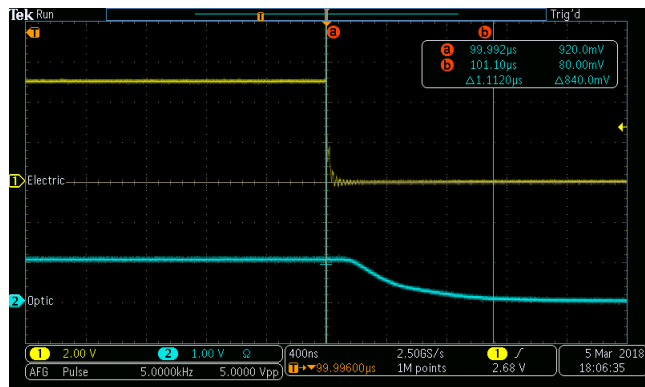


Figure 68 – Switch Fall Speed (S_f) Measurement.

B.6 Optical Coupler Measurements

The characterization of an optic coupler usually aims to obtain the excess loss, the insertion loss and the coupling ratio. Assuming a 2x2 coupler with inputs a and b , while the outputs are c and d , the following equations may be used for the characterization:

$$\text{Excess Loss (dB)} = 10 \log_{10} \frac{P_{a,b}(\text{mW})}{P_c(\text{mW}) + P_d(\text{mW})}, \quad (56)$$

$$\text{Insertion Loss (dB)} = 10 \log_{10} \frac{P_{a,b}(\text{mW})}{P_{c,d}(\text{mW})}, \quad (57)$$

and

$$\text{Coupling Ratio (\%)} = \frac{P_{c,d}(\text{mW})}{P_c(\text{mW}) + P_d(\text{mW})} \cdot 100. \quad (58)$$

These equations can be used with power measurements at any wavelength to obtain the coupler characteristics at that wavelength. Usually, a full spectrum characterization is the most helpful for the tester, requiring a broadband source and an OSA, as demonstrated in Figure 34. The procedures are:

Optical Coupler Characterization

1. Inspect and clean connectors with the light source turned off;
2. Measure the power of the light source with a power meter to guarantee that it is below the limit of the OSA;
3. Assemble the setup from Figure 34a;
4. Measure the broadband light source;
5. Assemble the setup from Figure 34b;
6. Measure the power output from each coupler output;
7. Use Equations 56-58 with the data obtained from the OSA.

The procedure above should generate results similar to Figure 35. To obtain the result at a specific wavelength it is possible to compute the values only at the desired wavelength as shown in Tables 9 and 10. Other parameters such as directivity and uniformity may also be measured by following the procedure above, however they were not taken into account in this text.

B.7 Optical Filter Measurements

An optical filter is usually characterized for its finesse and insertion loss. For precision during this measurement, an OSA and a broadband light source are required, as demonstrated by the characterization setup in Figure 30. The procedures are:

Optical Filter Characterization

1. Inspect and clean connectors with the light source turned off;
2. Measure the power of the light source with a power meter to guarantee that it is below the limit of the OSA;
3. Assemble the setup from Figure 30a;
4. Measure the broadband light source;
5. Assemble the setup from Figure 30b;
6. Measure the power output from the filter;
7. Compute the finesse and insertion loss.

By subtracting the measurement of the output from the input, both characteristics of the filter are obtained. The peak value is the insertion loss of the device, while the 3 dB attenuation points characterize the finesse. The measurements obtained from the OSA should be similar to Figure 31.